Thermal and Concentration Analyses of Cilia Induced Flow

By:

Sidra Shaheen
Reg. No. 88-FBAS/PHDMA/S17

Supervised By:

Dr. Khadija Maqbool

Department of Mathematics and Statistics
Faculty of Basic and Applied Sciences
International Islamic University, Islamabad
Pakistan
2021

Cilia- Physiological effect

Fluid dynamics

Heat- Transmission

Diffusion

Thermal and Concentration Analyses of Cilia Induced Flow

By:

Sidra Shaheen
Reg. No. 88-FBAS/PHDMA/S17

A Thesis

Submitted in the Partial Fulfilment of the

Requirements for the degree of

DOCTOR OF PHILOSOPHY

IN

MATHEMATICS

Supervised By:

Dr. Khadija Maqbool

Department of Mathematics and Statistics
Faculty of Basic and Applied Sciences
International Islamic University, Islamabad
Pakistan
2021

Author's Declaration

I, **Sidra Shaheen** Reg. No. **88-FBAS/PHDMA/S17** hereby state that my Ph. D. thesis titled : **Thermal and Concentration Analyses of Cilia Induced Flow** is my own work and has not been submitted previously by me for taking any degree from this university, International Islamic University Islamabad, Pakistan or anywhere else in the country/world.

At any time, if my statement is found to be incorrect even after my Graduation the university has the right to withdraw my Ph. D degree.

Name of Student: (**Sidra Shaheen**)

Reg. No. **88-FBAS/PHDMA/S17**

Dated: **21/09/2021**

Plagiarism Undertaking

I Solemnly declare that research work presented in the thesis titled: **Thermal and Concentration Analyses of Cilia Induced Flow** is solely my research work with no significant contribution from any other person. Small contribution/help wherever taken has been duly acknowledged and that complete thesis has been written by me.

I understand the zero tolerance policy of the HEC and University, **International Islamic University, Sector H-10, Islamabad, Pakistan** towards plagiarism. Therefore, I as an Author of the above titled thesis declare that no portion of my thesis has been plagiarized and any material used as a reference is properly referred/cited.

I undertake that if I am found guilty of any formal plagiarism in the above titled thesis even after award of Ph. D degree and HEC and the University has the right to publish my name on the HEC/University Website on which names of students are placed who submitted plagiarized thesis.

Student/Author Signature: Sidra Shaheen

Name: **(Sidra Shaheen)**

Certificate of Approval

This is to certify that the research work presented in this thesis, entitled: **Thermal and Concentration Analyses of Cilia Induced Flow** was conducted by **Ms. Sidra Shaheen,** Reg. No. **88-FBAS/PHDMA/S17** under the supervision of **Dr. Khadija Maqbool** no part of this thesis has been submitted anywhere else for any other degree. This thesis is submitted to the **Department of Mathematics & Statistics, FBAS, IIU, Islamabad** in partial fulfillment of the requirements for the degree of **Doctor of Philosophy in Mathematics, Department of Mathematics & Statistics, Faculty of Basic & Applied Science, International Islamic University, Sector H-10, Islamabad, Pakistan.**

Student Name: Sidra Shaheen **Signature:** Sidra Shaheen

Examination Committee:

a) **External Examiner 1:**
Name/Designation/Office Address **Signature:** _____

Dr. Muhammad Afzal Rana
Professor
Department of Mathematics,
Riphah International University, Islamabad, Pakistan.

b) **External Examiner 2:**
Name/Designation/Office Address) **Signature:** _____

Dr. Sohail Nadeem
Professor
Department of Mathematics,
Quaid-e-Azam University, Islamabad, Pakistan.

c) **Internal Examiner:**
Name/Designation/Office Address) **Signature:** _____

Dr. Ambreen Afsar Khan
Assistant Professor

Supervisor Name:
Dr. Khadija Maqbool **Signature:** _____

Name of HOD:
Dr. Ambreen Afsar Khan **Signature:** _____

Name of Dean:
Prof. Dr. Muhammad Irfan Khan **Signature:** _____

Dedication

I dedicate

this thesis to my parents

(Mr. and Mrs. Allah Ditta)

Acknowledgements

Words are insufficient to describe my gratefulness and appreciation to the ALLAH Almighty, the creator of the universe, who gave me strength, ability, courage and patience to successfully complete my thesis. I pay tributes to the Holy Prophet Muhammad (PBUH), whose personality showed the right path to mankind and His teachings make us ponder to explore the world.

I would like to extend my gratitude to my respected supervisor **Dr. Khadija Maqbool**, for her patient guide, enthusiastic encouragement and useful critiques of this research work. This thesis would not be possible without her worthy comments, suggestions, advice and assistance for keeping my progress on schedule. I pay my respects to all my teachers who enabled me for making my dream true.

I owe my deepest gratitude to my parents **Mr. and Mrs. Allah Ditta** for their support financially and morally aided me to focus on my studies. They always kept me motivated on my core task. Their encouragement, guidance and sustenance since my childhood enabled me to unfold my hidden abilities. Special Thanks to my Brothers **M Abdullah, M Asadullah** and my sister **Iqra Shaheen** for their moral support and prayers.

I am also thankful to my Ph.D. class fellows especially **Hira Mehboob** who always helped me with all aspects of academia.

In the end, I am grateful to Allah Almighty for bestowing me with such a wonderful husband, **Muhammad Bilal Arain,** whose love, care, encouragement and support have been a pillar of strength for me during this time consuming process.

Sidra Shaheen

Preface

Ciliary transport is a complex feature exists on some of biological surfaces in the presence of thermal and concentration fields. Cilia are small but complex additional structures that protrude from the walls of the vessels. Cilia with an average length of around 0.1 mm can easily found and thus contribute to many advanced biological transport systems. Cilia exists in groups or clusters unlike the flagella, which generally occurs as pairs or single structures. They manifest whip-like movements that appear in plants, cells, sea creatures and physiological organs. They play a huge part across the spectrum and biological properties. The mathematical modeling of moving cilia has significance to estimate the various variables that are effected in this mechanism. Although experiments together with mathematical model of ciliary transport estimates the role of frequency, length, velocity and number of cilia in fluid dynamics and provide the awareness of ciliary importance in occurrence of diseases (related to cilia). Motivated by these facts, the cynosure of current thesis is based on the study of different fluid models with cilia induced flow in thermal and concentration field with different effects like magnetic field effect, thermophorectic and Brownian motion effects, viscous dissipation effect and inertial effects in different geometries and mathematical tools. Under such assumptions, the governing equations of above mentioned biological flows are modelled using continuity, momentum, energy and concentration equation. The resulting partial differential equations are developed with or without long wavelength approximation. The resulting linear and nonlinear system of equation has been evaluated by the perturbation method, Adomian decomposition method and Homotopy perturbation method. The effects of emerging parameters are shown through graphs plotted by the software Mathematica. The impacts of physical parameters such

as Hartmann number, porosity parameter, Weissenberg number, cilia length, power law index, fluid parameters and Brinkman number are illustrated by the graphs. It is found that ciliary flow enhances heat and mass transfer. This thesis comprises nine chapters which are described in following manners.

The introduction of fluid mechanics, basic information about cilia, non-dimensional numbers, fundamental laws, governing equations and explanation of methodology pertinent to the problems presented in thesis are included in chapter one.

Chapter two develops the mathematical model of MHD convective flow and mixing induced by cilia present in the bronchial airways under the effect of microscopic temperature and concentration gradient for symplectic and antiplectic wave pattern. To solve the partial differential equations Homotopy perturbation method is used. The behavior of physical variables are estimated by graphical results. This study is submitted in **Kuwait Journal of Science and technology**.

Chapter three extends the work presented in chapter two where effect of nanoparticles on Jeffrey fluid due to ciliary movement has been obtained. The finding are discussed and displayed by the graphs. This investigation is published in **Rheologica Acta, (2020), https://doi.org/10.1007/s00397-020-01222-8.**

The rheological behavior of the fluid simulated with the non-Newtonian fluid under the action of nanoparticles has been considered in chapter four. The mathematical modelling has been made by the envelop model approach for the stokes flow of tangent hyperbolic fluid with entropy generation. The governing equations are simplified and solved analytically by Homotopy perturbation method and software "MATHEMATICA". The graphical results show the effects of viscoelastic parameter, nanoparticles, cilia length and Brinkman number on the velocity, temperature and

entropy generation. This work is published in the **Journal of Thermal Analysis and Calorimetry, (2021).**

Chapter five illustrates the mathematical modeling of Tangent hyperbolic fluid (blood) under the effect of magnetic field and copper nanoparticles passing through cylindrical tube. Metachronal wavy motion is produced. Momentum and energy equations are modeled for Tangent hyperbolic nano-fluid by using small Reynolds' number and long wavelength approximation and solved by Adomian decomposition method with the help of software "MATHEMATICA". The effects of emerging parameters have been discussed through graphs. This analysis is published in **Mathematical Biosciences and Engineering, 16(4): 2927–2941, (2019).**

In chapter six, thermal analysis of cilia-induced flow of mucus clearance through an idealized two-dimensional model of the human airway is presented. The effect of viscous dissipation is also considered. Perturbation technique is employed to solve the resulting non-linear equations. Impact of various parameters along with the characteristics of ciliary motion are presented through graphs and discussed in detail. This effort is published in **SN applied Sciences, (2021).**

Chapter seven involves the thermal and concentration analysis on the flow of power law fluid model through a ciliated tube. To simplify the problem long wavelength and small Reynolds number approximation is used and exact solution for velocity is obtained. Homotopy Perturbation technique is employed to solve the non-linear coupled equations of temperature and concentration profiles. The impact of physical parameters along the characteristics of ciliary motion are presented through graphs and discussed in detail. This work is submitted in **Communication in Theoretical Physics (2021).**

Chapter eight involves thermal and diffusion effects in peripheral layer due to ciliary movement. The fluid flow is modeled using the linear Phan-Thien-Tanner (PTT) fluid model. After incorporating long wavelength and low Reynolds number approximations, the resulting equations are solved and exact solution for velocity of fluid, temperature and concentration fields are achieved. The effect of important parameters along the properties of ciliary motion are illustrated by the graphs and discussed in graphical results section. The results emerged in this chapter (chap. eight) are accepted for publication in **Journal of Central South University**

Contents

Nomenclature

$\boldsymbol{V}$	Velocity field vector
u, v	Velocities in wave frame
x, y	Rectangular coordinates in wave frame
X, Y	Rectangular coordinates in fixed frame
R, Z	Cylindrical coordinates in fixed frame
r, z	Cylindrical coordinates in wave frame
P, p	Pressure in fixed and wave frame
$\boldsymbol{I}$	Identity tensor
$\boldsymbol{S}$	Cauchy stress tensor
$\boldsymbol{B}$	Magnetic field
$\boldsymbol{J}$	Current density
$\boldsymbol{R}$	Darcy's resistance
$\boldsymbol{g}$	Gravitational acceleration
T	Fluid temperature
C	Fluid Concentration
D	Diffusion constant
c_p	Specific heat
j	Embedding parameter
h	Half length of channel
t	Time
m	Power law index

k_{nf}	Thermal conductivity of nanofluid
k_1	Non-dimensional porosity parameter
k_f	Thermal conductivity of fluid
k_s	Thermal conductivity of solid nano particles
D_a	Dimensionless parameter for Darcy's Resistance
M	Hartmann number
c	Wave speed
a	Wave amplitude
Q	Volume flow rate
Re	Reynolds number
S_H	Schmidt number
Pr	Prandtl number
S_T	Soret number
Br	Brinkman number
Gr_T	Thermal Grashof number
Gr_C	Concentration Grashof number
k	Thermal conductivity
Nt	Thermophoretic parameter
Nb	Brownian motion parameter
We	Weissenberg number
$\boldsymbol{L}$	Symmetric part of the velocity gradient
Ns	Entropy generation
Be	Bejan number

Greek Letters

ρ_f	Fluid density
ρ_{nf}	Nano fluid density
ρ_s	Density of solid nano particles
λ	Wavelength
λ_1, λ_2	Viscoelastic parameters
β	Non-dimensional wave number
β_1	Coefficient of thermal expansion
β_1^*	Coefficient of concentration expansion
ϵ	Cilia length
α	Eccentricity of elliptical path
ψ	Stream function
$\dot{\gamma}$	Shear rate
σ	Electrical conductivity of the fluid
η	Viscosity of fluid
η_∞	Infinite shear rate viscosity
φ	Solid volume fraction of nano particles
η_0	Zero shear rate viscosity
θ	Dimensionless temperature
ϕ	Dimensionless concentration
Γ	Time constant
$\boldsymbol{\tau}$	Extra stress tensor

Chapter 1

Introduction

1.1 Bio Fluid Mechanics

Biofluid mechanics is a branch of fluid mechanics which includes fluid flow inside and outside of the living organisms. The modern challenges associated with the mathematical modeling of biological fluid flows have mainly observed in human circulatory system and respiratory system. Biofluid mechanics is rapidly increasing in diagnosis and decision-making for treatment of clinical diseases. The relationship between mucus flow phenomena in respiratory tract and blood flow in circulatory system with pathophysiological observations has increased by measurement techniques and capabilities of computational models. When tbese physiological models combine in medical study, a powerful set of tools becomes available for the diagnosis, assessment and prediction of treatment outcomes.

1.1.1 Types of Fluids

Fluid mechanics is further divided into Newtonian fluids (stress and deformation rate vary linearly) and the non-Newtonian fluids (stress and strain rate vary nonlinearly). Newtonian fluid models include viscous fluid model while the most familiar non-Newtonian fluid models include Jeffrey, Maxwell, Tangent hyperbolic, Power law and Phan-Thien-Tanner (PTT) fluid models.

1.2 Muco Ciliary Clearance

During respiration, respiratory system helps to pass the huge quantity of air into lungs. This environmental air is mostly polluted with small particles, bacteria and viruses and

they contaminated the airways. A superficial epithelium is present in respiratory system which consist of two types of cells the first one is goblet cells (source of mucus production 20%) and second is ciliary cells (80%). The ciliated epithelium consists of muco ciliary escalator which plays the basic role to protect the whole respiratory system. The main purpose of mucus is to trap the foreign particles and force generated by motion of cilia moves this mucus layer into digestive tract for removal. In nasal cavity and lower airways the debris laden mucus can be cleared with coughing and sneezing. Muco ciliary clearance (MCC) is dynamically regulated by both the inhaled environmental stimuli as well as host factors such as neurotransmitters and cytokines. A detailed knowledge of muco-ciliary clearance (MCC) is important for the correct diagnosis and treatment of respiratory tract diseases (including asthma, diffuse bronchitis, cilia infections etc) and essential for sustaining the correct beating frequency and coordination of cilia motion.

1.2.1 Mucus

Many parts of human bodies like vagina, digestive tract, lungs, eyes, and other moist surfaces are protected and lubricated by a complex biological liquid called mucus. Mucus consists of 95% water and 5% mucins. For the rapid passage of some gases, specific proteins, ions and many nutrients, mucus plays a role of guard to protect respiratory system from dust particles, viruses and bacteria's, Its efficiency and regularity based on its biochemical properties with different length scale. By considering mucus at macro level, its properties are different from solids and liquids. At nanoscale level mucus behaves as fluid with very low viscosity.

1.2.2 Ciliary Structure

A single epithelial cell consists of nearly 50–200 cilia. The length of single cilium is 0.5–0.7 μm and has a radius of about 0.1–0.15 μm and are present at upper surface of ciliated cells. Every cilium consists of a group of interconnected microtubules. Microtubules (axoneme) consists of filaments called ploto filaments which are derived from α- and β-tubulin dimers. The major component i.e. β-tubulin (type IV isotope) is present abundantly in respiratory cilia. The cross-section area of cilia shows the arrangement of these microtubules. In moving cilia, it consists of 9 doublet pair of microtubules organized in a circular manner around two central microtubules called 9+2 arrangement. Each cilium has a two strokes i.e. forward which is called effective stroke and backward which is called recovery stroke. During the effective stroke the cilia is fully extended, and tips of cilia makes a contact with mucus layer which provides the forward direction to the flow of mucus blanket then cilia bends 90° and goes back to the initial point within the thin (PCL) fluid layer.

1.2.3 Metachronal Wave

A cilium, collectively called cilia, exhibit two phase stroke, power stroke (effective stroke) and recovery stroke. Power stroke in which a cilium swings in full extension weakly, while in a recovery stroke it reaches to the base and slowly return to the original position. The high friction effective stroke is followed by low friction recovery stroke. Cilium undergoes a cyclic motion with these two strokes, which generates force to induced relative motion between the cell and its surrounding fluid. Since cilia are close together on a single organism and move in coordination. This coordination produce a collective behavior of cilia beating which forms a wave, called metachronal wave. This wave can have different types, depending on the direction of propagation with effective

stroke. If both (wave and power stroke) are in same direction, it is **symplectic** metachronal wave, or in opposite direction, called **antiplectic** metachronal wave, or perpendicular to each other, known as **diplectic** metachronal wave.

1.3 Nano Fluids

Nanofluids are stable and dilute suspension of solid particles typically of size less than 100nm in a liquid. This stable suspension of nanoparticles in the base fluids offer enhanced thermal conductivity as well as heat transfer performance in comparison with the base fluid. The term nano fluid was first coined by Choi. Different studies has been discussed the evaluation of thermo physical properties of nanofluids. Oxide ceramics, nitric ceramics, carbon nanotube, metals, semiconductors were used as nanoparticles in the preparation of nanofluids. While water, ethlyene glycol and oil can be used as base fluid. Choi investigated that addition of very small volume fraction of nanoparticles in the base fluid can double the thermal conductivity of the nanofluid. Later many other researchers showed that the thermal conductivity of the nanofluid can be enhanced up to 20% by adding small volume fraction of nanoparticles to the base fluid. There are lot of nanoparticles in blood that are commonly one thousand times smaller than a human hair and presence of theses nanoparticles produce many severe diseases such as neutropenia, blood cancer, eosinophillia, leukocytosis etc. In many cases common methods cannot be used to eliminate these particles.

1.4 Heat Transfer

Heat transfer is known as thermal energy, it is a form of energy which flow from one region to another or between the systems and surroundings as a result of temperature differences. Heat is transferred primarily through three modes conduction, convection are radiation.

1.4.1 Effect of Heat Transfer on Ciliary Flow

The most important factor influencing ciliary activity is the temperature. Change in temperature modify the different degrees of moisture and humidity which are necessary to maintain normal physiological conditions in ciliated cells. In general, the effect of temperature on ciliary movement is much like its effect on most biological processes with increase in temperature. Experiments showed that there was a rapid rise in the temperature from the standard 20°C, it always resulted in acceleration of the movement. This acceleration was markedly increased with a gradual increase in temperature until 40°C was reached. An acute rise to 50°C paralyzed the movement of cilia. Temperatures between 20° and 30°C did not affect the movement of cilia, but cilia were very sensitive to temperatures above 35°C. By decreasing the temperature from 20° to 15°C and 10°C, the ciliary movement became decidedly slower, until at 5°C it ceased. It was found that the most suitable temperature for ciliary movement was between 37° and 38°C.

1.4.2 Entropy Generation

Entropy generation is the process which is associated with thermodynamic irreversibility of flow and second law of thermodynamics. Therefore, energy is reduced due to decreasing entropy which is used by system to do work. To increase the efficiency of engineering systems (Heat engines) the study of entropy generation is important. Which can be done by decreasing the entropy generation effects in the system. Bejan was the first researcher who proved that there are many factors which can increase entropy generation like frictional forces, magnetic field and viscous dissipation.

1.5 Concentration Gradient

Diffusion takes place due to concentration difference of a specie. Diffusion has many applications in industrial and in biological process, e.g. evaporation of fluids, removal of contamination from liver, kidneys and respiratory tract and purification of alcohol.

1.5.1 Effect of Concentration Gradient on Ciliary Flow

Cilia play an important role in respiratory tract where three mass transfer exit. If the cilia beat frequency is low then it decreases the mass transfer, if cilia beat frequency is moderate then cilia do not take active part in mass transport and third regime is active regime where cilia have very high beat frequency and increases mass transfer actively. Cilia beat frequency may vary with the age and health conditions so knowing the cilia beat frequency one can predict the mass transfer rate in respiratory tract.

Another example of mass transfer with the help of cilia are coral reefs. Corals can enhance mass transport with the help of cilia present on the surface of their bodies.

1.5.2 Thermophoretic Effects

Thermophoresis is the force that occurs due to the presence of a temperature gradient, and it does not depend on size of particles. As a result of interactions between fluid and nano particles, nanoparticles in a temperature gradient experience a force directed from high temperature to low temperature. Insulating materials are greatly affected by thermophoresis as compared to highly conducting (e.g., metallic) particles. For high density particles temperature difference starts establishing in the particle which introduce complexities.

1.5.3 Nanoparticle Effects in Diffusion

Nanoparticles are important in the fields of biology and medicine. They can bind many drugs, proteins and target cancer cells. Interaction of respiratory mucus with

nanoparticles helps in targeted drug delivery and cancer treatment which has great applications in biomedical science. These nanoparticles should penetrate in the mucus to reduce rapid clearance and achieve the pharmacokinetic profile required for better outcomes. Recent studies show that mucus-diffusing nanoparticle can enhance the distribution, retention, and efficiency of vaginally administered drugs. Similarly, nanoparticles that can penetrate easily in airway mucus may achieve reduced clearance and improved airway distribution, retention, and pharmacokinetic profile.

1.6 Two Layer Flows

Two layered flows have major applications in engineering and biomedical sciences. Recent studies shows that in many of engineering problems if flow is considered in two layers with different viscosities, less power is required to run the systems. In respiratory tract, ciliated epithelium is covered by airway surface liquid (ASL) which mainly consist of two different layers. The first one is mucus layer which is a non-homogenous, non-Newtonian, viscoelastic fluid and second layer is periciliary liquid layer (PCL) which is considered as a watery lubricating (nearly Newtonian) fluid layer with much small viscosity. To keep the respiratory tract clear from inhaled pollutants like viruses and bacteria's, transport of ASL which is facilitated by periodic ciliary actions has great importance. We have considered fluids in both layers with different viscosities and densities.

1.7 Laws of Fluid Mechanics

The fundamental laws of fluid mechanics which describe the fluid behavior are mass, momentum and energy conversations and are applicable in all physical problems.

1.7.1 Continuity Equation

Law of conservation of mass is mathematically represented by the continuity equation. This law states that neither mass can be generated nor demolished or the mass is conserved. For compressible fluid, the continuity equation is defined as follow

$$\frac{d\rho}{dt} + \rho(\nabla . V) + (V . \nabla)\rho = 0, \tag{1.1}$$

1.7.2 Momentum Equation

Momentum equation can be derived from law of conservation of momentum and can be represented by the following equation

$$\rho\left(\frac{\partial V}{\partial t} + (V . \nabla)\mathbf{V}\right) = -\nabla P + \nabla . \tau + \rho \boldsymbol{b}_f, \tag{1.2}$$

1.7.3 Energy Equation

The convective heat transfer problem requires a solution for the temperature distribution through the flow. The equation for achieving this ultimate form is the energy equation. Mathematically we can write

$$\rho c_p \left(\frac{dT}{dt}\right) = k\nabla^2 T + \tau . \boldsymbol{L} + \rho\bar{\gamma}, \tag{1.3}$$

where T denotes the temperature, τ represents the extra stress tensor, k is the thermal conductivity, c_p represents the specific heat and $\bar{\gamma}$ is the radial heating.

1.7.4 Concentration Equation

The mass transfer problem requires a solution for the concentration difference through the flow. Mathematically it can be given as follows

$$\left(\frac{dC}{dt}\right) = D\nabla^2 C. \tag{1.4}$$

Where C is concentration and D is the Diffusion constant.

1.8 Dimensionless Numbers

1.8.1 Hartmann Number

It is interpreted as the ratio of electromagnetic forces to the viscous forces. It appears in the magnetohydrodymics flow problems. Mathematically, it is defined as follows

$$M = B_0 a \sqrt{\frac{\sigma}{\mu}}, \tag{1.5}$$

where B_0, a , σ, μ are magnetic field intensity, mean width of channel/tube, fluid conductivity and fluid viscosity, respectively.

1.8.2 Darcy's number

It is the ratio of volume pores in the medium to the volume of bulk fluid in the medium. Mathematically, it is given as follows

$$D_a = \frac{a^2}{k}. \tag{1.6}$$

1.8.3 Reynolds Number

The Reynolds number is the ratio of inertial forces to the viscous forces. In fluid mechanics, the Reynolds number is a dimensionless number used to predict that flow is laminar or turbulent. Its mathematical form is as follow

$$Re = \frac{\rho u a}{\mu}. \tag{1.7}$$

1.8.4 Wave Number

The ratio of channel width to the wavelength of metachronal wave is called wave number. Usually it is represented by β and it can be written as

$$\beta = \frac{a}{\lambda}. \tag{1.8}$$

1.8.5 Weissenberg Number

The ratio of elastic forces to the viscous forces is actually the Weissenberg number. This dimensionless number is used to study the non-Newtonian viscoelastic fluid. It is usually denoted by We. Mathematically, it is defined as

$$We = \frac{mU_f}{a}. \tag{1.9}$$

1.8.6 Prandtl Number

It describes the ratio of momentum to thermal diffusivity and measure the heat transfer between moving fluid and solid surface. Mathematically, it is given by the following relation

$$P = \frac{\mu c_p}{k_1}. \tag{1.10}$$

1.8.7 Eckert Number

It is the ratio of advective mass transfer to the heat dissipation potential. It simply shows the relation between enthalpy and kinetic energy of the flow and is denoted by E_c. Mathematical representation is as follow

$$E_c = \frac{{U_f}^2}{c_p \Delta T}. \tag{1.11}$$

1.8.8 Brinkman Number

It is expressed as a ratio of viscous heat generation to the heat transfer rate and is essential for short distance velocity changes flow i.e. lubricant flow. It is denoted by Br in the product of Eckert and Prandtl number i.e. $Br = EcPr.$

1.8.9 Thermal Grashof Number

The ratio of buoyancy forces due to convective heat transfer to the viscous forces is called thermal Grashof number. This non-dimensional parameter is a measure of free or natural convection. Mathematically, the Grashof number is defined as

$$Gr = \frac{g\beta \Delta T l^3}{\nu^2}, \tag{1.12}$$

in which g denotes the gravitational acceleration, β denotes the volume expansion, l be the characteristics length, ΔT is the change in temperature and ν is for the viscous forces.

1.8.10 Concentration Grashof Number

The ratio of buoyancy forces due to concentration gradient to the viscous forces is known as concentration Grashof number. Mathematically, the Grashof number is defined as

$$Gr = \frac{g\beta \Delta C l^3}{\nu^2}, \tag{1.13}$$

in which g denotes the gravitational acceleration, β denotes the volume expansion, l be the characteristics length, ΔC is the change in concentration and ν is for the viscous forces.

1.9 Literature Review

The study of ciliary flow is very rich in history. The oldest known organelle cilia are discovered by Lee-Wenheok in 1674-1675 due to their motality. Wilson et al. [1] described the metachronism of moving cilia and they distinguish cilia from flagella by length, number and frequency of beating but they were considered "Different modification of a single type". Mathematical model for cilia was first introduced by Gray that microorganisms execute with small velocity in water [2], Taylor [3] studied the ciliary motion of microorganisms for finite and infinite length models. During 1960's Porter [4], Satir [5], Sleigh [6], and many other researchers studied the ciliary structure and they recognized that 9+2 pattern is universal for motile cilia and 9+0 pattern is universal for non-motile cilia.

During last three decades of nineteenth century, Blake [7 & 8] used the envelope model to study the movement of different microorganisms. Katz [9] and Lardner [10] presented the propulsion of fluid due to cilia in mammalian reproductive systems and then Blake [11] used this model to study both female and male reproductive system. Brennen [12 & 13] used the envelope model to study the locomotion of ciliated microorganisms. Sanderson [14], Agarwal [15], Fulford, [16] and Sleigh [17] described the detailed study of motile cilia in respiratory tract. They studied the mechanism of mucociliary transport but a proper mathematical model for ciliary motion is given by Gueron et al. [18]. Since cilia has very complex structure, small size and high speed, therefore some assumptions to solve problems related to ciliary flow has been used in this research. The most common of these assumptions are long wavelength and low

Reynolds' number approximation. In literature many researchers [19-23] used these approximations to investigate the fluid flow due to ciliary motion.

Ciliary transport plays an important role in many biological process which includes mucus flow in respiratory tract [24, 25, 26], the movement of ovum in the fallopian tube [27, 28, 29] and the movement of spermatozoa in the ductus efferent of the male reproductive tract [30, 31, 32]. The abnormalities in human airways cilia cause periciliary dyskinesia (PCD). These patients have sinusitis and chronic bronchitis such as chronic obstructive pulmonary disease (COPD), asthma, infection, lobar pneumonia, influenzal pneumonia. Lee et al. [33] studied both layers of respiratory tract i.e, PCL and mucus layer with Newtonian fluid Model and presented the diseases related to defects in cilia. Maqbool et al. [34-39] discussed the mathematical modeling of ciliary flow in upper and lower respiratory tract in normal as well as in diseased conditions and also they discussed the effect of heat transfer on ciliary activity with the effect of magnetic field and porous medium. Siddiqui et al. [40] analyzed the magnetohydrodynamics flow of viscous fluid induced by the ciliary propulsion in a porous medium which has an application to control diseases in respiratory tract. Recently, Shaheen et al. [41] discussed the mathematical modeling of magnetically actuated muco ciliary pumping in bronchial tube in diseased condition with Darcy's law and constant magnetic field. Due to its numerous importance, the study of motile cilia has key role in biofluid dynamics.

Heat transfer in biological flows and specifically in ciliary flows has wide-range of applications in medical sciences [42 & 43], bioengineering [44 & 45] and microfabrication technologies [46 & 47]. Some more applications include the thermal treatment of tumors [48], thermal control of respiratory system [49], heat transfer through blood [50] and heat transfer regulation in organs of the body, etc. Main

applications of temperature gradient in biological systems are thawing and freezing process for preserving the biological material, cryosurgery, infrared radiators, and microwave methods. Computational and mathematical thermal analysis is considered as a critical modern tool in biological flows.

Heat transfer has large impact on ciliary flow as described by Umbeda [51]. He studied the impact of heat transfer on PCL layer and showed that by increasing temperature frequency of cilia can be made normal required for muco ciliary clearance. Mills *et al.* [52] have used computational fluid dynamics to study the thermal transport in artificially ciliated microfluidic systems. Heat transfer analysis of Rabinowitsch fluid flow due to metachronal wave of cilia is investigated by Akber et al. [53]. Nadeem et al. [54] studied the effect of cilia on the heat transfer and concluded that cilia enhance the transport of heat in the fluid. Akbar et al. [55 & 56] observed the influence of Hartmann layer and the analysis of heat transfer on transportation of copper nanofluids due to the metachronal wave of beating cilia. Recently, Abrar et al. [57] discussed the entropy generation during cilia transport of water based titanium dioxide nanoparticles in the presence of viscous dissipation. They obtained closed form exact solution for velocity, temperature and entropy generation. A mathematical modeling for cilia induced nanofluid flow through the human male reproductive tract is discussed by Imran et al. [58]. They observed that by increasing thermophoretic effects frictional forces at boundary also enhances significantly. Manzoor *et al.* [59] studied the forced convective MHD flow of eclectically conducing Jeffrey biofluid in a ciliated channel, and Adomian decomposition method has been applied on the mixed convective electromagnetic fluid flow in the vertical ciliated channel with variable viscosity by Farooq et al. [60]. Farah et al. [61] studied the electro-osmotic flow of Jeffrey fluid with

effects of heat source/sink and obtained the solution by using Adomian decomposition method.

Mass diffusion is also important phenomenon in industry. Mass diffusion has many applications such as nutrients' diffusion from the blood to tissues [62], membrane separation process [63], reverse osmosis [64], combustion process [65], diffusion of chemical impurities [66] and drug delivery in respiratory tract [67]. Biologically-inspired pumping systems (artificial cilia) have great applications in engineering as they achieve high efficiency. Industrial applications of mass diffusion also contains feature of two-phase flows.

Khan et al. [68] provided effects of thermophoresis and Brownian motion on Eyring–Powell fluid flow due to ciliary motion which has great applications in human oviduct. They solved the resulting differential equation by Homotopy perturbation method and show the impact of various parameters on concentration difference graphically. Shaheen et al. [69] analyzed the thermal and concentration gradient effects on the peristaltic motion of non-Newtonian Jeffrey six constant fluid with ciliated boundary. Abdelsalam et al. [70] studied the theoretical analysis of thermal and concentration gradient on a fluid flowing due to ciliary motion with inclined magnetic field. Farooq et al. [71] studied the combined thermal and concentration gradient effects in human body during flow of different physiological fluids. This research has major applications in male reproductive tract. Recently many researchers [72-77] studied the effects of thermophoresis and Brownian motion on the biological fluids which has many applications in drug delivery systems in respiratory tract.

1.10 Research Methodology

In this thesis some analytical techniques are used to solve the linear and nonlinear problems appearing in the next chapters. Some of the these suitable techniques are described below

- Perturbation method
- Adomian decomposition method
- Homotopy perturbation method

1.10.1 Perturbation Method

The perturbation method is used to solve the nonlinear problems analytically. To approximate the perturbation solution [78], we assume β as a small or large variable and the unknown function u of the differential equation can be express as

$$u = u_0 + u_1\beta + u_2\beta^2 + u_3\beta^3 + \cdots , \tag{1.14}$$

and substitute in differential equation to alter the nonlinear equation into numbers of linear problems depending on the large or small parameter of the equation and then solution is approximated by the sum of sub linear equation's solution. This technique has its vital role in development of science and engineering. The problems in which small or large parameter is not present, perturbation method cannot be used.

1.10.2 Adomian Decomposition Method

An efficient method to solve linear and nonlinear, initial and boundary value problem is Adomian decomposition method (ADM) [79, 80]. ADM doesn't need any restrictive assumptions such as small or large parameter. Nonlinear differential equation can be written in the following form

$$u(x) = f(x) - \mathcal{L}^{-1}(Ru) - \mathcal{L}^{-1}(Nu), \tag{1.15}$$

in which unknown function u decompose into a sum of an infinite number of components and calculated in a recursive manner, $f(x)$ is inhomogeneous term, $\mathcal{L}^{-1}$ is the inverse operator of linear highest order derivative, Ru is the linear part of the equation and can be decompose in the infinite sum of component of u_m where $m = 0, 1, 2, 3 \ldots$, and Nu represent the nonlinear part of the equation and can be decompose into an infinite series of Adomian polynomials A_m where $m = 0, 1, 2, 3 \ldots$, which are based on trigonometric and algebraic identities and on Taylor series. Finally, the partial sum of the equation is the solution of required equation.

1.10.3 Homotopy Perturbation Method

The Homotopy perturbation technique [81] is a powerful and efficient technique to find the approximate solution of linear and nonlinear equation. HPM combines the two different methods that are perturbation and Homotopy method. This method is applicable when the exact solution of an equation is not possible. It starts with the initial approximation which can be freely selected and satisfiy the boundary conditions of the problem. The Homotopy structure can be written as

$$\begin{aligned} \mathcal{H}(v, j) &= (1 - j)[\mathcal{L}(v) - \mathcal{L}(w_0)] + j[A(v) - f(r)] \\ &= 0, \end{aligned} \qquad (1.16)$$

in which $\mathcal{L}$ is the linear part, A can be decompose into a linear and nonlinear part, u_0 is the initial guess which satisfy the considered equation and $j \in [0,1]$ is an embedding parameter.

Homptopy perturbation method leads to a solution in terms of power series. In this way, a strict nonlinear equation reduce into solvable linear and nonlinear equation.

Chapter 2

Effect of Viscous Dissipation and Thermophoretic Diffusion on Muco Ciliary Clearance

In this chapter we have modeled the MHD convective flow of viscous fluid induced by cilia, which is resembled with the mucus flow through bronchial airways under the effect of microscopic temperature gradient and magnetic field. The ciliary flow is modeled by the symplectic and antiplectic pattern that forms the metachronal wave. The governing equations are modeled in fixed and wave frame with long wavelength and low Reynolds' number approximation. The results show that symplectic metachronal waves are the most efficient regarding the fluid flow. The flow is studied with the help of temperature gradient, diffusion law, viscous dissipation and thermophoretic effects and the expressions for velocity, temperature and concentration profile are solved by the help of analytical technique HPM and software "MATHEMATICA". The graphical results of stream function show that presence of magnetic field and porous medium help to increase the pumping phenomena, whereas thermal and concentration Grashof number assist to slow the pumping of mucus through bronchial airways.

2.1 Mathematical Model

Consider a viscous flow in a tube of finite length L. Assume infinite number of continuously beating cilia are present at the inner walls of tube generating symplectic metachronal wave which moves towards positive z-axis with wave speed c. As cilia are present at the internal walls of the tube and due to continuously beating of cilia, fluid flow is established. We will use envelope model approach to discuss the transport of mucus by ciliary movement which is already used in literature [82] for the flow induced by cilia.

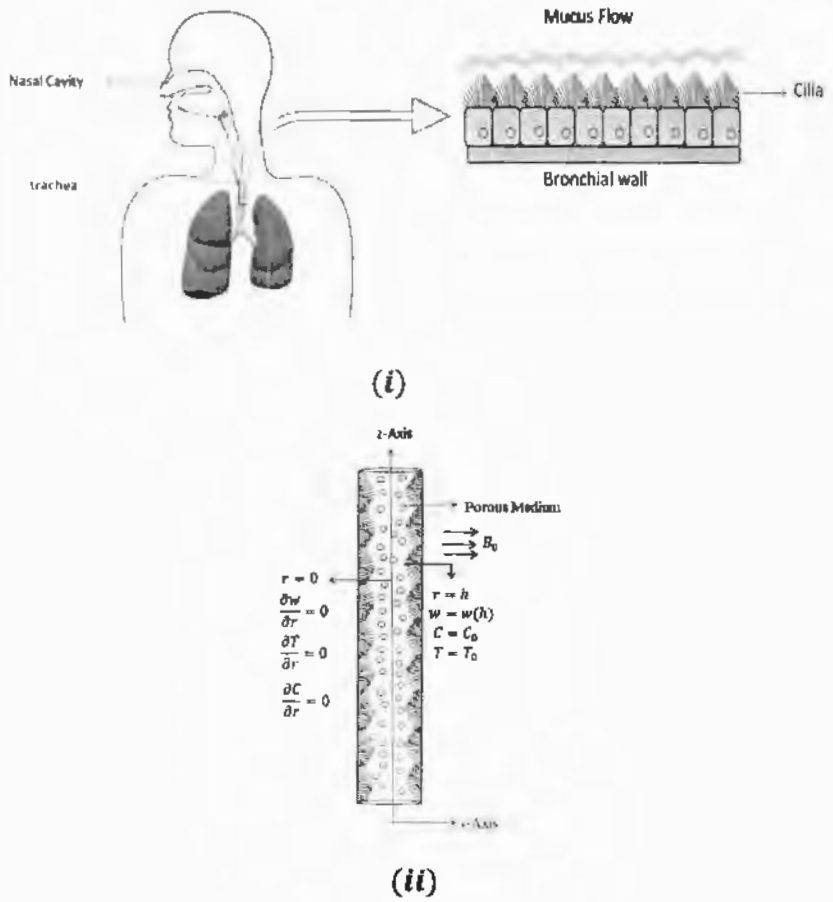

Fig. 2.1: Geometry of the problem.

The position of the ciliary flow near the tip of cilia is governed by the following equation given in Ref. [83]

$$R = H = F(Z,t) = a + a\epsilon\cos\left(\frac{2\pi}{\lambda}(Z - ct)\right), \tag{2.1}$$

$$Z = G(Z, Z_0, t) = Z_0 + a\epsilon\alpha\sin\left(\frac{2\pi}{\lambda}(Z - ct)\right). \tag{2.2}$$

R and Z components of velocity are given as follow

$$U = \dot{R}|_{Z=Z_0} = \dot{F} + F'\dot{Z} = \dot{F} + F'W, \tag{2.3}$$

$$W = \dot{Z}|_{Z=Z_0} = \dot{G} + G'\dot{Z} = \dot{G} + G'W. \tag{2.4}$$

The transformation from fixed to wave frame by using Galilean transformation are given in Ref. [30]

$$z = Z - ct, \qquad r = R, \qquad w = W - c, \qquad u = U, \tag{2.5}$$
$$p(t,r,z) = P(T,R,Z),$$

where U is the radial and W is the axial velocities.

The governing equations for the magnetodynamic diffusive convective flow of a viscous fluid with thermophoretic and viscous dissipation effect [84] are given as follows

$$\frac{1}{r}\frac{\partial}{\partial r}(ru) + \frac{\partial w}{\partial z} = 0, \tag{2.6}$$

$$\rho E(u) = \eta\nabla^2 u - \frac{\eta u}{k_1} - \frac{\partial p}{\partial r}, \tag{2.7}$$

$$\rho E(w) = \eta\nabla^2 w - \left(\sigma B_0^2 + \frac{\eta}{k_1}\right)(w + c) + \rho_f g\beta_1(T - T_0) + \rho_f g\beta_1^*(C - C_0) - \frac{\partial p}{\partial z}, \tag{2.8}$$

$$\rho c_p E(T) = k\nabla^2 T + 2\eta\left(\frac{\partial u}{\partial z}\right)^2 + 2\eta\left(\frac{\partial w}{\partial r}\right)^2 + \eta\left(\frac{\partial u}{\partial r} + \frac{\partial w}{\partial z}\right)^2 \tag{2.9}$$

$$E(C) = D\nabla^2 C + \frac{D_{kT}}{T_0}\nabla^2 T, \tag{2.10}$$

where $E = u\frac{\partial}{\partial r} + w\frac{\partial}{\partial z}$

Boundary conditions are suggested by [84] in the following manner

$$\frac{\partial C}{\partial r} = 0, \qquad \frac{\partial T}{\partial r} = 0, \qquad \frac{\partial w}{\partial r} = 0, \qquad at \ \ r = 0, \tag{2.11a}$$

$$T = T_0, \qquad w = w(h), \qquad C = C_0 \ \ at \ \ r = h. \tag{2.11b}$$

To non-dimensionalize the problem we use following parameters

$$z^* = \frac{z}{\lambda}, \qquad r^* = \frac{r}{a}, \qquad u^* = \frac{u}{\beta c}, \qquad w^* = \frac{w}{c}, \qquad h^* = \frac{h}{a}, \qquad p^* = \frac{a\beta}{c\mu}p,$$

$$\beta = \frac{a}{\lambda}, \qquad S_{ij}{}^* = \frac{a}{\mu c}S_{ij}, \qquad \lambda_1{}^* = \frac{c\lambda_1}{a}, \qquad Re = \frac{\rho ac}{\mu}, \qquad Pr = \frac{\mu c_p}{k},$$

$$\theta = \frac{T - T_0}{T_1 - T_0}, \phi = \frac{C - C_0}{C_1 - C_0}, Gr_T = \frac{g\beta_1 a^3(T_1 - T_0)}{\nu^2}, Gr_C = \frac{g\beta_1{}^* a^3(C_1 - C_0)}{\nu^2}, \tag{2.12}$$

$$S_H = \frac{\mu}{D\rho}, \quad S_T = \frac{\rho D k_T}{\mu(C_1 - C_0)}, \qquad M = \sqrt{\frac{\sigma}{\mu}}aB_0^2, \quad D_a = \frac{k}{a^2}.$$

After dropping $(*)$ Eqs. (2.6)-(2.11) in non-dimensional form are given by the following expressions

$$\frac{1}{r}\frac{\partial}{\partial r}(ru) + \frac{\partial w}{\partial z} = 0, \tag{2.13}$$

$$Re\beta\rho[E(w)] = F_1(w) + \beta^2\frac{\partial^2 w}{\partial z^2} \left(M^2 + \frac{1}{D_a}\right)(w + 1) + Gr_T\theta + Gr_C\phi - \frac{\partial p}{\partial z}, \tag{2.14}$$

$$Re\beta^2[E(u)] = \beta^2\left[F_1(u) + \beta^2\frac{\partial^2 u}{\partial z^2} - \frac{u}{r^2}\right] + \frac{\beta}{D_a}u - \frac{\partial p}{\partial r}, \tag{2.15}$$

$$\beta E(\theta) = F_1(\theta) + \frac{\partial^2\theta}{\partial z^2} + Br\left(\beta^2\left(\frac{\partial u}{\partial z}\right)^2 + \left(\frac{\partial u}{\partial r} + \frac{\partial w}{\partial z}\right)^2\right) + Br\left(\frac{\partial w}{\partial r}\right)^2, \tag{2.16}$$

$$\beta E(\phi) = F_1\left(\frac{\phi}{S_H} + S_T\theta\right). \tag{2.17}$$

Where $F_1 = \frac{\partial^2}{\partial r^2} + \frac{1}{r}\frac{\partial}{\partial r}$,

with boundary conditions

$$w = w(h) = -(1 + 2\pi\epsilon\alpha\beta\cos(2\pi z)), \tag{2.18a}$$

$$u = u(h) = 2\pi\epsilon(\sin(2\pi z)) + \beta 2\pi\epsilon\alpha\sin(2\pi z)\cos(2\pi z), \tag{2.18b}$$

at

$$r = h(z) = a + \epsilon\alpha a\cos(2\pi z),$$

and

$$\frac{\partial w}{\partial r} = \frac{\partial \theta}{\partial r} = \frac{\partial \phi}{\partial r} = 0 \qquad at \;\; r = 0. \tag{2.19}$$

By applying low Reynolds' number and long wavelength approximation one can get following equations

$$F_1(w) = \left(M^2 + \frac{1}{D_a}\right)(w + 1) - Gr_T\theta - Gr_C\phi - \frac{\partial p}{\partial z}, \tag{2.20}$$

$$\frac{\partial p}{\partial r} = 0, \tag{2.21}$$

$$F_1(\theta) + Br\left(\frac{\partial w}{\partial r}\right)^2 = 0, \tag{2.22}$$

$$F_1(\phi) + S_H S_T F_1(\theta) = 0, \tag{2.23}$$

where the boundary conditions are

$$w = w(h) = -1 - 2\pi\epsilon\alpha\beta\cos(2\pi z), \theta = 0, \phi = 0, at \;\; r = h, \tag{2.24}$$

$$\frac{\partial w}{\partial r} = \frac{\partial \theta}{\partial r} = \frac{\partial \phi}{\partial r} = 0 \qquad at \;\; r = 0. \tag{2.25}$$

The flow rate of mucus in human trachea ranges from 5-20 mm/min, therefore it is important to calculate flow rate of mucus from the airways to the ciliated epithelium. Volume flow rate can be calculated by integrating Eq. (2.13) and volume flow rate is defined as follows:

$$q = 2\int_0^h rwdr, \tag{2.26}$$

so that dimensional and non-dimensional volume flow rate are related as

$$Q = 2\int_0^l rwdr = 2\int_0^l r(w+1)dr = q + h^2. \tag{2.27}$$

The average volume flow rate can be written as follows

$$\bar{Q} = \frac{1}{T}\int_0^T Qdt^* = q + 1 + 0.5\epsilon^2. \tag{2.28}$$

2.2 Homotopy Perturbation Solution

To obtain the solution of governing equations, homotopy perturbation method is described as

$$\mathcal{H}(w,j) = (1-j)[\mathcal{L}(w) - \mathcal{L}(w_0)]$$
$$+j\left(\mathcal{L}(w) + \left(M^2 + \frac{1}{D_a}\right)w + \left(M^2 + \frac{1}{D_a}\right) - Gr_T\theta - Gr_C\phi - \frac{\partial p}{\partial z}\right), \tag{2.29}$$

$$\mathcal{H}(j,\theta) = (1-j)[\mathcal{L}(\theta) - \mathcal{L}(\theta_0)] + j\left(\mathcal{L}(\theta) + Br\left(\frac{\partial w}{\partial r}\right)^2\right), \tag{2.30}$$

$$\mathcal{H}(j,\phi) = (1-j)[\mathcal{L}(\phi) - \mathcal{L}(\phi_0)] + j\left(\mathcal{L}(\phi) + S_H S_T \frac{1}{r}\frac{\partial}{\partial r}\left(r\frac{\partial\theta}{\partial r}\right)\right). \tag{2.31}$$

The linear operator and initial guesses are chosen as follows

$$\mathcal{L} = \frac{1}{r}\frac{\partial}{\partial r}\left(r\frac{\partial}{\partial r}\right), \tag{2.32}$$

$$w_0 = \frac{1}{4}\frac{dp_0}{dz}(r^2 - h^2) + w(h), \tag{2.33}$$

$$\theta_0 = \frac{r^2 - h^2}{4}, \phi_0 = \frac{r^2 - h^2}{4}. \tag{2.34}$$

According to homotopy perturbation method

$$w = w_0 + jw_1 + j^2w_2 + \cdots, \tag{2.35a}$$

$$\theta = \theta_0 + j\theta_1 + j^2\theta_2 + \cdots, \tag{2.35b}$$

$$\phi = \phi_0 + j\phi_1 + j^2\phi_2 + \cdots. \tag{2.35c}$$

$$p = p_0 + jp_1 + j^2p_2 + \cdots. \tag{2.35d}$$

where is $j \in [0,1]$ is the homotopy perturbation parameter and $j = 0$ gives initial guess and $j = 1$ gives the final solution. With the help of Eqs. (2.35a) - (2.35d), second order solution for the velocity and temperature profile are given as follow

$$w = w(h) + \frac{1}{4}\left(A_1 + \frac{dp}{dz} + \left(M^2 + \frac{1}{D_a}\right)(w(h) + 1)\right)(r^2 - h^2) + \frac{1}{16}A_2(r^4 - h^4) + \frac{1}{36}A_3(r^6 - h^6) + \frac{1}{64}\left(-Gr_T\theta - Gr_C\phi + \left(M^2 + \frac{1}{D_a}\right)^2\frac{dp}{dz}\right)(-3h^4 - 4r^2h^2 + r^4). \tag{2.36}$$

$$\theta = \left(\frac{1}{16}A_4 - \frac{1}{32}Br\left(\frac{dp}{dz}\right)^2\right)(r^4 - h^4) + \frac{1}{35}A_5(r^6 - h^6), \tag{2.37}$$

$$\phi = \left(\frac{1}{4} + A_6 - S_HS_T\right)(r^2 - h^2) + \frac{1}{16}A_7(r^4 - h^4). \tag{2.38}$$

Integrating Eq. (2.36) pressure gradient in terms of volume flow rate can be written as

$$\frac{dp}{dz} = \frac{-A_9 + \sqrt{-4A_{10}A_8 + A_9^2 + 4A_8q}}{2A_8}. \tag{2.39}$$

The stream function can be calculated by the following relation

$$w = \frac{1}{r}\frac{\partial\psi}{\partial z}, \qquad u = -\frac{1}{r}\frac{\partial\psi}{\partial r}, \tag{2.40}$$

$$\psi = A_{11}r^8 + A_{12}r^6 + A_{13}r^4 + A_{14}r^2. \tag{2.41}$$

where A_1 to A_{14} are defined in Appendix.

2.3 Graphical Results

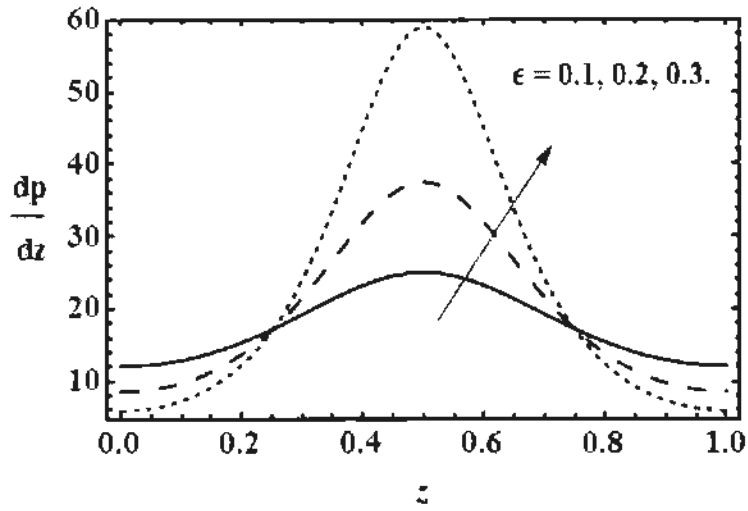

Fig. 2.2: Impact of cilia length parameter ϵ on pressure gradient $\frac{dp}{dz}$ for $M = 1$, $D_a = 0.1, Gr_T = 1, Gr_C = 1$.

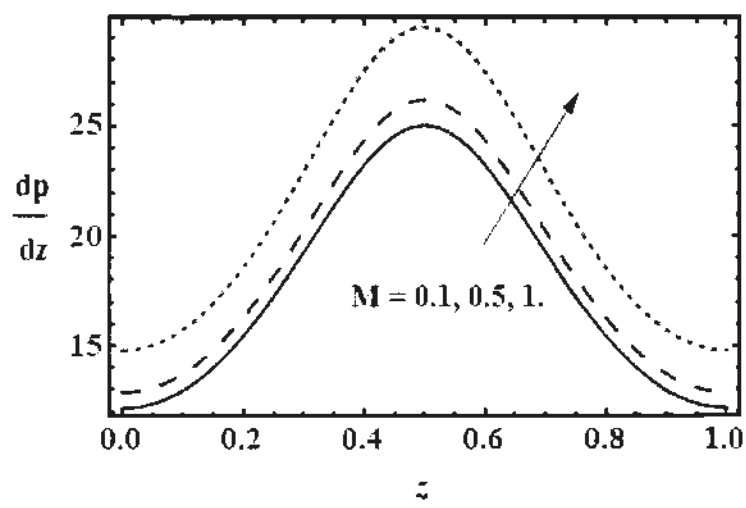

Fig. 2.3: Influence of Hartmann number M on pressure gradient $\frac{dp}{dz}$ for $\epsilon = 0.1$, $D_a = 0.1, Gr_T = 1, Gr_C = 1$.

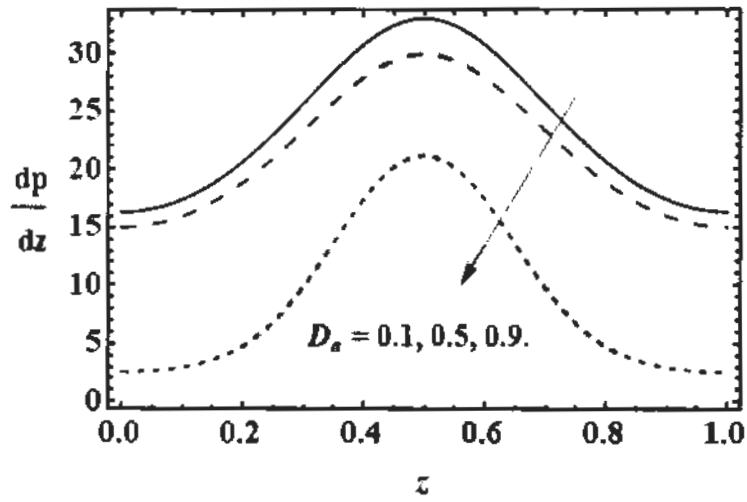

Fig. 2.4: Impact of Darcy's number D_a on pressure gradient $\frac{dp}{dz}$ for $\epsilon = 0.1$, $M = 0.1, Gr_T = 1, Gr_C = 1.$

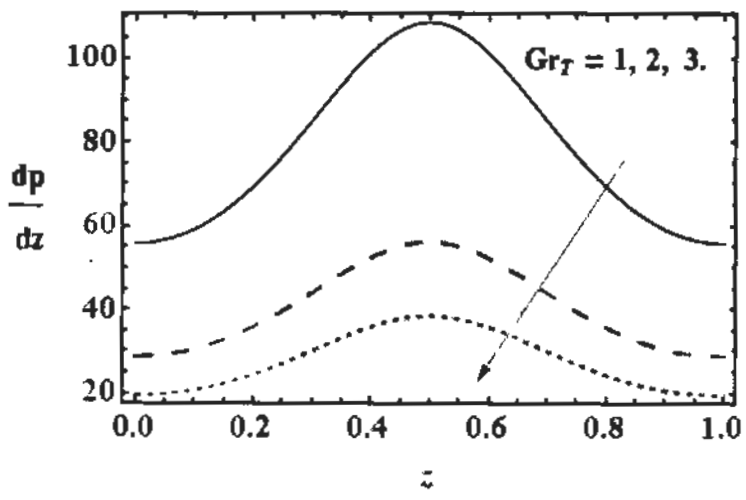

Fig. 2.5: Impact of thermal Grashof number Gr_T on pressure gradient $\frac{dp}{dz}$ for $\epsilon = 0.1, M = 0.1, D_a = 0.1, Gr_C = 1.$

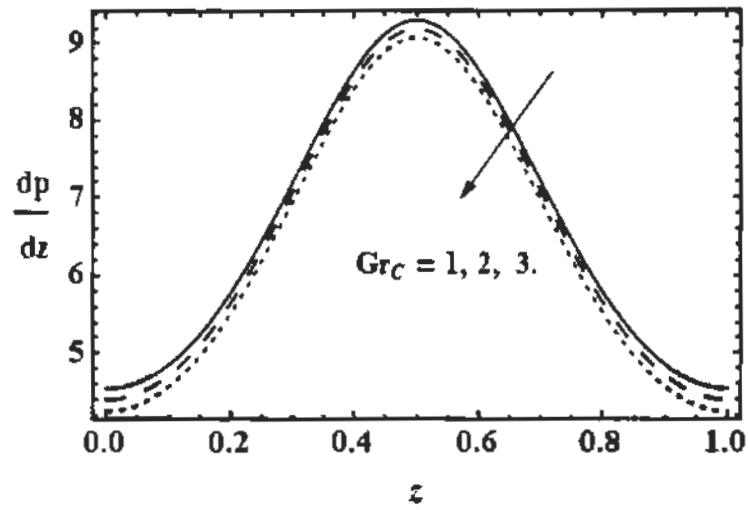

Fig. 2.6: Impact of concentration Grashof number $\mathrm{Gr_C}$ on pressure gradient $\frac{dp}{dz}$ for $\epsilon = 0.1, M = 0.1, D_a = 1, Gr_T = 1.$

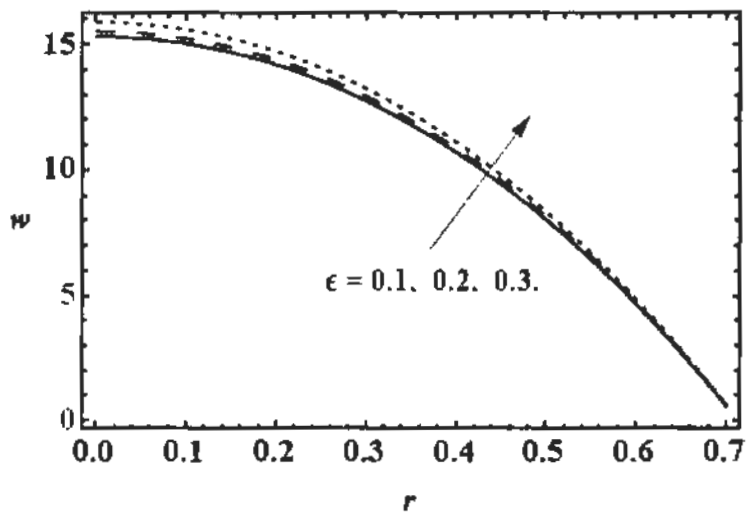

Fig. 2.7: Impact of cilia length parameter ϵ on axial velocity w for $M = 1$, $D_a = 0.1, Gr_T = 1, Gr_C = 1.$

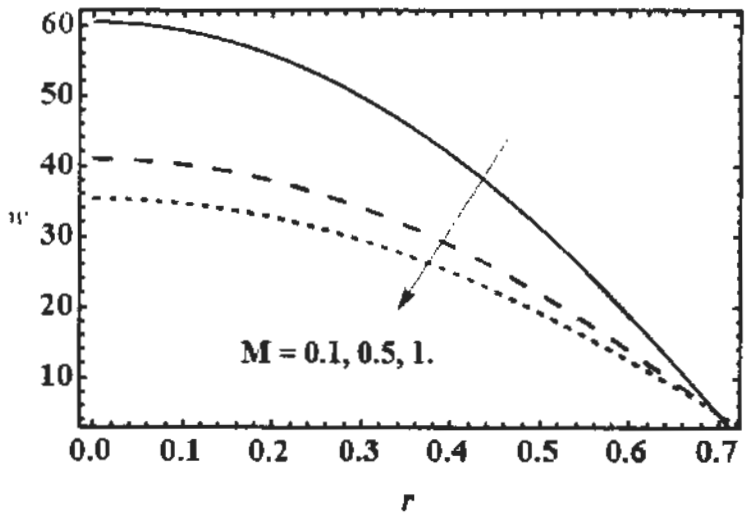

Fig. 2.8: Impact of Hartmann number M on axial velocity w for $\epsilon = 0.2$, $D_a = 0.1, Gr_T = 1, Gr_C = 1.$

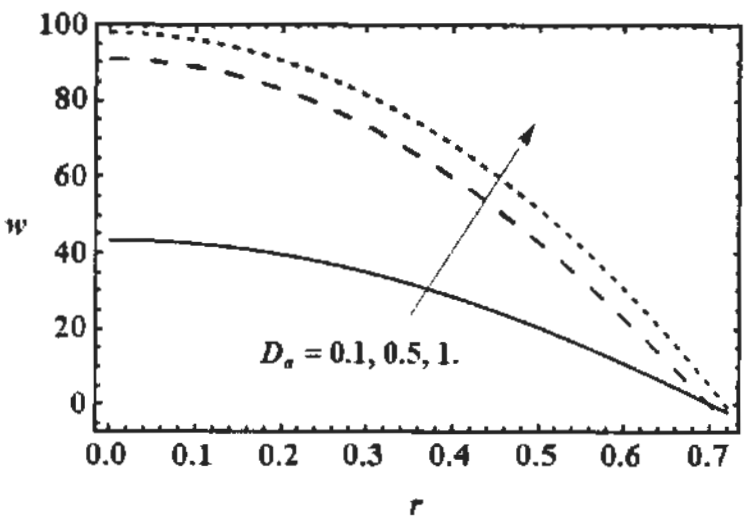

Fig. 2.9: Impact of Darcy's number D_a on axial velocity w for $\epsilon = 0.1$, $M = 0.1, Gr_T = 1, Gr_C = 1.$

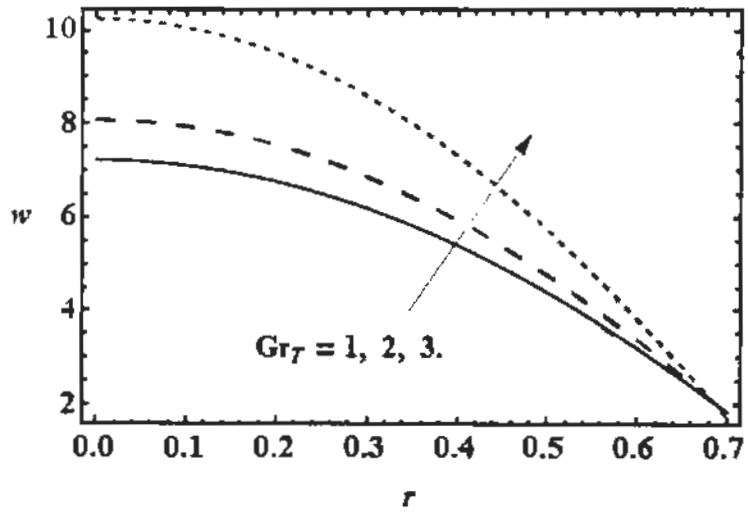

Fig. 2.10: Impact of thermal Grashof number Gr_T on axial velocity w for $\epsilon = 0.1$, $M = 0.1, D_a = 0.1, Gr_C = 1.$

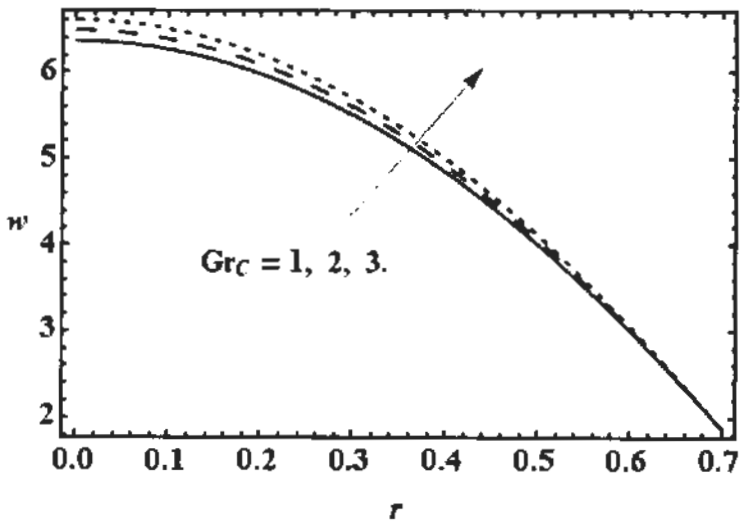

Fig. 2.11: Impact of concentration Grashof number Gr_C on axial velocity w for $\epsilon = 0.1, M = 0.1, D_a = 0.1, Gr_T = 1$

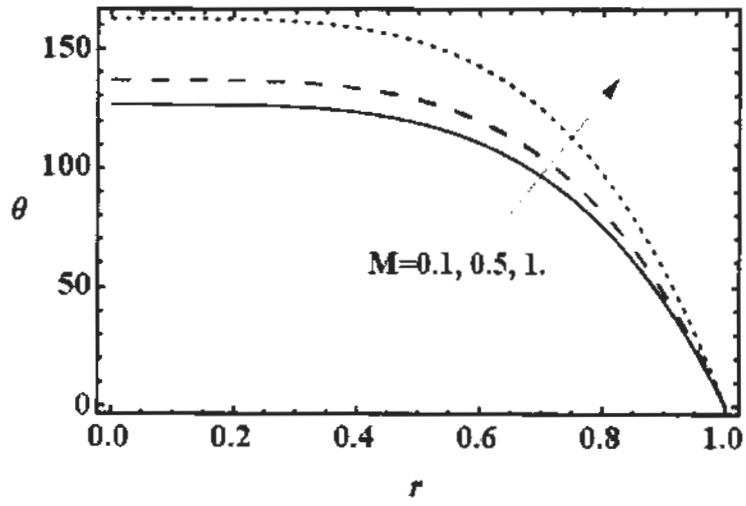

Fig. 2.12: Impact of cilia Hartmann number M on temperature field θ for $\epsilon = 0.1, D_a = 0.1, Gr_T = 1, Gr_C = 1.$

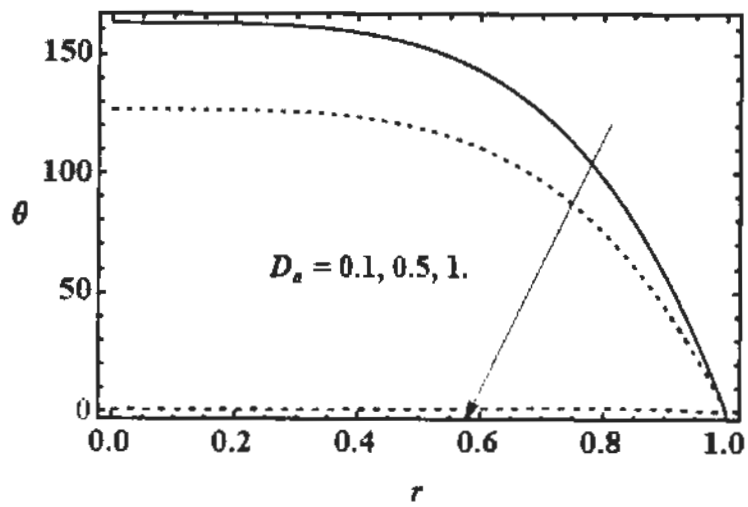

Fig. 2.13: Impact of Darcy's number D_a on temperature field θ for $\epsilon = 0.1, M = 0.1, Gr_T = 1, Gr_C = 1.$

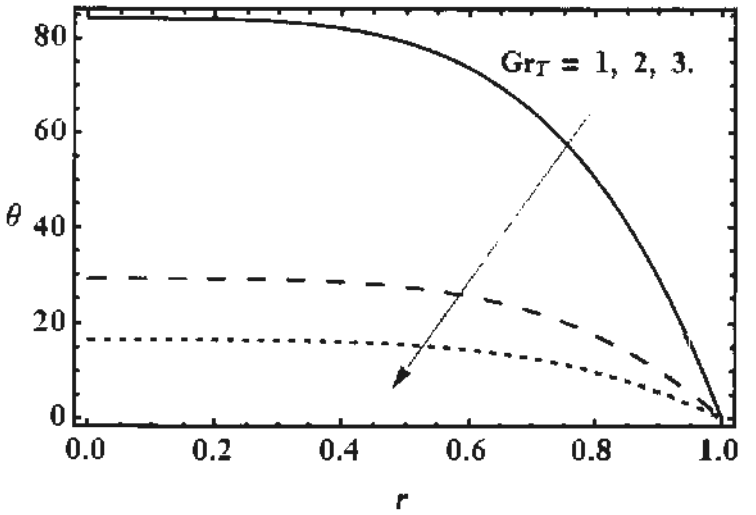

Fig. 2.14: Impact of thermal Grashof number Gr_T on temperature field θ for $\epsilon = 0.1, M = 0.1, D_a = 0.1, Gr_C = 1.$

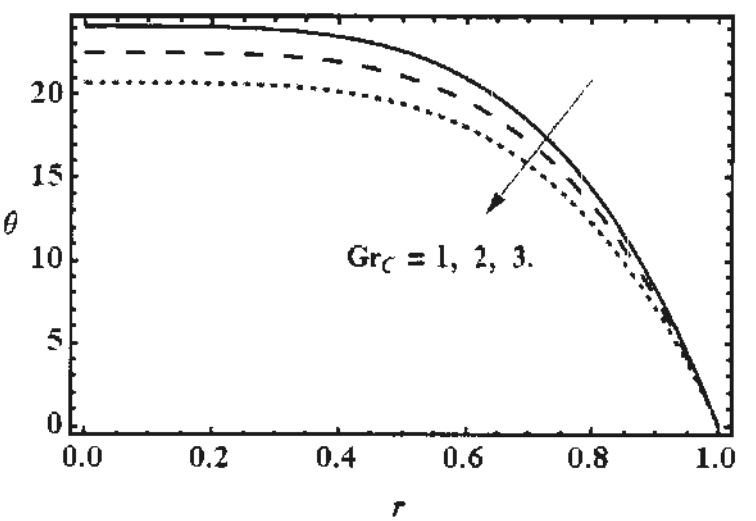

Fig. 2.15: Impact of concentration Grashof number Gr_C on temperature profile θ for $\epsilon = 0.1, M = 0.1, D_a = 1$ *and* $Gr_T = 1.$

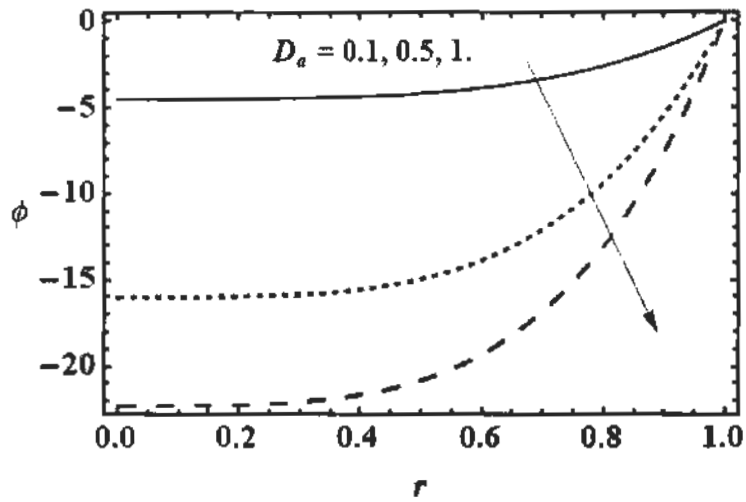

Fig. 2.16: Impact of Darcy's number D_a on concentration field ϕ for $M = 1, S_H = 1$ and $S_T = 1$.

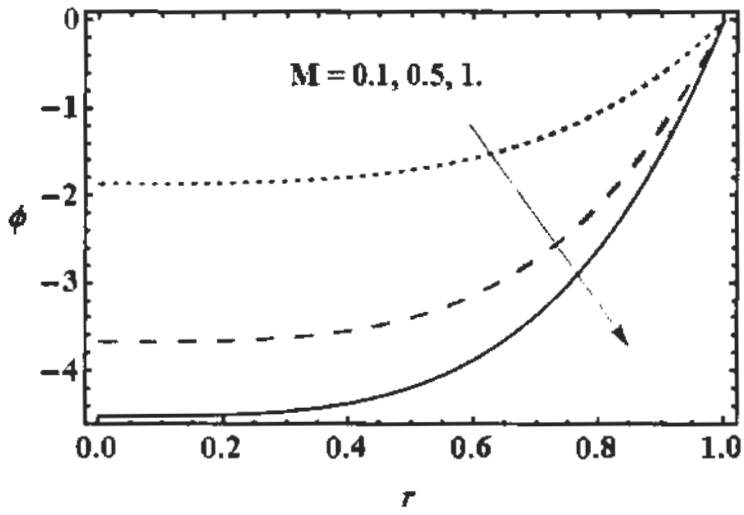

Fig. 2.17: Impact of Hartmann number M on concentration field ϕ for $S_H = 1, S_T = 1$ and $D_a = 0.1$.

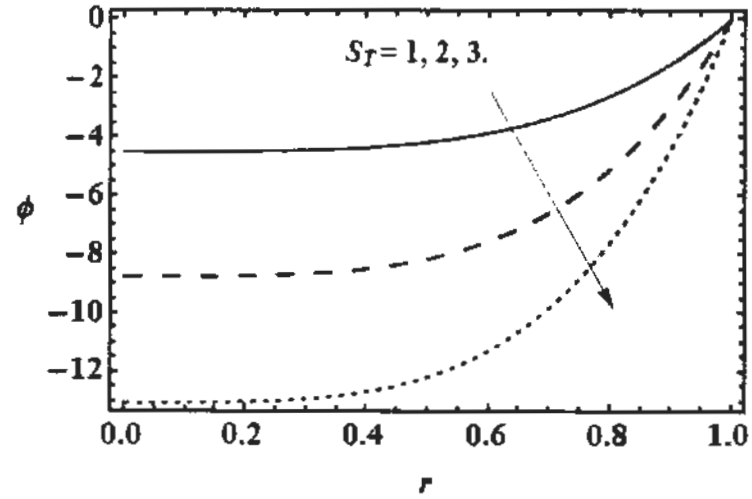

Fig. 2.18: Impact of Schmidt number S_T on concentration field ϕ for $M = 1, D_a = 0.1$ and $S_T = 1$.

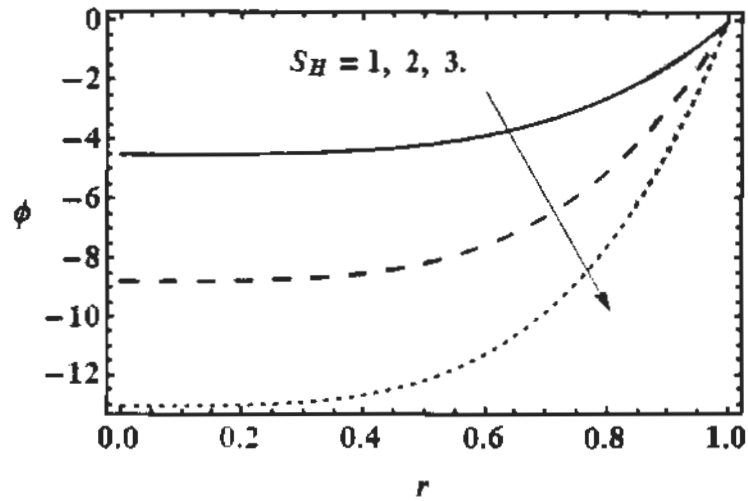

Fig. 2.19: Impact of Soret number S_H on concentration profile ϕ for $S_H = 1, D_a = 0.1$ and $M = 0.1$.

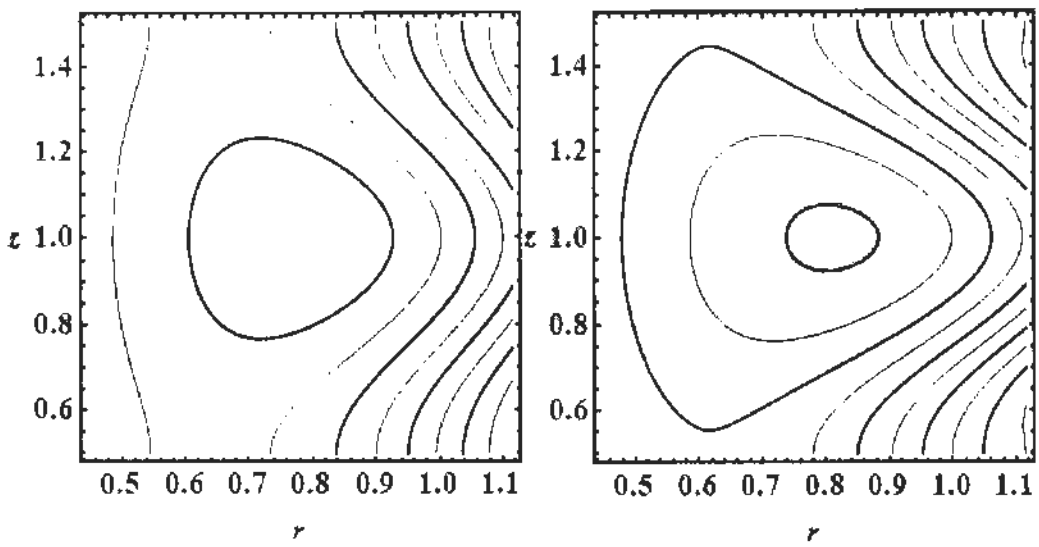

$(i)\ \epsilon = 0.1$ $(ii)\ \epsilon = 0.15$

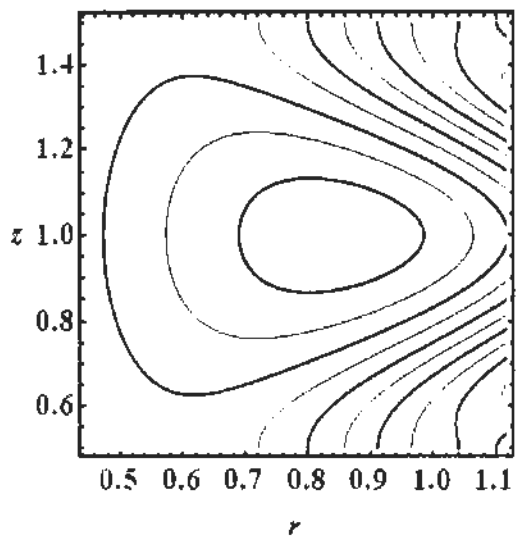

$(iii)\ \epsilon = 0.2$

Fig. 2.20: Contour plots for distinct values of cilia length parameter ϵ for $Gr_T = 1$, $Gr_C = 1, M = 1, D_a = 0.1$.

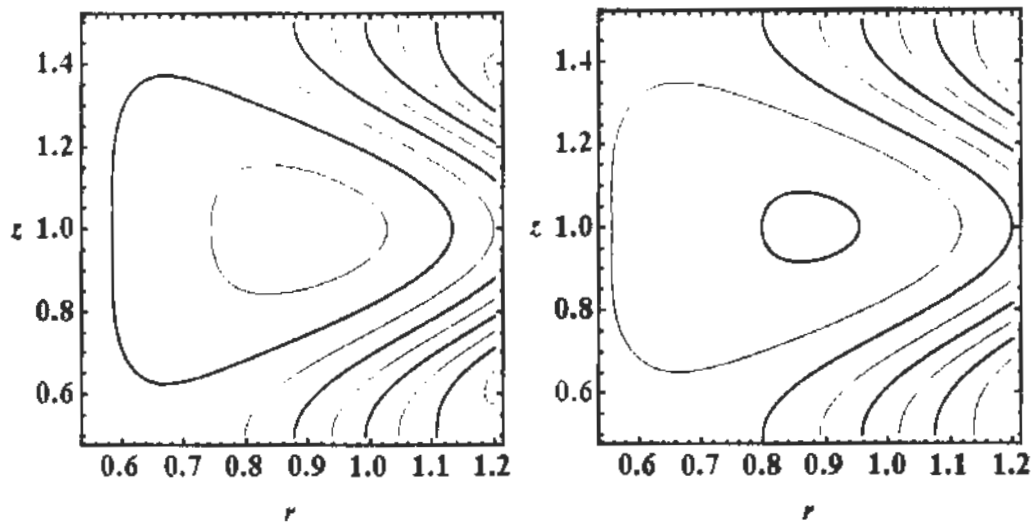

$(i)\ M = 0.1$ $(ii)\ M = 1$

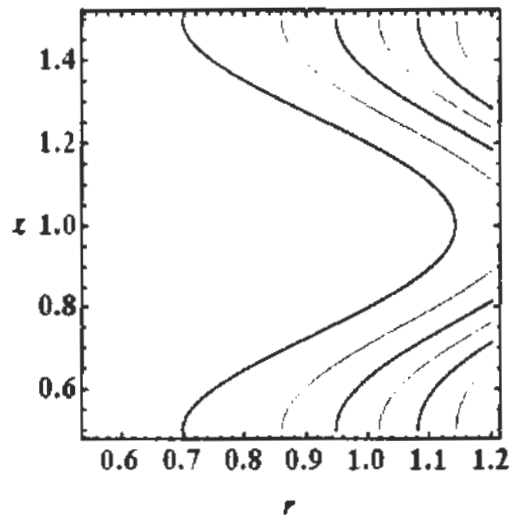

$(iii)\ M = 2$

Fig. 2.21: Contour plots for distinct values of Hartmann number M for $\epsilon = 0.1$, $D_a = 0.1, Gr_T = 1, Gr_C = 1$.

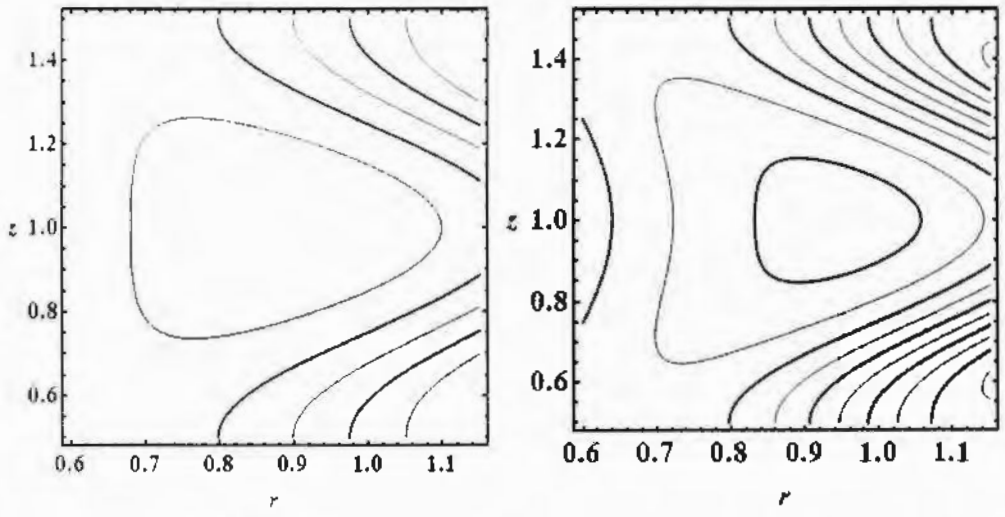

(i) $D_a = 0.1$ (ii) $D_a = 0.5$

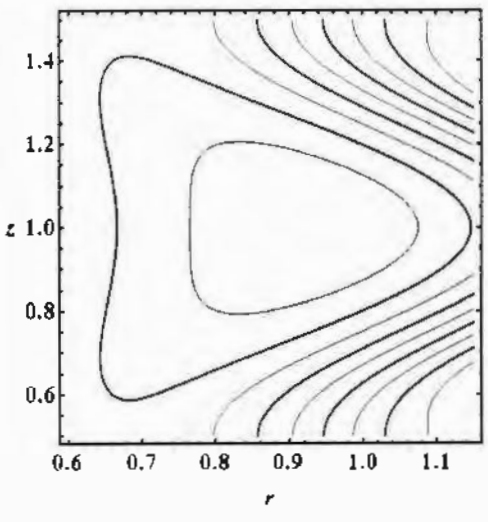

(iii) $D_a = 1$

Fig. 2.22: Contour plots for distinct values of Darcy's number D_a for $\epsilon = 0.1$, $M = 0.1, Gr_T = 1, Gr_C = 1.$

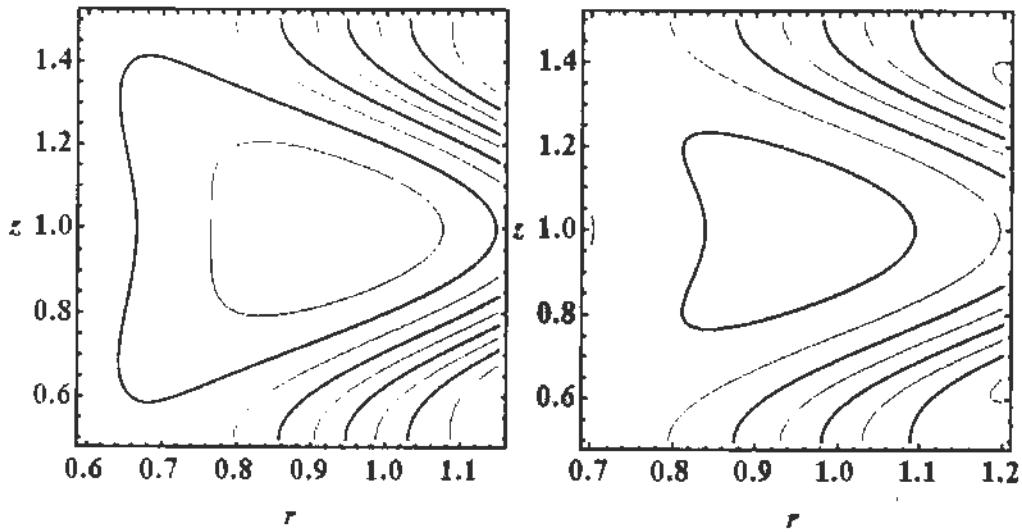

(*i*) $Gr_T = 1$ (*ii*) $Gr_T = 2$

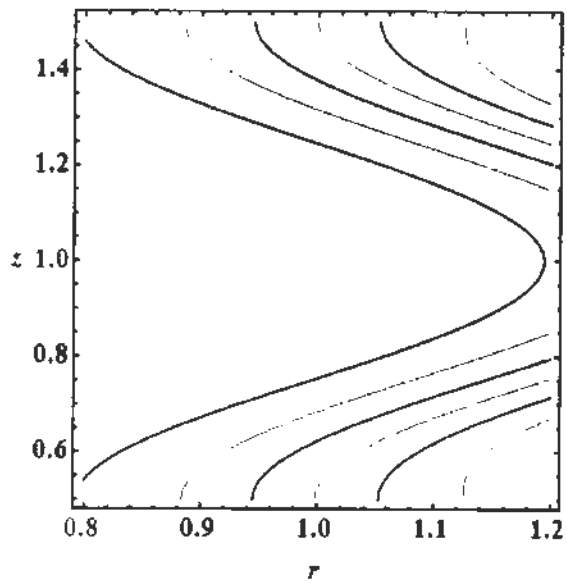

(*iii*) $Gr_T = 3$

Fig. 2.23: Contour plots for distinct values of thermal Grashof number $\mathrm{Gr_T}$ for $D_a = 0.1, Gr_C = 1, \epsilon = 0.1$ *and* $M = 0.1$.

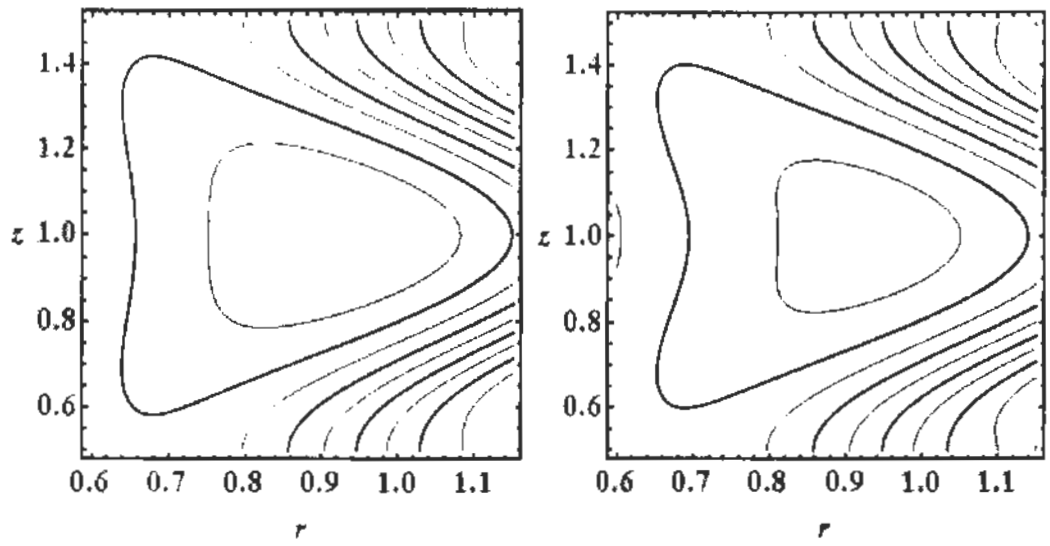

$(i)\ Gr_C = 1$ $(ii)\ Gr_C = 2$

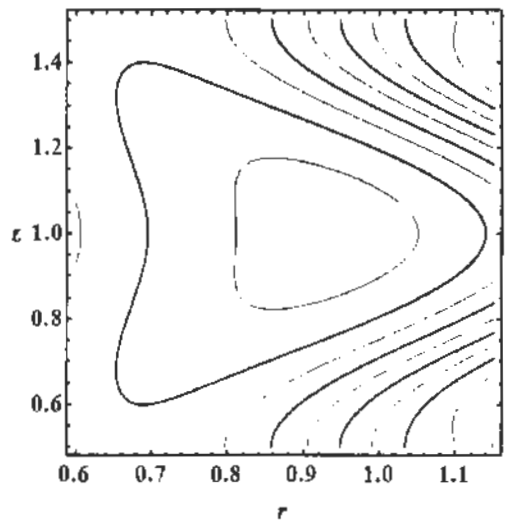

$(iii)\ Gr_C = 3$

Fig. 2.24: Contour plots for distinct values of concentration Grashof number Gr_C for $D_a = 1, Gr_T = 1, \epsilon = 0.1$ *and* $M = 0.1$.

2.4 Discussion

The thermophorectic diffusion and viscous dissipation effects on mucociliary clearance has been considered in this research. We study the effects of prominent parameters magnetic parameter M, Darcy's number D_a, thermal and solutal Grashof number on pressure gradient, velocity, temperature and concentration field for $\alpha = 0.2, \beta = 0.2$ and $\bar{Q} = 1$. Figs. $2.2 - 2.6$ represent the effects of cilia length parameter ϵ, magnetic parameter M Darcy's number D_a and Grashof number on pressure gradient. It is noticed that pressure gradient increases along the axial direction of the tube as we increase ϵ and M and decrease can be observed with the increasing value of Darcy's parameter D_a, thermal and concentration Grashof number. Figs. $2.7 - 2.11$ depict the impact of ϵ, M, D_a, Gr_T and Gr_C on axial velocity. It is depicted that velocity in axial direction increases as we increase the cilia length parameter ϵ and permeability of porous medium D_a and velocity is retarded with the increasing magnetic parameter M, thermal and concentration Grashof number. The fluid velocity near the center of the tube become mounted due to poiseuille nature of the flow.

Figs. $2.12 - 2.15$ portray the variation of temperature field for distinct values of magnetic parameter M, Brinkmann number Br and Grashof number. It can be seen that by employig magnetic field heat transfer rises but the temperature profile shows the retarded behavior with the increasing value of D_a, Br, Gr_T and Gr_C. The Darcy's number D_a, Brinkmann number Br, thermal Grashof Gr_T and solutal Grashof Gr_C are poor conductor of heat for viscous fluid.

In Figs. $2.16 - 2.19$, the influence of magnetic parameter M, Darcy's number D_a, Schmidt number S_H and Soret number S_T on concentration field is observed. It is evident that magnitude of concentration profile increases as we increase M, D_a, S_H and S_T. The coneentration of molecules became high in the presence of

heating effects, magnetic field and porous medium.

The trapping phenomena of mucociliary clearance for different values of ϵ, M, D_a, Gr_T and Gr_C has been shown in Figs. $2.20 - 2.24$ and it can be seen that by rising the values of ϵ and D_a number of boluses as well as size of boluses increase. The size and number of boluses decreases as we increase M, Gr_T and Gr_C. The mucus (fluid) become thin when ciliary length become high to clear the airway mucus but viscous dissipation and thermophoretic effects make the fluid (mucus) thick.

2.5 Conclusions

The mathematical analysis of mucociliary clearance with the effect of viscous dissipation, thermophoresis, magnetic field and porous medium has been discussed. The diffusive convective transfer of heat and mass of ciliary flow in a vertical symmetric tube is modeled with the help of mass, momentum, energy and concentration laws. Homotopy perturbation solution of velocity, temperature and concentration have been constructed upto the second order with the help of software "MATHEMATICA". The flow features e.g velocity, stream function and pressure gradient are analyzed for different values of involved parameters and following observations have noted.

- Pressure gradient increases by increasing values of cilia length, Hartmann and porosity parameter, but decreases with rising value of concentration and thermal Grashof number.
- Axial flow velocity decelerates with the increasing value of ϵ, M, Gr_T and Gr_C but flow velocity accelerates with the increasing value of D_a.
- Temperature profile deereases with growing values of D_a, Br, Gr_T and Gr_C but increase can be seen in temperature profile by rising value of M.
- Concentration profile decelerated with the increasing values of D_a, M, S_H and S_T.
- Trapping phenomena shows the size of bolus reduces by rising M, D_a, Gr_T and

Gr_C but bolus size tends to increase with the rising value of ϵ.

The magnitude of concentration level can be increased in presence of magnetic field and thermophoretic effect but heat transfer and axial flow can be increased with the high length of cilia and porous medium.

Chapter 3

Thermal and Concentration Field Analysis of Jeffrey Nanofluid Flow

In this chapter, we discuss the effect of nanoparticles on Jeffrey fluid parameter due to ciliary movement. The mathematical modelling has been made by the envelop model approach for the stokes flow of Jeffrey fluid. The governing partial differential equations are solved by HPM and software "MATHEMATICA". The graphical results show the effects of viscoelastic parameter, cilia length and thermal and concentration Grashof numbers on the pressure gradient, velocity, temperature and concentration profile.

3.1 Mathematical Model

Consider a Jeffrey nanofluid [85] flow (mucus contains dust particles) in a respiratory tract resembled with a tube having finite length. Assume infinite number of continuously beating cilia are present at the inner walls of tube generating symplectic metachronal wave which moves

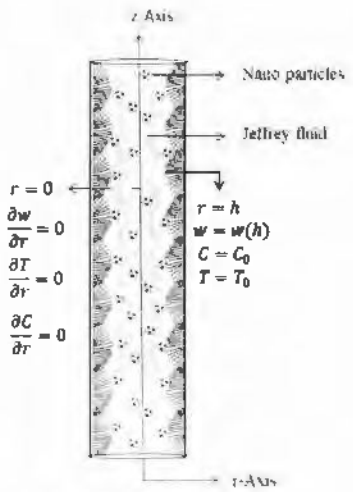

(i)

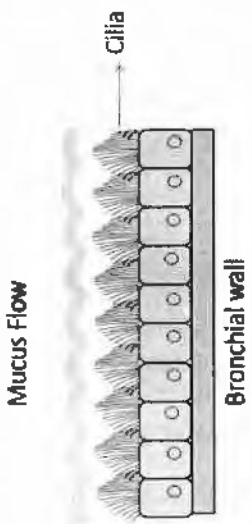

(ii)

Fig. 3.1: Geometry of the problem.

towards a positive $z - axis$ with wave speed c. As we have considered the cilia which are present on the inner surface of the trachea and due to continuously beating of cilia, fluid flow is established.

The governing equations for the Jeffrey nanofluid flow through a ciliated tube with thermophoresis, Brownian motion and buoyancy effects are given as follow

$$\frac{1}{r}\frac{\partial}{\partial r}(ru) + \frac{\partial w}{\partial z} = 0, \tag{3.1}$$

$$\rho_f\left(\frac{\partial}{\partial t}+V.\nabla\right)V=\rho_f g\beta_1{}^*(C-C_0)+\rho_f g\beta_1(T-T_0)+\nabla.\boldsymbol{\tau}, \tag{3.2}$$

$$\boldsymbol{\tau}=-\mathrm{p}\mathbf{I}+\mathbf{S}, \tag{3.3}$$

$$\left(\rho c_p\right)_f\left(\frac{\partial}{\partial t}+V.\nabla\right)T \tag{3.4}$$

$$=k\nabla^2T+trace(\boldsymbol{S}.\boldsymbol{L})+\left(\rho c_p\right)_p\left(D_B\nabla C.\nabla T+\frac{D_T}{T_0}\nabla T.\nabla T\right),$$

$$\left(\frac{\partial}{\partial t}+V.\nabla\right)C=D_B\nabla^2C+\frac{D_T}{T_0}\nabla^2T, \tag{3.5}$$

where

$$\boldsymbol{S}=\frac{\eta}{1+\lambda_1}\left(\boldsymbol{A_1}+\lambda_2\frac{d\boldsymbol{A_1}}{dt}\right), \tag{3.6}$$

with boundary conditions

$$w=w(h)=\frac{-\left(\frac{2\pi}{\lambda}\right)\left[\epsilon a\alpha c\sin\left(\frac{2\pi}{\lambda}\right)z\right]}{1-\left(\frac{2\pi}{\lambda}\right)\left[\epsilon a\alpha\cos\left(\frac{2\pi}{\lambda}\right)z\right]}, \tag{3.7a}$$

$$u=u(h)=\frac{\left(\frac{2\pi}{\lambda}\right)\left[\epsilon a\alpha c\sin\left(\frac{2\pi}{\lambda}\right)z\right]}{1-\left(\frac{2\pi}{\lambda}\right)\left[\epsilon a\alpha\cos\left(\frac{2\pi}{\lambda}\right)z\right]}, \tag{3.7b}$$

$$T=T_0, \qquad C=C_0, \tag{3.7c}$$

at

$$r=\pm h(z)=\pm\left[a+\epsilon a\alpha\cos\left(\frac{2\pi}{\lambda}\right)z\right].$$

and

$$\frac{\partial w}{\partial r}=0 \qquad at\ \ r=0. \tag{3.8a}$$

The temperature and concentration profile are constant at center of the tube therefore

$$\frac{\partial T}{\partial r}=0, \qquad \frac{\partial C}{\partial r}=0, at\ \ r=0. \tag{3.8b}$$

In above equations V is the velocity profile, $\boldsymbol{\tau}$ is the extra stress tensor and ρ_f is the density of fluid.

To non-dimensionalize the above system we use following parameters

$$z^* = \frac{z}{\lambda}, \quad u^* = \frac{u}{\beta c}, \quad r^* = \frac{r}{a}, \quad w^* = \frac{w}{c}, \quad p^* = \frac{a\beta}{c\mu}p, \quad h^* = \frac{h}{a},$$

$$\beta = \frac{a}{\lambda}, \quad S_{ij}{}^* = \frac{a}{\eta c}S_{ij}, \quad \lambda_1{}^* = \frac{c\lambda_1}{a}, \quad Re = \frac{\rho ac}{\mu}, \quad Pr = \frac{\eta c_p}{k},$$

$$\theta = \frac{T - T_0}{T_1 - T_0}, \phi = \frac{C - C_0}{C_1 - C_0}, Nb = \frac{(\rho c)_p D_B (C_1 - C_0)}{(\rho c)_f \alpha_f}, \tag{3.9}$$

$$Nt = \frac{(\rho c)_p D_T (C_1 - C_0)}{(\rho c)_f \alpha_f} Gr_T = \frac{g\beta_1 \alpha^3 (T_1 - T_0)}{\nu^2}, Gr_C = \frac{g\beta_1{}^* \alpha^3 (C_1 - C_0)}{\nu^2}.$$

Using Eq. (3.9) into Eqs. (3.1)-(3.8), we can obtain following form of equations after dropping the asterisk

$$\frac{1}{r}\frac{\partial}{\partial r}(ru) + \frac{\partial w}{\partial z} = 0, \tag{3.10}$$

$$Re\beta E(w) = \frac{1}{r}\frac{\partial}{\partial r}\left(\frac{r}{1+\lambda_1}\left(\frac{\partial w}{\partial r} + \beta^2 \frac{\partial u}{\partial z}\right)\right) - \frac{\partial p}{\partial z} + \beta^2 \frac{\partial^2 w}{\partial z^2} + Gr_T \theta + Gr_C \phi, \tag{3.11}$$

$$Re\beta^2 E(u) = \beta^2 \left[F_1(u) + \beta^2 \frac{\partial^2 u}{\partial z^2} - \frac{u}{r^2}\right] - \frac{\partial p}{\partial r}, \tag{3.12}$$

$$\beta RePrE(\theta) = F_1(\theta) + \beta^2 \frac{\partial^2 \theta}{\partial z^2} + Nb\left(\frac{\partial \theta}{\partial r}\frac{\partial \phi}{\partial r} + \beta^2 \frac{\partial \theta}{\partial z}\frac{\partial \phi}{\partial z}\right) + Nt\left(\left(\frac{\partial \theta}{\partial r}\right)^2 + \beta^2\left(\frac{\partial \theta}{\partial z}\right)^2\right) + Br\frac{\partial w}{\partial r}\left(\frac{1}{1+\lambda_1}\left(\frac{\partial w}{\partial r} + \beta^2 \frac{\partial u}{\partial z}\right)\right), \tag{3.13}$$

$$\beta E(\phi) = F_1(\phi) + \beta^2 \frac{\partial^2 \phi}{\partial z^2} + \frac{Nt}{Nb}\left(\frac{\partial^2 \theta}{\partial r^2} + \frac{1}{r}\frac{\partial \theta}{\partial r}\right), \tag{3.14}$$

with boundary conditions

$$w = w(h) = -(1 + 2\pi\epsilon\alpha\beta\cos(2\pi z)), \tag{3.15}$$

$$u = u(h) = 2\pi\epsilon(\sin(2\pi z)) + \beta 2\pi\epsilon\alpha \sin(2\pi z)\cos(2\pi z), \tag{3.16}$$

at

$$r = h(z) = a + \epsilon\alpha a\cos(2\pi z),$$

$$\frac{\partial w}{\partial r} = \frac{\partial \theta}{\partial r} = \frac{\partial \phi}{\partial r} = 0 \qquad at \;\; r = 0. \tag{3.17}$$

Using long wavelength $(\lambda \to \infty)$ and low Reynolds' number $(Re \to 0)$ approximation [34] we can find following forms of equations

$$F_1(w) - (1 + \lambda_1)\left(-Gr_T\theta - Gr_C\phi + \frac{\partial p}{\partial z}\right) = 0, \tag{3.18}$$

$$\frac{\partial p}{\partial r} = 0, \tag{3.19}$$

$$F_1(\theta) + Nb\frac{\partial \theta}{\partial r}\frac{\partial \phi}{\partial r} + Nt\left(\frac{\partial \theta}{\partial r}\right)^2 - \frac{Br}{1 + \lambda_1}\left(\frac{\partial w}{\partial r}\right)^2 = 0, \tag{3.20}$$

$$F_1(\phi) + \frac{Nt}{Nb}F_1(\theta) = 0, \tag{3.21}$$

with boundary conditions

$$w = w(h) = -1 - 2\pi\epsilon\alpha\beta\cos(2\pi z), \theta = 0, \phi = 0, at \;\; r = h, \tag{3.22}$$

$$\frac{\partial w}{\partial r} = \frac{\partial \theta}{\partial r} = \frac{\partial \phi}{\partial r} = 0 \qquad at \;\; r = 0. \tag{3.23}$$

Volume flow rate is defined as

$$q = 2\int_0^h rwdr, \tag{3.24}$$

so that dimensional and non-dimensional volume flow rate are related as

$$Q = 2\int_0^l rwdr = 2\int_0^l r(w + 1)dr = q + h^2. \tag{3.25}$$

The average volume flow rate can be written as follows

$$\bar{Q} = \frac{1}{T}\int_0^T Qdt^* = q + 1 + 0.5\epsilon^2. \tag{3.26}$$

3.2 Homotopy Perturbation Solution

To obtain the solution of governing equations we use, homotopy perturbation method which is described as follow

$$\mathcal{H}(j,w) = (1-j)[\mathcal{L}(w) - \mathcal{L}(w_0)] + j\left(\mathcal{L}(w) - (1+\lambda_1)\left(-Gr_T\theta - Gr_C\phi + \frac{dp}{dz}\right)\right), \tag{3.27}$$

$$\mathcal{H}(j,\theta) = (1-j)[\mathcal{L}(\theta) - \mathcal{L}(\theta_0)] + j\left(\mathcal{L}(\theta) - Nb\left(\frac{\partial\theta}{\partial r}\frac{\partial\phi}{\partial r}\right) - Nt\left(\frac{\partial\theta}{\partial r}\right)^2 + \frac{Br}{1+\lambda_1}\left(\frac{\partial w}{\partial r}\right)^2\right), \tag{3.28}$$

$$H(j,\phi) = (1-j)[\mathcal{L}(\phi) - \mathcal{L}(\phi_0)] + j\left(\mathcal{L}(\phi) - \frac{Nt}{Nb}\frac{1}{r}\frac{\partial}{\partial r}\left(r\frac{\partial\theta}{\partial r}\right)\right). \tag{3.29}$$

The linear operator and initial guesses are chosen as

$$\mathcal{L} = \frac{\partial^2}{\partial r^2} + \frac{1}{r}\frac{\partial}{\partial r}, \tag{3.30}$$

$$w_0 = \frac{1}{4}\frac{dp_0}{dz}(1+\lambda_1)(r^2-h^2) + w(h), \tag{3.31}$$

$$\theta_0 = \frac{r^2-h^2}{4}, \phi_0 = \frac{r^2-h^2}{4}. \tag{3.32}$$

According to Homotopy perturbation method

$$w = w_0 + jw_1 + j^2w_2 + \cdots, \tag{3.33a}$$

$$\theta = \theta_0 + j\theta_1 + j^2\theta_2 + \cdots, \tag{3.33b}$$

$$\phi = \phi_0 + j\phi_1 + j^2\phi_2 + \cdots. \tag{3.33c}$$

$$p = p_0 + jp_1 + j^2p_2 + \cdots. \tag{3.33d}$$

where $j\epsilon[0,1]$ is the Homotopy perturbation parameter and $j = 0$ gives initial guess and $j = 1$ gives the final solution. With the help of Eqs. $(3.33a) - (3.33d)$, solution for the velocity, temperature and concentration profiles are given as follow

$$w \cong w_0 + w_1 + w_2 = A_{15} + A_{16}(r^2-h^2) + A_{17}(r^4-h^4) + A_{18}(r^6-h^6). \tag{3.34}$$

Using Eq. (3.39) in Eq. (3.33) and solving Eqs. (3.33) & (3.34) under the boundary

conditions given in Eqs. (3.27) & (3.28) temperature and concentration profile can be obtained as follow

$$\theta \cong \theta_0 + \theta_1 + \theta_2 = A_{19}(r^2 - h^2) + A_{20}(r^4 - h^4) + A_{21}(r^6 - h^6), \tag{3.35}$$

$$\phi \cong \phi_0 + \phi_1 + \phi_2 = A_{22}(r^2 - h^2) + A_{23}(r^4 - h^4). \tag{3.36}$$

After integrating Eq. (3.34) one can get following pressure gradient in terms of volume flow rate

$$\frac{dp}{dz} = \frac{-A_{24} + \sqrt{-4A_{25}A_{26} + A_{24}^2 + 4A_{24}q}}{2A_{24}}, \tag{3.37}$$

where A_{15} to A_{24} are defined in Appendix.

The solution obtained by the Homotopy perturbation method is convergent as expressions of velocity, temperature and concentration profiles are in the form of power series with decaying coefficients.

3.3 Graphical Results

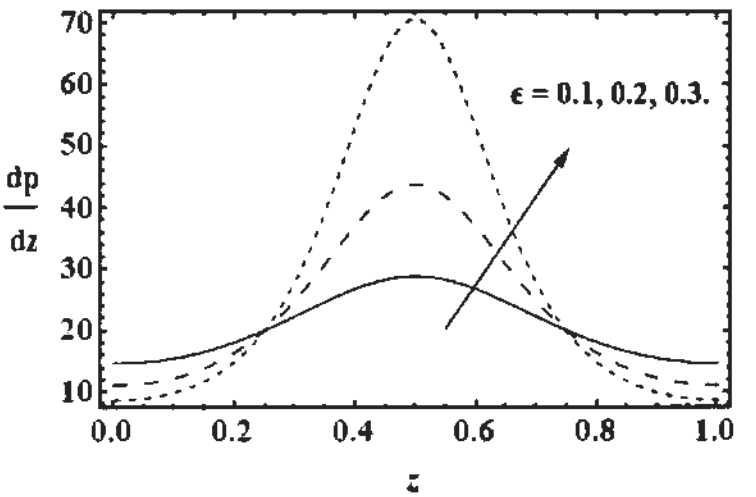

Fig. 3.2: Influence of cilia length parameter ϵ fraction on pressure gradient $\frac{dp}{dz}$ for $\lambda_1 = 0.3, Gr_T = 1$ and $Gr_C = 1$.

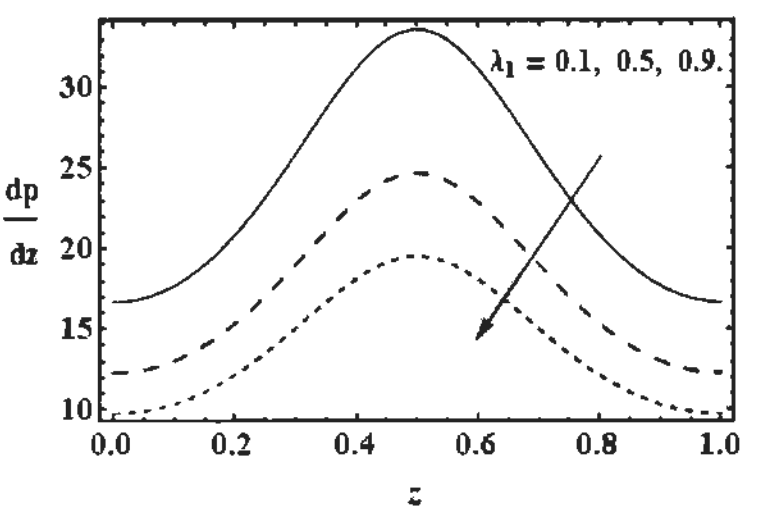

Fig. 3.3: Influence of Jeffrey fluid parameter λ_1 on pressure gradient $\frac{dp}{dz}$ for $\epsilon = 0.2$, $Gr_T = 1$ and $Gr_C = 1$.

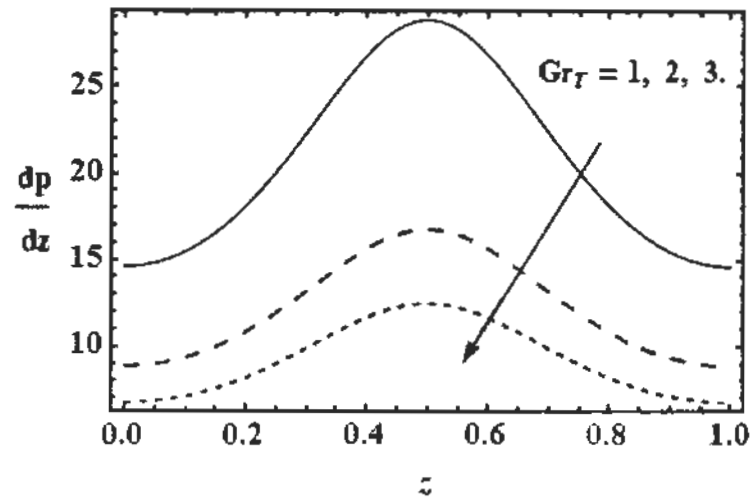

Fig. 3.4: Influence of thermal Grashof number Gr_T on pressure gradient $\frac{dp}{dz}$ for $\epsilon = 0.2$,

$\lambda_1 = 0.3$ and $Gr_C = 1$.

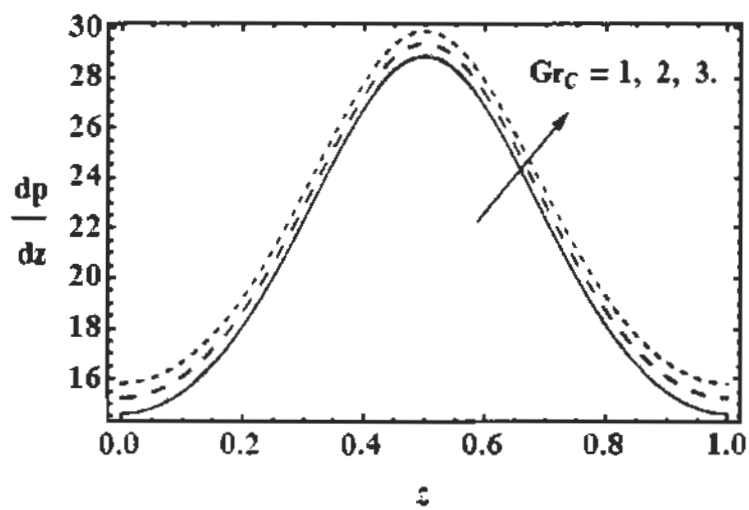

Fig. 3.5: Influence of concentration Grashof number Gr_C on pressure gradient $\frac{dp}{dz}$ for

$\epsilon = 0.2, \lambda_1 = 0.3$ and $Gr_T = 1$.

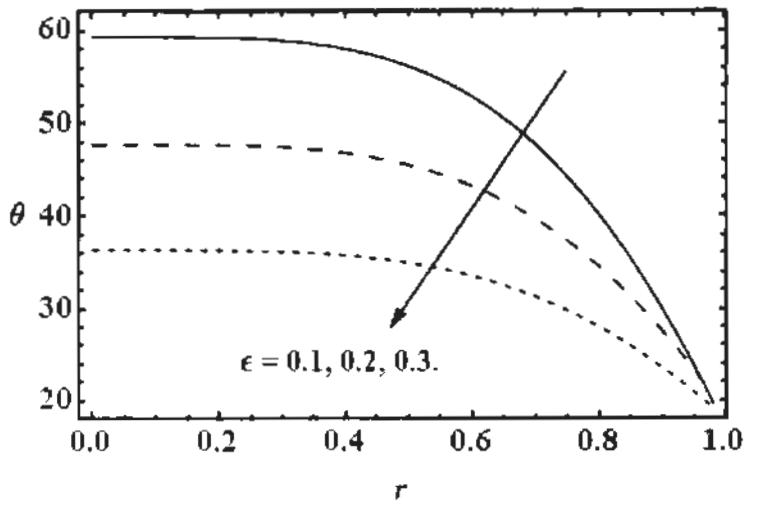

Fig. 3.6: Influence of cilia length parameter ϵ on temperature profile θ for $\lambda_1 = 0.3, Gr_T = 1, Gr_C = 1, Nt = 4$ and $Nb = 1$.

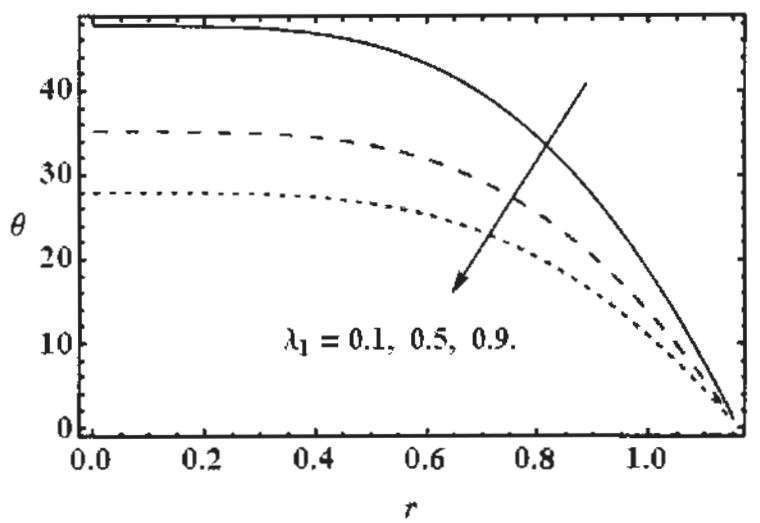

Fig. 3.7: Influence of Jeffrey fluid parameter λ_1 on temperature profile θ for $\epsilon = 0.2,\ Gr_T = 1, Gr_C = 1, Nt = 4$ and $Nb = 1$.

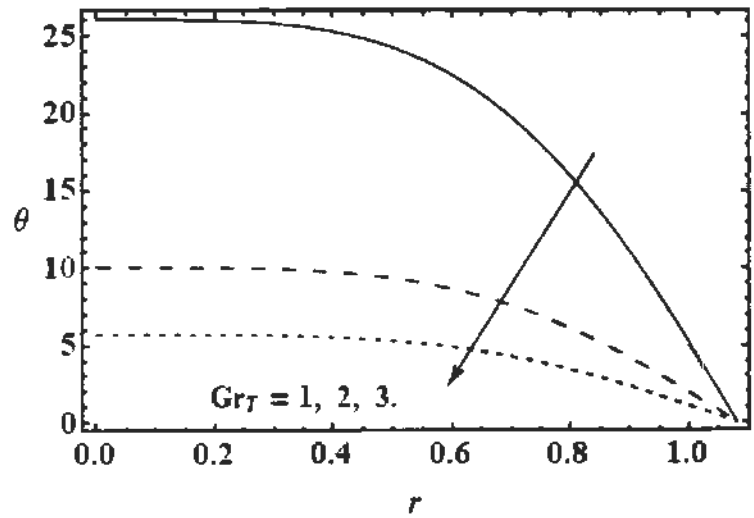

Fig. 3.8: Influence of thermal Grashof number Gr_T on temperature profile θ for $\epsilon = 0.2,\ \lambda_1 = 1, Gr_C = 1, Nt = 4$ and $Nb = 1$.

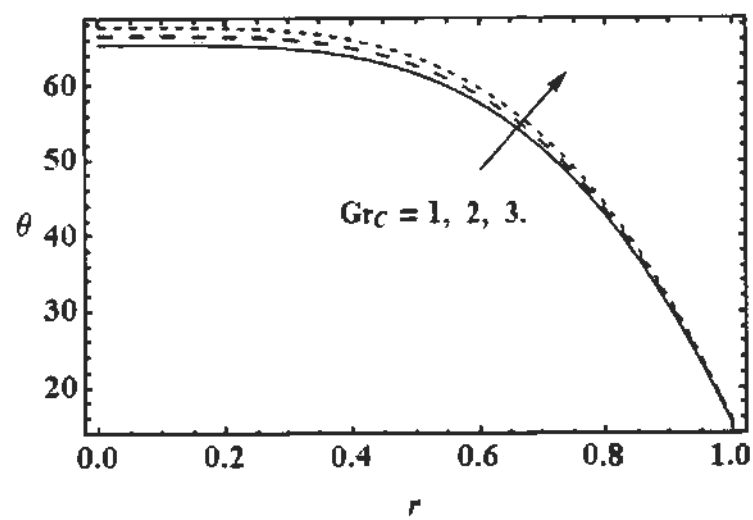

Fig. 3.9: Influence of concentration Grashof number Gr_C on temperature profile θ for $\epsilon = 0.2,\ \lambda_1 = 1, Gr_T = 1, Nt = 4$ and $Nb = 1$.

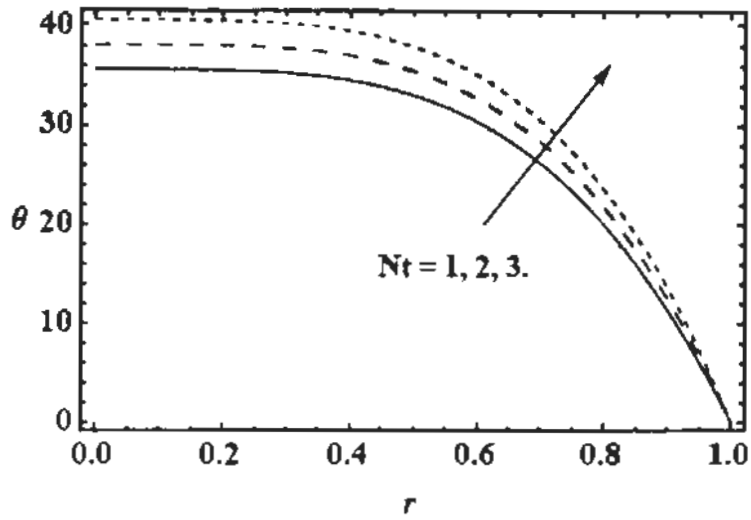

Fig. 3.10: Influence of thermophoretic constant Nt on temperature profile θ for $\epsilon = 0.2,\ \lambda_1 = 1, Gr_T = 1,\ Gr_C = 1$ and $Nb = 1$.

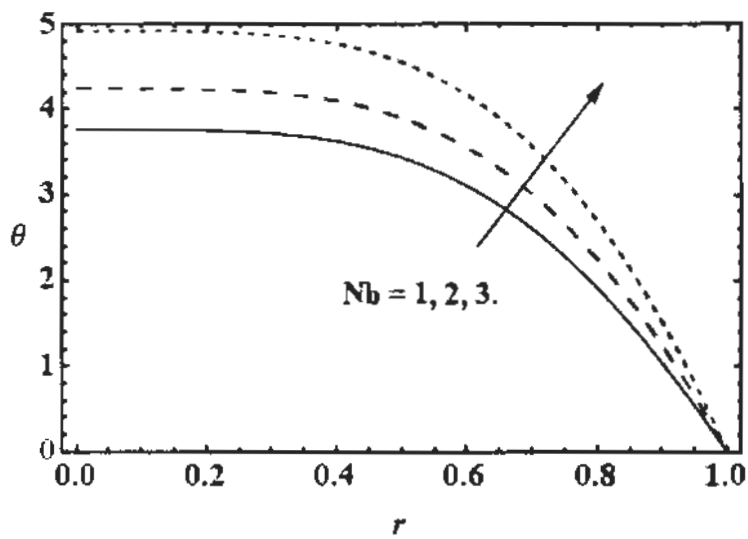

Fig. 3.11: Influence of Brownian motion constant Nb on temperature profile θ for $\epsilon = 0.2,\ \lambda_1 = 1, Gr_T = 1,\ Gr_C = 1$ and $Nb = 1$.

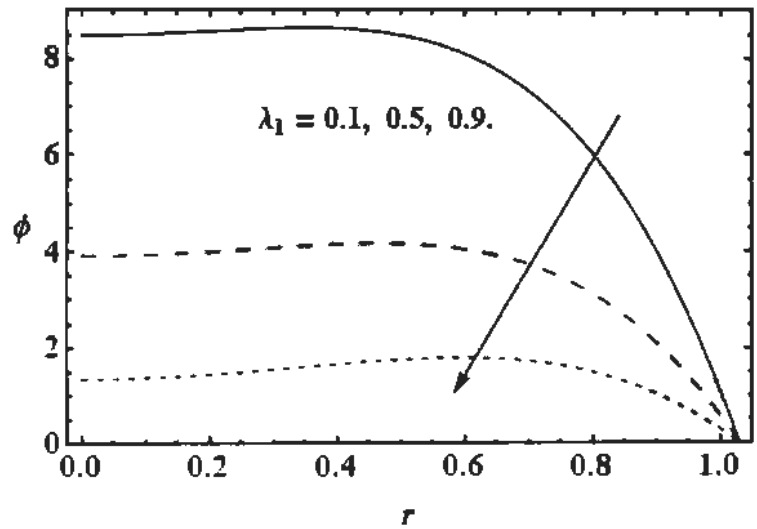

Fig. 3.12: Influence of Jeffrey fluid parameter λ_1 on concentration profile ϕ for $Nt = 4$ and $Nb = 1$.

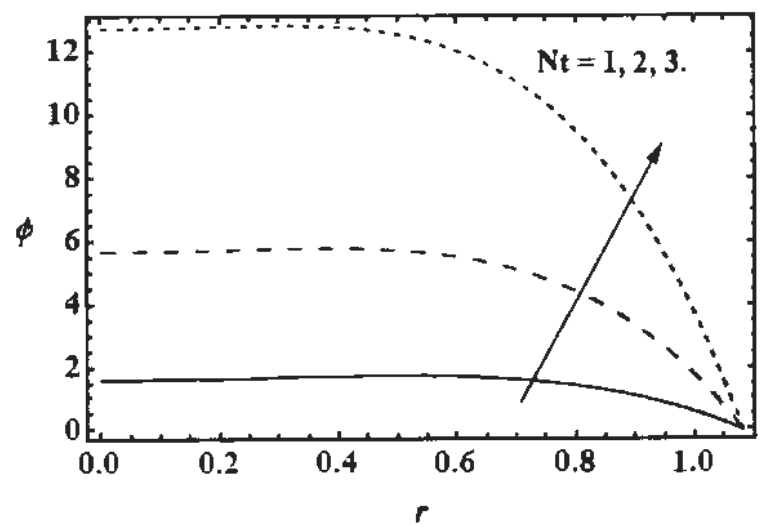

Fig. 3.13: The effect of thermophoretic constant Nt on concentration profile ϕ for $\lambda_1 = 0.3$ and $Nb = 1$.

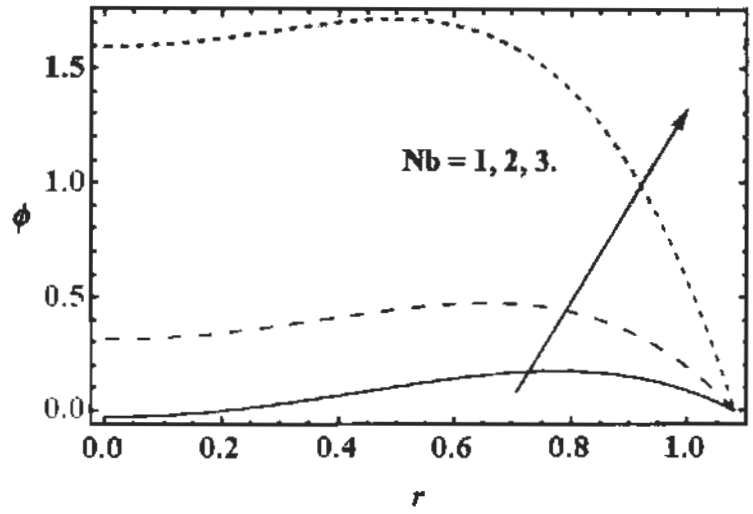

Fig. 3.14: Influence of Brownian motion constant Nb on concentration profile ϕ for $\lambda_1 = 0.3$ and $Nt = 1$.

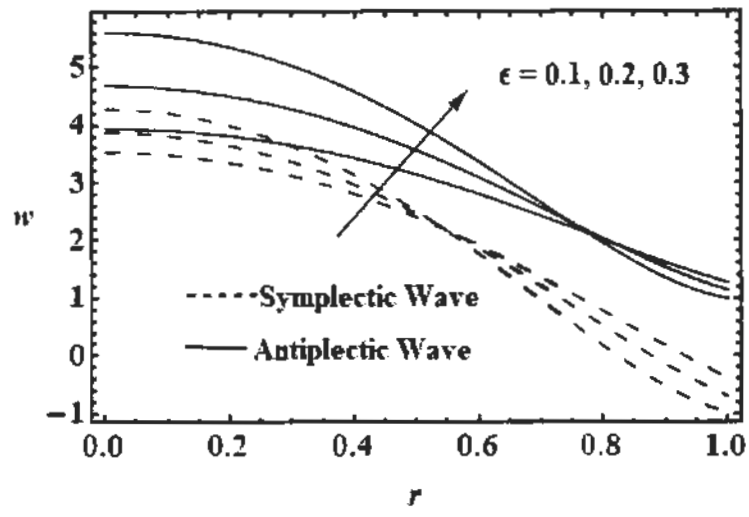

Fig. 3.15: Comparison of symplectic and antiplectic wave pattern of different values of cilia length parameter ϵ for $\lambda_1 = 0.3, Gr_T = 1$ and $Gr_C = 1$.

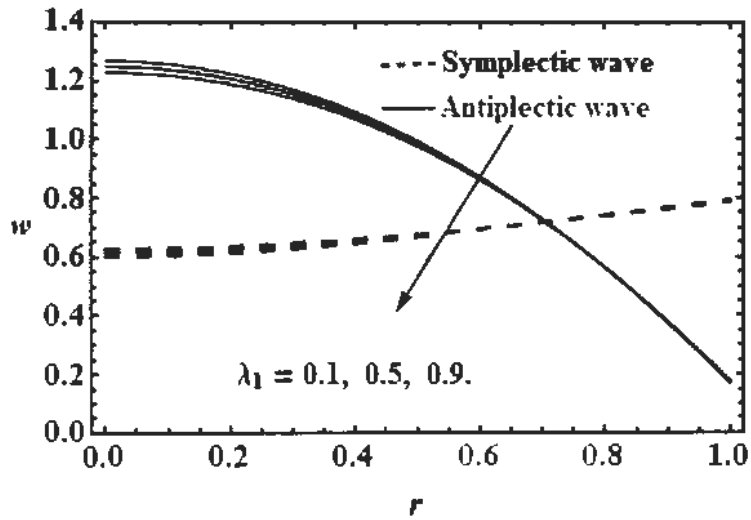

Fig. 3.16: Comparison of symplectic and antiplectic wave pattern of different values of Jeffrey fluid parameter λ_1 for $\epsilon = 0.3, Gr_T = 1$ and $Gr_C = 1$.

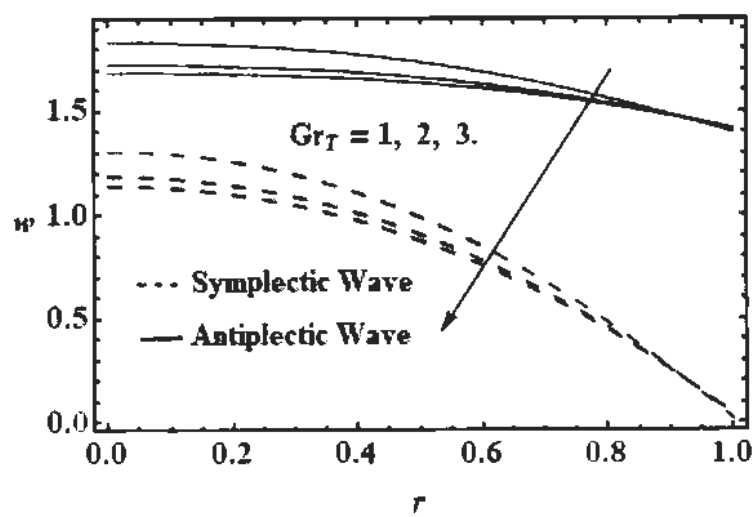

Fig. 3.17: Comparison of symplectic and antiplectic wave pattern of different values of thermal Grashof number Gr_T for $\epsilon = 0.2, \lambda_1 = 0.3$ and $Gr_C = 1$.

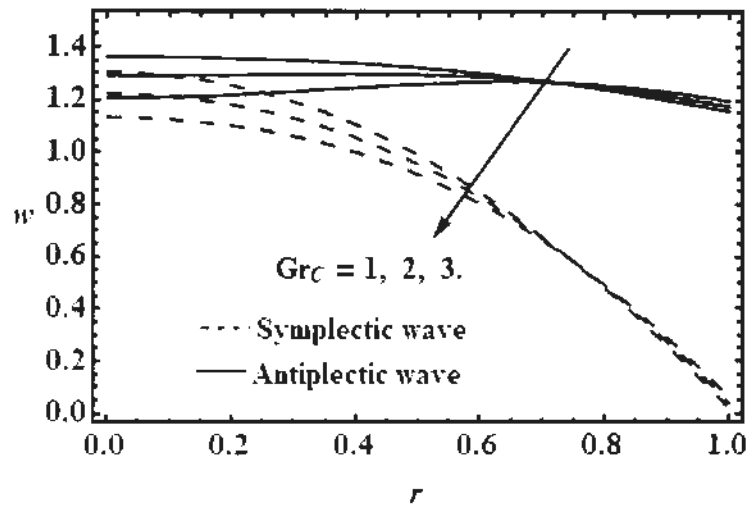

Fig. 3.18: Comparison of symplectic and antiplectic wave pattern of different values of concentration Grashof number Gr_C for $\epsilon = 0.2, \lambda_1 = 0.3$ and $Gr_T = 1$.

3.4 Discussion

The mathematical model of microsystem of respiratory tract contains mucociliary clearance as Jeffrey nanofluid flow through ciliated tube is governed by the energy, concentration and momentum equation with the effects of thermophoresis and Brownian motion. The results of velocity, temperature, concentration profile and pressure gradient are presented through graphs. For the biological relevance of the present study we have presumed $\alpha = 0.4, \beta = 0.4,$

$z = 0.1$ from Ref. [30].

Pressure gradient in the ciliary flow is a vital agent for the mucociliary clearance and its variations depend upon distinct values of cilia length ϵ, Jeffrey parameter (viscoelastic parameter) λ_1, thermal Grashof number Gr_T and solutal Grashof number Gr_C that are expressed through Figs. $3.2 - 3.5$. It is noted that pressure deviation mounted for the increasing values of cilia length parameter ϵ and solutal Grashof number Gr_C but deviation decreases with the increasing value of viscosity (Jeffrey)

parameter λ_1 and thermal Grashof number Gr_T. These graphs show that when the buoyancy forces are dominant over the temperature difference, then pressure gradient decreases for the ciliary flow but in contrast when the buoyancy forces became dominant over the concentration difference the increase in pressure gradient is required for the Jeffrey nanofluid flow. The increasing values of Jeffrey parameter λ_1 show that pressure gradient increases for the ciliary flow due to thickness of the fluid flow. Since the temperature difference effect the mucus flow near the ciliated bed therefore, heat transfer altered due to the cilia length parameter ϵ, Jeffrey parameter λ_1, thermal Grashof number Gr_T and solutal Grashof number Gr_C which is shown in Figs. 3.6 – 3.11. These figures display that the decay in transfer of heat is observed with the increasing values of cilia length parameter ε, Jeffrey parameter λ_1 and thermal Grashof number Gr_T but solutal Grashof number Gr_C, thermophoretic parameter and Brownian motion parameter cause to rise in transfer of heat. It is noticed that the presence of nanoparticles (Nb and Nt) and buoyancy force due to concentration difference Gr_C help to enhance the thermal conductivity of the fluid that results to increase the temperature profile, whereas Jeffrey parameter λ_1, cilia length parameter ϵ and thermal Grashof number Gr_T cause to reduce the thermal conductivity of the fluid which results to decrease the temperature profile.

The diffusion of nano particles in the mucus are influenced by the Jeffrey parameter λ_1, thermophoretic parameter Nt and Brownian motion parameter Nb that are displayed through Figs. 3.12 – 3.14. It is observed that concentration profile decreases with the increasing values of Jeffrey parameter λ_1 and Brownian motion parameter Nb whereas concentration profile increases with the increasing values of thermophoretic parameter Nt. It is viewed that increasing values of Nb and λ_1 makes the diffusion process slow which results to decay the concentration profile

but thermophoretic effect causes to accelerate the diffusion process which results to increase the concentration profile.

The variation of ϵ, λ_1, Gr_T and Gr_C has been displayed for axial velocity using the symplectic and antiplectic wave pattern. Figs. $3.15 - 3.18$ indicate that axial velocity is maximum at the center of the tube $r = 0$ due to the presence of pressure gradient. Axial velocity increases for the increasing values of cilia length parameter ϵ i.e the cilia length help to accelerate the axial velocity near the center of ciliated tube. The increasing values of λ_1, Gr_T and Gr_C cause to decrease the axial velocity in the region $-0.5 \leq r \leq 0.5$. It is noticed that Jeffrey parameter λ_1 and buoyancy forces (Gr_T and Gr_C) decelerate the fluid flow in the axial direction. It is also observed that magnitude of the velocity profile is high in the antiplectic wave pattern when compared with symplectic wave pattern. Thus for the fast movement of the axial flow antiplectic wave pattern is suitable and for the slow motion of axial velocity symplectic wave pattern is a best choice.

3.5 Conclusions

In this research, the analysis of micro-system of respiratory tract contains mucus clearance as Jeffrey nanofluid through cilia beating subject to the surrounding temperature has been done with the effects of thermophoresis and Brownian motion. In humans, the physiological part for respiration is small airways, it is already proved [38] that micro-system of ciliary motion plays a key role in clearance of mucus present in small airways.

The flow of mucus under the influence of surrounding temperature and environment (clean and dusty) has been observed in this study and main results of this study are listed below

- The thickness of the nanofluid (Jeffrey fluid with dust or viruses) causes to reduce

the flow rate, heat transfer (θ) in mucus, diffusion of nanoparticles in mucus (ϕ) and pressure gradient $\left(\frac{dp}{dz}\right)$ for the mucoclearance.

- The cilia length parameter ϵ causes to increase the velocity (w) and pressure gradient $\left(\frac{dp}{dz}\right)$ along the trachea length but it causes to reduce the heat transfer (θ).
- Buoyancy force due to temperature difference (Gr_T) causes to decrease the pressure gradient, temperature and axial velocity.
- Buoyancy force due to concentration difference (Gr_C) causes to increase the pressure gradient and temperature profile but it helps to reduce the axial velocity.
- Thermophoretic number causes (Nt) to increase the temperature and concentration profile.
- Temperature profile increases and concentration profile decreases by increasing Brownian motion parameter (Nb).
- By considering Jeffrey parameter $(\lambda_1 = \lambda_2 = 0)$ the results of linear viscous fluid can be retrieved.

This study helps how one can control the mucociliary clearance with the help of temperature and surrounding environment. The present study will hopefully provide significant applications in bioengineering, medical sciences, and medical equipment, such as cilia based microdevices for the clearance of viscoelastic fluid from dust and viruses.

Chapter 4

Mathematical Study of Entropy Generation on Tangent Hyperbolic Nanofluid Flow

In this chapter, we discuss the effect of nanoparticles and entropy generation due to ciliary movement. The mathematical modeling has been made by the envelop model approach for the Stokes flow of tangent hyperbolic fluid. The governing partial differential equations are solved by Homotopy perturbation method and software "MATHEMATICA". The graphical results show the effects of viscoelastic parameter, nanoparticles, cilia length and Brinkman number on the velocity, temperature and entropy generation.

4.1 Mathematical Model

Consider a two dimensional flow of Tangent hyperbolic copper nanofluid in a tube having width $2h$. Blood is considered as base fluid and copper nanoparticles are immersed in blood. Assume infinite number of continuously beating cilia are present at the inner walls of tube generating symplectic metachronal wave which moves towards positive z-axis with wave speed c.

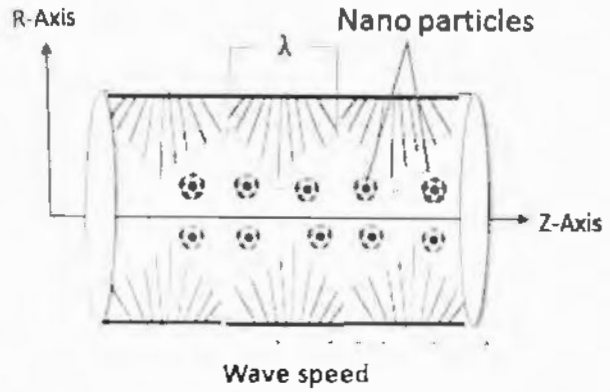

Figure 4.1: Geometry of ciliated tube.

Governing equations for an incompressible tangent hyperbolic nanofluid [86] are defined as follows:

$$\nabla . \boldsymbol{V} = 0, \tag{4.1}$$

where

$$V = [u, 0, w], \tag{4.2}$$

and

$$\rho_f \frac{d\boldsymbol{V}}{dt} = div\boldsymbol{\tau}, \tag{4.3}$$

$$(\rho c)_f \frac{dT}{dt} = k_{nf}\nabla^2 T + trace(\boldsymbol{S}.\boldsymbol{L}), \tag{4.4}$$

where **V** is the velocity components.

Here the appropriate stress tensors for the tangent hyperbolic fluid model is as follows:

$$\boldsymbol{\tau} = -p\boldsymbol{I} + \boldsymbol{S}, \tag{4.5}$$

$$\boldsymbol{S} = [(\eta_\infty + (\eta_0 + \eta_\infty)\tanh(\Gamma\dot{\gamma})^m)\dot{\gamma}_i], \tag{4.6}$$

where

$$\dot{\gamma} = \sqrt{\frac{1}{2}\boldsymbol{\pi}},$$
$$where \quad \boldsymbol{\pi} = trace(gradV + gradV^T)^2, \tag{4.7}$$

where $\boldsymbol{\pi}$ is second order tensor we study the above equation for the case where $\eta_\infty = 0$ and $\Gamma\dot{\gamma} < 1$. The elements of extra stress tensor can be written as

$$\dot{\gamma}_i = \boldsymbol{L} + \boldsymbol{L}^T, \tag{4.8}$$

$$\boldsymbol{S} = \eta_0((\Gamma\dot{\gamma})^m)\dot{\gamma}_i = \eta_0(1 + \Gamma\dot{\gamma} - 1)^m\dot{\gamma}_i = \eta_0\big(1 + m(\Gamma\dot{\gamma} - 1)\big)\dot{\gamma}_i, \tag{4.9}$$

where thermal conductivity of Cu+blood nano-fluid is defined as follow

$$\begin{aligned}
\rho_{nf} &= (1-\varphi)\rho_f + \varphi\rho_s, \\
\eta_{nf} &= \frac{\eta_f}{(1-\varphi)^{2.5}}, \\
\big(\rho c_p\big)_{nf} &= (1-\varphi)\big(\rho c_p\big)_f + \varphi\big(\rho c_p\big)_s, \\
\alpha_{nf} &= \frac{k_{nf}}{\big(\rho c_p\big)_{nf}}, \\
k_{nf} &= k_f\left(\frac{k_s + 2k_f - 2\varphi\big(k_f - k_s\big)}{k_s + 2k_f + 2\varphi\big(k_f - k_s\big)}\right),
\end{aligned} \tag{4.10}$$

where k_{nf} is the thermal conductivity of nano-fluid, k_f is the thermal conductivity of base fluid, k_s is the thermal conductivity of solid nano particles and φ is the solid volume fraction. The Mathematical model for geometry of cilia tips in the wave frame is

$$h = 1 + \epsilon\cos 2\pi z, \tag{4.11a}$$

$$w(h) = -1 - 2\pi\epsilon\alpha\beta\cos 2\pi z, \tag{4.11b}$$

where ϵ is the cilia length parameter, α is the eccentricity of elliptic wave and β is the wave number.

The governing equations of motion for tangent hyperbolic fluid model in a tube are specified as follows

$$\frac{1}{r}\frac{\partial}{\partial r}(ru) + \frac{\partial w}{\partial z} = 0, \tag{4.12}$$

$$\rho_f E(w) = \frac{1}{r}\frac{\partial}{\partial r}(rS_{rz}) + \frac{\partial S_{zz}}{\partial z} - \frac{\partial p}{\partial z}, \tag{4.13}$$

$$\rho_f E(u) = F_1(S_{rr}) + \frac{\partial S_{zr}}{\partial z} - \frac{\partial p}{\partial r}, \tag{4.14}$$

$$(\rho c)_f E(T) = k_{nf}\left(F_1(T) + \frac{\partial^2 T}{\partial z^2}\right) + S_{zr}\frac{\partial w}{\partial r}, \tag{4.15}$$

where ρ_f is the fluid density, u and w are the radial and axial components of velocity, c is the wave speed and η_f is the apparent viscosity of fluid.

The following non-dimensional parameters can be introduced for further analysis

$$z^* = \frac{z}{\lambda}, \quad u^* = \frac{u}{\beta c}, \quad r^* = \frac{r}{a}, \quad w^* = \frac{w}{c}, \quad p^* = \frac{a\beta}{c\mu}p, \quad h^* = \frac{h}{a},$$

$$\beta = \frac{a}{\lambda}, \quad S_{ij}{}^* = \frac{a}{\eta_f c}S_{ij}, \quad \lambda_1 = \frac{c\lambda_1}{a}, \quad Re = \frac{\rho a c}{\eta_f}, \quad We = \frac{\Gamma c}{a},$$

$$\alpha_f = \frac{k}{(\rho c)_f}, \quad \theta = \frac{T - T_0}{T_0}, \quad Br = \frac{a^2\eta_f}{k_f T_0}, \quad Pr = \frac{\eta_f c_p}{k_f}, \quad Ec = \frac{c^2}{c_p T_0}. \tag{4.16}$$

In terms of dimensionless parameters the momentum equations and shear stresses are

$$\frac{1}{r}\frac{\partial}{\partial r}(ru) + \frac{\partial w}{\partial z} = 0, \tag{4.17}$$

$$Re\beta E(w) = -\frac{\partial p}{\partial z} + F_1(S_{rz}) + \beta\frac{\partial S_{zz}}{\partial z}, \tag{4.18}$$

$$Re\beta^2 E(u) = -\frac{\partial p}{\partial r} + \beta\left(F_1(S_{rr})\right) + \beta^2\frac{\partial S_{zr}}{\partial z} - \beta\frac{\partial S_{\theta\theta}}{\partial z}, \tag{4.19}$$

$$\beta(\rho c)_f E(\theta) = k_{nf}\left(F_1(\theta) + \beta^2\frac{\partial^2\theta}{\partial z^2}\right) + S_{zr}\frac{\partial w}{\partial r}, \tag{4.20}$$

$$S_{rz} = \left(1 + m\left(We\frac{\partial w}{\partial r} - 1\right)\right)\frac{\partial w}{\partial r}. \tag{4.21}$$

Using long wavelength approximation ($\beta \to 0$) the governing equations and boundary conditions are as follow

$$\frac{\partial p}{\partial z} = (1-m)(F_1(w)) + mWe\frac{1}{r}\frac{\partial}{\partial r}\left(r\left(\frac{\partial w}{\partial r}\right)^2\right) \tag{4.22}$$

$$-\frac{\partial p}{\partial r} = 0, \tag{4.23}$$

$$\frac{k_{nf}}{k_f}(F_1(\theta)) = -Br\frac{\eta_{nf}}{\eta_f}\left(1 + m\left(We\frac{\partial w}{\partial r} - 1\right)\right)\left(\frac{\partial w}{\partial r}\right)^2. \tag{4.24}$$

$$\frac{\partial w}{\partial r} = 0, \quad \frac{\partial \theta}{\partial r} = 0 \qquad at \quad r = 0, \tag{4.25a}$$

$$w = w(h), \quad \theta = 0 \qquad at \quad r = h. \tag{4.25b}$$

Integration of Eq. (4.17) over the tube width is as follow

$$\int_0^h \left[\frac{1}{r}\frac{\partial(ru)}{\partial r} + \frac{\partial w}{\partial z}\right] rdr = 0, \tag{4.26}$$

$$hu(h) + \frac{1}{2}\frac{\partial q}{\partial z} - h\frac{\partial h}{\partial z}w(h) = 0, \tag{4.27}$$

where $q = 2\int_0^h rwdr$.

Eq. (4.27) takes the followig form

$$\frac{\partial q}{\partial z} = 2h\left(\frac{\partial h}{\partial z}w(h) - u(h)\right). \tag{4.28}$$

The relation between q and dimensionless volume flow rate Q is given by

$$Q = 2\int_0^h RWdR = 2\int_0^h (w+1)rdr = q + h^2, \tag{4.29}$$

The mean volume flow rate for the time period $T = \frac{\lambda}{c}$ is

$$\bar{Q} = \frac{1}{T}\int_0^T Qdt^* = q + 1 + \frac{\epsilon^2}{2}, \tag{4.30}$$

where λ is the wavelength of metachronal wave, c is the wave speed and t^* is the mean averaged time.

4.2 Solution of the Problem

To obtain the solution of governing equations we use homotopy perturbation method [80] which is described as follow

$$\mathcal{H}(j,w) = (1-j)\big(\mathcal{L}(w) - \mathcal{L}(w_0)\big)$$
$$+j\left(\mathcal{L}(w) - \frac{1}{(1-\varphi)^{2.5}}\frac{\partial p}{\partial z} + \frac{1}{r}\frac{\partial}{\partial r}\left(rmWe\left(\frac{\partial w}{\partial r}\right)^2\right)\right), \tag{4.31}$$

$$\mathcal{H}(j,\theta) = (1-j)\big(\mathcal{L}(\theta) - \mathcal{L}(\theta_0)\big)$$
$$+j\left(\mathcal{L}(\theta) - \frac{Br}{(1-\varphi)^{2.5}}\frac{k_f}{k_{nf}}\left(1+m\left(We\frac{\partial w}{\partial r}-1\right)\right)\left(\frac{\partial w}{\partial r}\right)^2\right). \tag{4.32}$$

The linear operator and initial guesses are chosen as

$$\mathcal{L}(w) = (1-m)\left(\frac{\partial^2 w}{\partial r^2} + \frac{1}{r}\frac{\partial w}{\partial r}\right), \tag{4.33}$$

$$\mathcal{L}(\theta) = \frac{\partial^2 \theta}{\partial r^2} + \frac{1}{r}\frac{\partial \theta}{\partial r}. \tag{4.34}$$

$$w_0 = \frac{(1-\varphi)^{2.5}}{4(1-m)}\frac{dp_0}{dz}(r^2-h^2) + w(h), \tag{4.35}$$

$$\theta_0 = \frac{r^2-h^2}{4}. \tag{4.36}$$

According to homotopy perturbation method

$$w = w_0 + jw_1 + j^2 w_2 \ldots, \tag{4.37a}$$
$$\theta = \theta_0 + j\theta_1 + j^2\theta_2 \ldots, \tag{4.37b}$$
$$p = p_0 + jp_1 + j^2 p_2 \ldots, \tag{4.37c}$$

where $j \in [0,1]$ is the homotopy perturbation parameter and $j = 0$ gives initial guess and $j = 1$ gives the final solution. With the help of Eqs. (4.31) - (4.37), second order solution for the velocity and temperature profile are given as follow

$$w = w(h) + A_{27}(r^2-h^2) + A_{28}(r^3-h^3), \tag{4.38}$$

and

$$\theta = \frac{1}{(1-\varphi)^{2.5}}\frac{k_f}{k_{nf}}\left(\frac{A_{29}}{16}(r^4-h^4) + \frac{A_{30}}{25}(r^5-h^5) + \frac{A_{31}}{36}(r^6-h^6)\right) \tag{4.39}$$

$$+\frac{1}{(1-\varphi)^{2.5}}\frac{k_f}{k_{nf}}\left(\frac{A_{32}}{49}(r^7-h^7)+\frac{A_{33}}{64}(r^8-h^8)\right).$$

Integrating Eq. (4.27) using software "**MATHEMATICA**" and calculating pressure gradient in the following form

$$\frac{dp}{dz}=\frac{-A_{35}\pm\sqrt{A_{35}^2-4A_{34}A_{36}}}{2A_{34}}. \tag{4.40}$$

4.3 Entropy Generation

Entropy generation can be written as

$$S'''_{gen}=\frac{k_f}{T_\infty^2}\left(\left(\frac{\partial T}{\partial r}\right)^2+\left(\frac{\partial T}{\partial z}\right)^2\right)+\frac{1}{T_0}\tau_{zr}\frac{\partial w}{\partial r}. \tag{4.41}$$

Dimensionless form of entropy generation can be written as

$$N_S=\frac{S'''_{gen}}{S'''_G}=\left(\frac{\partial\theta}{\partial r}\right)^2+Br\Lambda\left(1+m\left(We\frac{\partial w}{\partial r}-1\right)\right)\left(\frac{\partial w}{\partial r}\right)^2, \tag{4.42}$$

$$S'''_G=\frac{k_f T_0^2}{\bar{\theta}_0^2 a^2}, \qquad \Lambda=\frac{\bar{\theta}_0}{T_0}. \tag{4.43}$$

4.4 Graphical Results

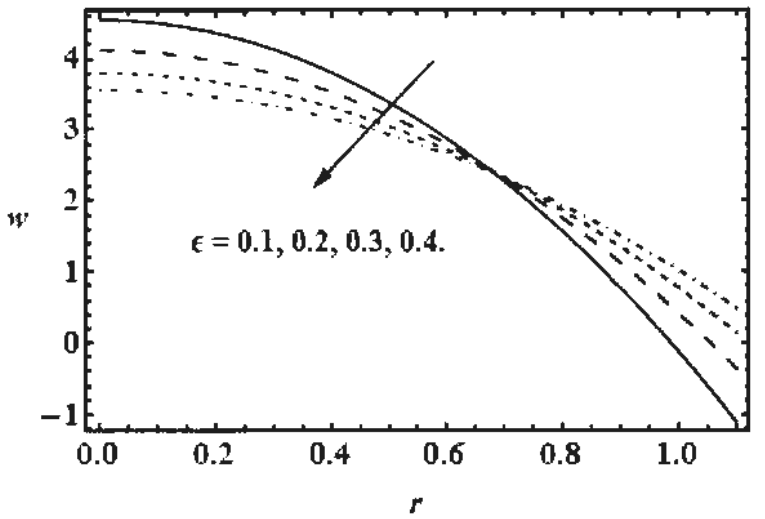

Fig. 4.2: Impact of cilia length parameter ϵ on axial velocity w for $m = 0.1$ and $\varphi = 0.2$.

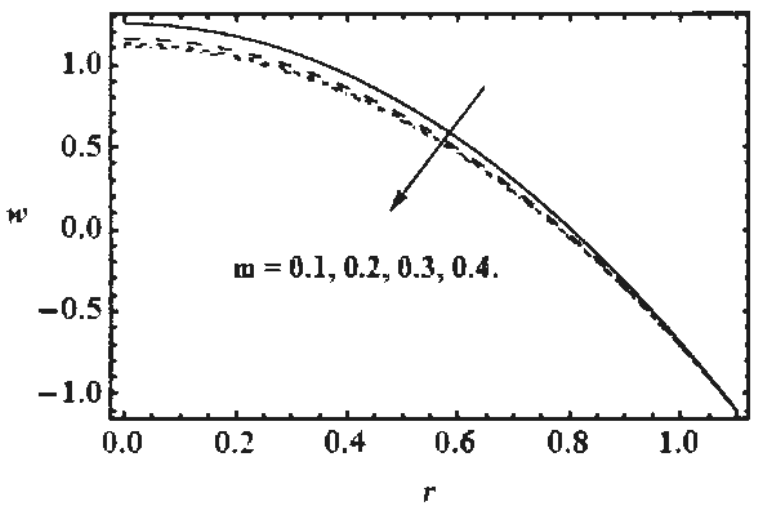

Fig. 4.3: Impact of power law index m on axial velocity w for $\epsilon = 0.2$ and $\varphi = 0.2$.

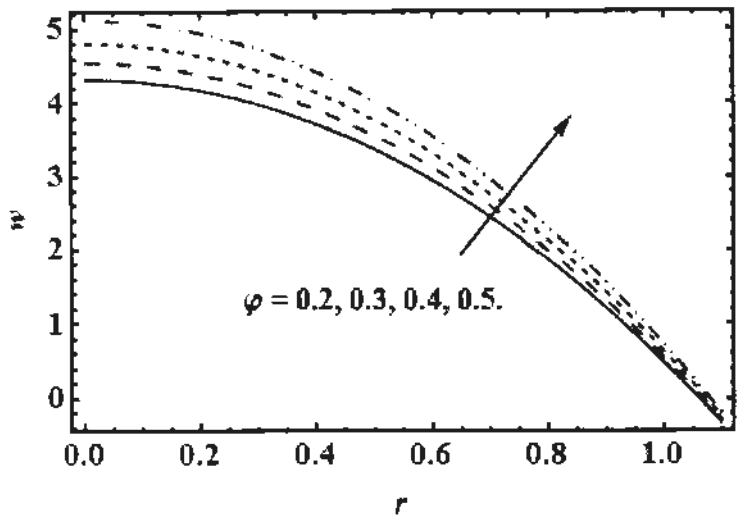

Fig. 4.4: Impact of nanoparticles volume fraction φ on axial velocity w for $\epsilon = 0.2$ and $m = 0.1$.

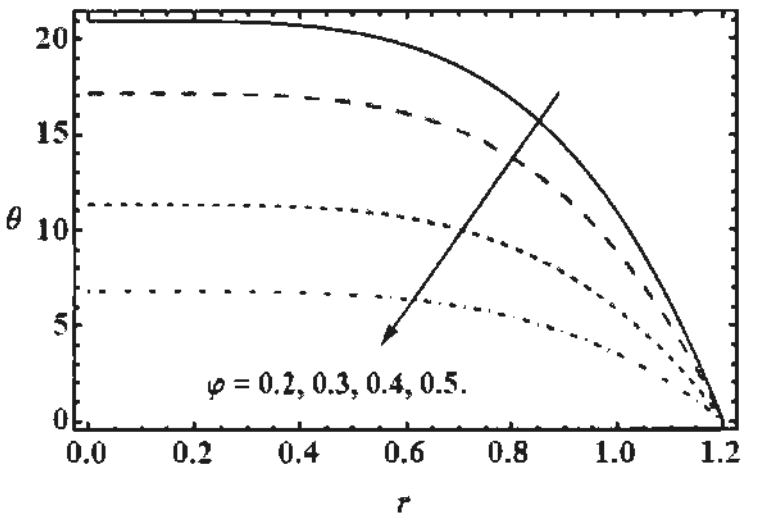

Fig. 4.5: Impact of nanoparticles volume fraction φ on temperature field θ for $Br = 1$ and $m = 0.1$.

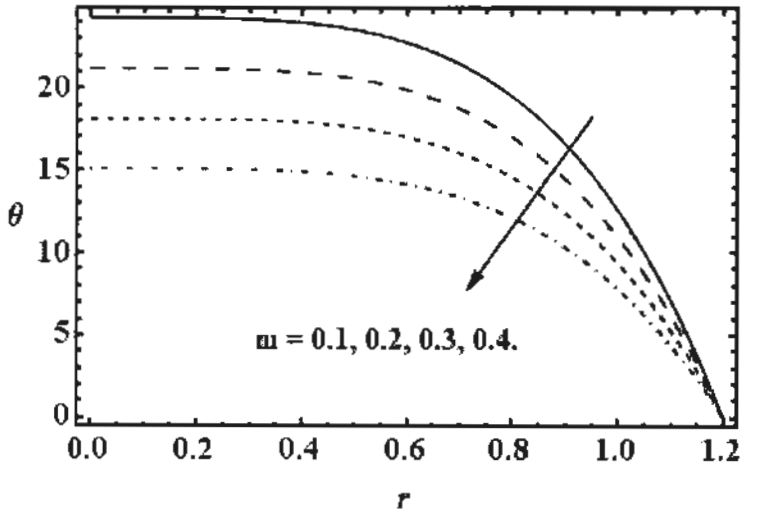

Fig. 4.6: Influence of power law index m on temperature profile θ for $Br = 1$ and $\varphi = 0.1$.

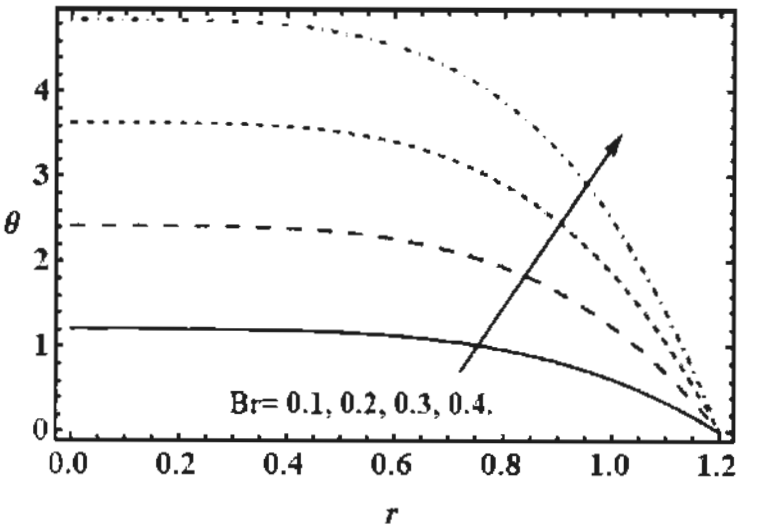

Fig. 4.7: Influence of Brinkman number Br on temperature profile θ for $\varphi = 0.1$ and $m = 0.1$.

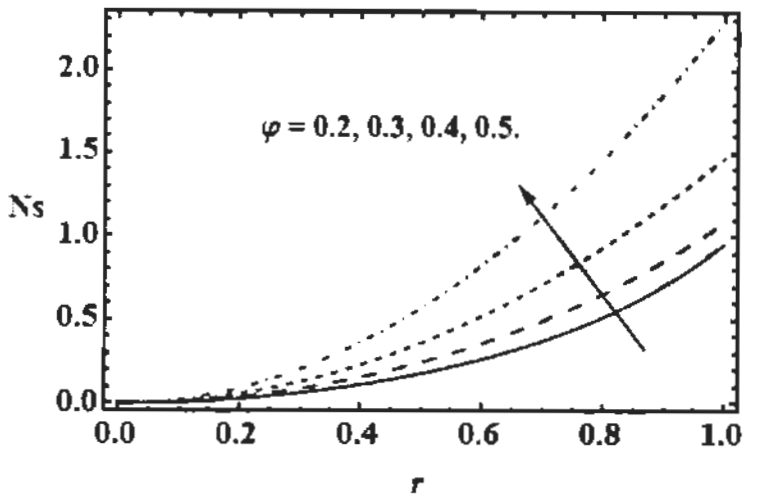

Fig. 4.8: Influence of nanoparticles volume fraction φ on entropy generation Ns for $Br = 1$ and $m = 0.1$.

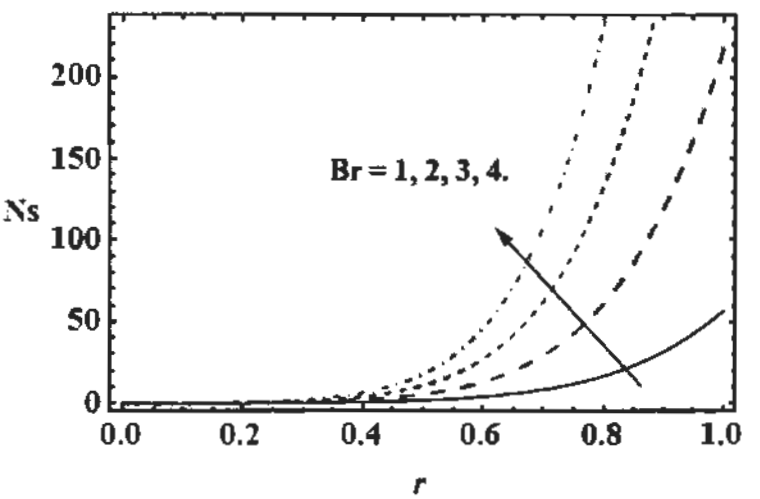

Fig. 4.9: Influence of Brinkman number Br on entropy generation Ns for $m = 0.1$ and $\varphi = 0.1$.

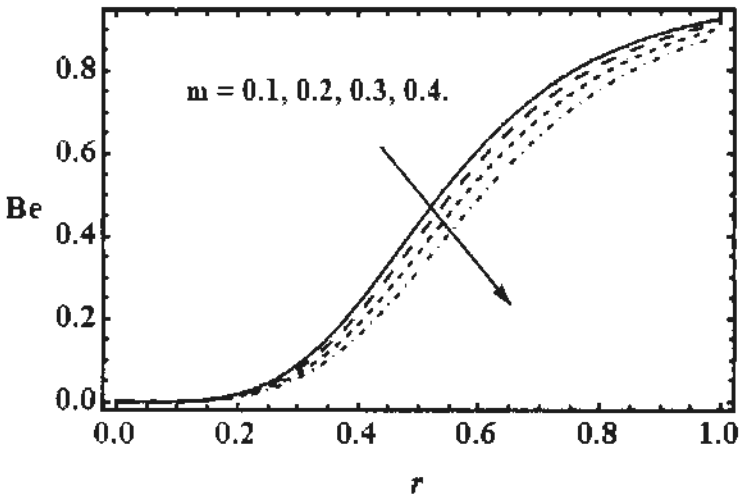

Fig. 4.10: Influence of power law index m on entropy generation Ns for $Br = 1$ and $\varphi = 0.1$.

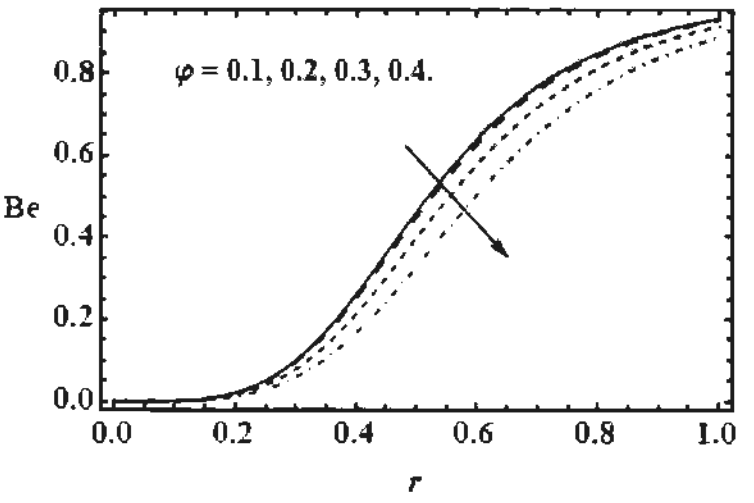

Fig. 4.11: Influence of nanoparticles volume fraction φ on Bejan number Be for $Br = 1$ and $m = 0.1$.

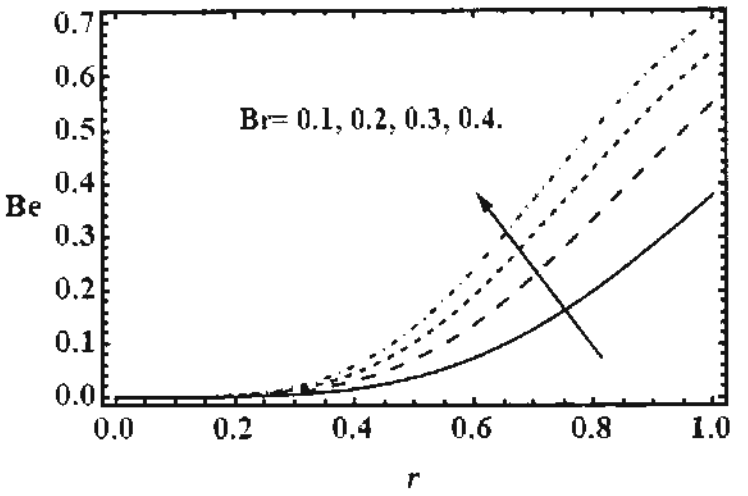

Fig. 4.12: Influence of Brinkman number Br on Bejan number Be for $m = 0.1$ and $\varphi = 0.1$.

4.5 Discussion

The mathematical model of tangent hyperbolic nanofluid flow through ciliated tube is governed by the energy and momentum equations. The profiles of velocity and temperature, pressure gradient, entropy generation and Bejan number are presented through plots.

In this section graphical results have shown the effects of different parameters of interest. The cilia induced flow of a tangent hyperbolic nanofluid in circular tube is investigated. The effect of emerging parameters for the entropy generation, and stream functions are observed.

Axial velocity for various values of, cilia length ϵ, power law index m and nanoparticle volume fraction of the fluid φ, are observed in figures 4.2 – 4.4. In Fig. 4.2 the velocity of fluid decreases by increasing cilia length parameter as increase in cilia length resist the fluid flow at the center of tube. Fig. 4.3 shows that velocity of fluid decreases by increasing power law index m because by increasing m fluid

behaves like a shear thickening fluid which causes the decrease in velocity of fluid. Fig. 4.4 shows that velocity increases by increasing nanoparticle volume fraction of the fluid because when nanoparticles are high in fluid, they will move quickly that increases the velocity of the fluid.

Temperature profile for different values of nanoparticle volume fraction of the fluid φ, power law index m and Brickman number Br are observed in Figs. $4.5 - 4.7$. It can be seen that temperature is maximum at the centre of tube and minimum at the ciliated walls where it is effected by ciliated walls. Fig 4.5 illustrates that by increasing nanoparticle volume fraction of the fluid φ, temperature profile decreases. Fig. 4.6 shows that by increasing power law index m temperature profile decreases. Brinkman number is the ratio of viscous heat generation to external heating. So by increasing Brinkman number viscous heat generation will increase as compared to external heating; therefore, temperature will increase.

In Figs $4.8 - 4.10$ entropy generation for different values of nanoparticle volume fraction of the fluid φ, power law index m and Brinkman number Br are observed. It can be depicted that entropy generation is maximum at the ciliated walls and minimum at the centre of tube.

In Figs. $4.11 - 4.13$ Bejan number for different values of nanofluid volume fraction φ, power law index m and Brinkman number Br is observed. Furthermore by increasing φ and m Bejan number decreases while by increasing Brinkman number Br Bejan number increases.

4.6 Conclusions

In this study we have developed a mathematical model of velocity and temperature profile in the presence of nanoparticles in base fluids. Ciliated surfaces are present at the boundaries of tube due to which fluid motion is produced. The continuous

movement of cilia creates elliptical envelop known as metachronal waves. The boundary conditions are defined at mean radius of cylinder therefore horizontal and vertical velocity are defined at the mean radius $(r = a)$. The governing differential equations involve the parameter depend upon, volume fractions of nanoparticles. The differential equations are solved by homotopy perturbation method (HPM). The following main points are concluded

- Axial velocity of the fluid increases by inserting nanoparticles.
- Thermal conductivity of fluid increases by adding nanoparticles.
- The entropy generation due to nanoparticles will decrease the viscosity on the wall so of tube and blood will flow with less/normal pressure.

Chapter 5

Heat Transfer Analysis for Tangent Hyperbolic Cilia Induced Nano Fluid Flow

In this chapter, we illustrate the mathematical modeling of tangent hyperbolic fluid (blood) under the effect of magnetic field, porous medium and copper nanoparticles passing through cylindrical tube. Momentum and energy equations are modeled for tangent hyperbolic nano-fluid and solved by Adomian decomposition method with the help of software "MATHEMATICA". The impact of various parameters have been discussed through graphs

5.1 Mathematical Model

Consider a tangent hyperbolic nano-fluid flow in a tube of mean radius a in a porous medium. Assume infinite number of continuously beating cilia are present at the inner walls of tube generating symplectic metachronal wave which moves towards positive z-axis with wave speed c.

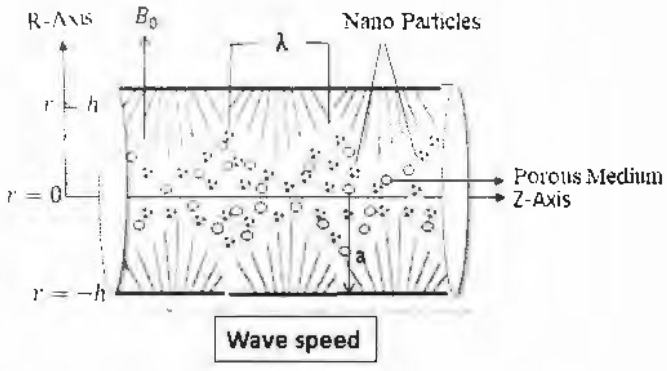

Figure 5.1: Geometry of ciliated tube.

Governing equations for an incompressible MHD tangent hyperbolic nano-fluid through porous medium are defined as [86]

$$\rho_f \frac{dV}{dt} = div\boldsymbol{\tau} + \sigma(\boldsymbol{J} \times \boldsymbol{B}) + \boldsymbol{R}, \tag{5.1}$$

$$(\rho c)_f \frac{dT}{dt} = k_{nf}\nabla^2 T + trace(\boldsymbol{\tau}.\boldsymbol{L}). \tag{5.2}$$

where $\boldsymbol{V} = (u, 0, w)$, $\boldsymbol{J}$ is the current density, $\boldsymbol{B}$ is the strength of magnetic field, R is the Darcy's resistance, T is the temperature profile, $\boldsymbol{L}$ is gradient of velocity and $\boldsymbol{\tau}$ is defined as follows.

$$\boldsymbol{\tau} = -p\boldsymbol{I} + \boldsymbol{S}, \tag{5.3}$$

$$\boldsymbol{S} = [(\eta_\infty + (\eta_0 + \eta_\infty)\tanh(\Gamma\dot{\gamma})^m)\dot{\gamma}_i], \tag{5.4}$$

$$\dot{\gamma} = \sqrt{\frac{1}{2}\boldsymbol{\pi}}, \qquad \dot{\gamma}_i = \boldsymbol{L} + \boldsymbol{L}^T, \tag{5.5}$$

$$where \ \ \boldsymbol{\pi} = trace(gradV + gradV^T)^2,$$

In this study we consider $\eta_\infty = 0$ and $\Gamma\dot{\gamma} < 1$.

Now stress tensor takes the following form

$$\dot{\gamma}_i = \boldsymbol{L} + \boldsymbol{L}^T, \tag{5.6}$$

$$\boldsymbol{S} = \eta_0((\Gamma\dot{\gamma})^m)\dot{\gamma}_i = \eta_0(1 + \Gamma\dot{\gamma} - 1)^m\dot{\gamma}_i = \eta_0\big(1 + m(\Gamma\dot{\gamma} - 1)\big)\dot{\gamma}_i, \tag{5.7}$$

where thermal conductivity of Cu+blood nano-fluid is defined as follows

$$\rho_{nf} = (1-\varphi)\rho_f + \varphi\rho_s,$$

$$\eta_{nf} = \frac{\eta_f}{(1-\varphi)^{2.5}},$$

$$\big(\rho c_p\big)_{nf} = (1-\varphi)\big(\rho c_p\big)_f + \varphi\big(\rho c_p\big)_s,$$

$$\alpha_{nf} = \frac{k_{nf}}{\big(\rho c_p\big)_{nf}},$$

$$k_{nf} = k_f\left(\frac{k_s + 2k_f - 2\varphi(k_f - k_s)}{k_s + 2k_f + 2\varphi(k_f - k_s)}\right), \tag{5.8}$$

where k_{nf} is the thermal conductivity of nano-fluid, k_f is the thermal conductivity of base fluid, k_s is the thermal conductivity of solid nano particles and φ is the solid volume fraction. The Mathematical model for geometry of cilia tips in the wave frame is

$$h = 1 + \epsilon \cos 2\pi z, \tag{5.9a}$$

$$w(h) = -1 - 2\pi\epsilon\alpha\beta \cos 2\pi z. \tag{5.9b}$$

The governing equations of motion of tangent hyperbolic fluid model in a tube are specified as follows.

$$\frac{1}{r}\frac{\partial}{\partial r}(ru) + \frac{\partial w}{\partial z} = 0, \tag{5.10}$$

$$\rho_f E(w) = F_1(S_{rz}) + \frac{\partial S_{zz}}{\partial z} - \left(\sigma {B_0}^2 + \frac{\eta_f}{k}\right)(w + c) - \frac{\partial p}{\partial z}, \tag{5.11}$$

$$\rho_f E(u) = F_1(S_{rr}) + \frac{\partial S_{zr}}{\partial z} - \frac{\partial p}{\partial r}, \tag{5.12}$$

$$(\rho c)_f E(T) = k_{nf}\left(F_1(T) + \frac{\partial^2 T}{\partial z^2}\right) + S_{zr}\frac{\partial w}{\partial r}. \tag{5.13}$$

where ρ_f is the fluid density, u and w are the radial and axial components of velocity, c is the wave speed, η_f is the apparent viscosity of fluid and k is the permeability parameter.

The following parameters can be introduced to non- dimensionalize above quantities

$$z^* = \frac{z}{\lambda}, \quad u^* = \frac{u}{\beta c}, \quad r^* = \frac{r}{a}, \quad w^* = \frac{w}{c}, \quad p^* = \frac{a\beta}{c\mu}p, \quad h^* = \frac{h}{a},$$

$$\beta = \frac{a}{\lambda}, \quad {S_{ij}}^* = \frac{a}{\mu c}S_{ij}, \quad \lambda_1 = \frac{c\lambda_1}{a}, \quad Re = \frac{\rho a\beta}{\mu}, \quad We = \frac{\Gamma c}{a},$$

$$\alpha_f = \frac{k}{(\rho c)_f}, \quad \theta = \frac{T - T_0}{T_0}, \quad M = \sqrt{\frac{\sigma}{\mu}}a{B_0}^2, \quad D_a = \frac{k}{a^2}, \tag{5.14}$$

$$Br = \frac{a^2\eta_f}{k_f T_0}, \qquad Pr = \frac{\mu c_p}{k_f}, \qquad Ec = \frac{c^2}{c_p T_0}.$$

where λ, a, c symbolize the wavelength, width of velocity and wave speed respectively. In terms of dimensionless parameters the momentum equations and shear stresses are

$$\frac{1}{r}\frac{\partial}{\partial r}(ru) + \frac{\partial w}{\partial z} = 0, \tag{5.15}$$

$$Re\beta[E(w)] = F_1(S_{rz}) + \beta\frac{\partial S_{zz}}{\partial z} - \left(M^2 + \frac{1}{D_a}\right)(w+1) - \frac{\partial p}{\partial z}, \tag{5.16}$$

$$Re\beta^2 E(u) = \beta\left(F_1(S_{rr})\right) + \beta^2\frac{\partial S_{zr}}{\partial z} - \beta\frac{\partial S_{\theta\theta}}{\partial z} - \frac{\partial p}{\partial r}, \tag{5.17}$$

$$\beta(\rho c)_f E(\theta) = k_{nf}\left(F_1(\theta) + \beta^2\frac{\partial^2\theta}{\partial z^2}\right) + S_{zr}\frac{\partial w}{\partial r}, \tag{5.18}$$

$$\tau_{rz} = \left(1 + m\left(We\frac{\partial w}{\partial r} - 1\right)\right)\frac{\partial w}{\partial r}. \tag{5.19}$$

After using long wavelength approximation ($\beta \to 0$) the boundary value problem takes the following form

$$\frac{\partial p}{\partial z} = (1-m)\left(F_1(w)\right) + mWe\frac{1}{r}\frac{\partial}{\partial r}\left(r\left(\frac{\partial w}{\partial r}\right)^2\right) - \left(M^2 + \frac{1}{D_a}\right)(w+1), \tag{5.20}$$

$$-\frac{\partial p}{\partial r} = 0, \tag{5.21}$$

$$\frac{k_{nf}}{k_f}\left(F_1(\theta)\right) = -Br\frac{\eta_{nf}}{\eta_f}\left(1 + m\left(We\frac{\partial w}{\partial r} - 1\right)\right)\left(\frac{\partial w}{\partial r}\right)^2. \tag{5.22}$$

$$\frac{\partial w}{\partial r} = 0, \qquad \frac{\partial \theta}{\partial r} = 0 \qquad at \quad r = 0, \tag{5.23a}$$

$$w = w(h), \qquad \theta = 0 \qquad at \quad r = h. \tag{5.23b}$$

Integration of Eq. (5.15) over the tube width is given as:

$$\int_0^h \left[\frac{1}{r}\frac{\partial(ru)}{\partial r} + \frac{\partial w}{\partial z}\right] r dr = 0, \tag{5.24}$$

$$hu(h) + \frac{1}{2}\frac{\partial q}{\partial z} - h\frac{\partial h}{\partial z}w(h) = 0, \tag{5.25}$$

where $q = 2\int_0^h rw dr$.

Eq. (5.25) can be written as

$$\frac{\partial q}{\partial z} = 2h\left(\frac{\partial h}{\partial z}w(h) - u(h)\right). \tag{5.26}$$

The relation between q and dimensionless volume flow rate Q is given by

$$Q = 2\int_0^h RWdR = 2\int_0^h (w+1)rdr = q + h^2, \tag{5.27}$$

The mean volume flow rate for the time period $T = \frac{\lambda}{c}$ is

$$\bar{Q} = \frac{1}{T}\int_0^T Qdt^* = q + 1 + \frac{\epsilon^2}{2}, \tag{5.28}$$

where λ is the wavelength of metachronal wave, c is the wave speed and t^* is the mean averaged time.

5.2 Solution of the Problem

To obtain the solution of governing equations, we use Adomian decomposition method [78-79].

$$\mathcal{L} + mWe\frac{1}{r}\frac{\partial}{\partial r}\left(r\left(\frac{\partial w}{\partial r}\right)^2\right) - \left(M^2 + \frac{1}{D_a}\right)(w+1) - \frac{\partial p}{\partial z} = 0. \tag{5.29}$$

The linear and inverse operator are chosen as follows

$$\mathcal{L} = \frac{1}{r}\frac{\partial}{\partial r}\left(r(1-m)\frac{\partial w}{\partial r}\right), \tag{5.30}$$

$$\mathcal{L}^{-1} = \int\left[\frac{1}{r(1-m)}\int r[.]\,dr\right]dr. \tag{5.31}$$

Applying $\mathcal{L}^{-1}$ on Eq. (5.29) we get

$$w = c_1 \ln r + c_2 - \mathcal{L}^{-1}\left[\begin{array}{c}\frac{M^2}{1-m}w + \frac{m}{1-m}mWe\frac{1}{r}\frac{\partial}{\partial r}\left(r\left(\frac{\partial w}{\partial r}\right)^2\right) \\ + \frac{m}{1-m}\mathcal{L}^{-1}{}_{rw}\left(M^2 + \frac{1}{D_a}\right)\end{array}\right]. \tag{5.32}$$

Adomian decomposition method yields the following infinite series

$$w = \sum_{n=0}^{\infty} w_n, \tag{5.33}$$

Initial guess and recursive relation can be chosen in a following manner.

$$w_0 = c_1 \ln r + c_2 \frac{1}{1-m}\left(M^2 + \frac{1}{D_a}\right)\frac{r^2}{4}, \tag{5.34}$$

$$w_{n+1} = -\mathcal{L}^{-1}\left[\frac{M^2}{1-m}w_n + \frac{m}{1-m}We\frac{1}{r}\frac{\partial}{\partial r}\left(r\left(\frac{\partial w_n}{\partial r}\right)^2\right)\right]. \tag{5.35}$$

With the help of boundary conditions, initial guess takes the following form.

$$w_0 = \frac{1}{4(1-m)}\frac{dp}{dz}(r^2 - h^2) + w(h), \tag{5.36}$$

$$w = w(h) + A_1(r^2 - h^2) + A_2(r^3 - h^3) + A_3(r^4 - h^4) + A_4(r^5 - h^5) + A_5(r^6 - h^6). \tag{5.39}$$

Using Eq. (5.39) in Eq. (5.24), we get

$$\begin{aligned}\theta = {} & A_6(r^4 - h^4) + A_7(r^5 - h^5) + A_8(r^6 - h^6) + A_9(r^7 - h^7) + \\ & A_{10}(r^8 - h^8) + A_{11}(r^9 - h^9) + A_{12}(r^{10} - h^{10}) \\ & + A_{13}(r^{11} - h^{11}) + A_{14}(r^{12} - h^{12}) + A_{15}(r^{13} - h^{13}) \\ & A_{16}(r^{14} - h^{14}) + A_{17}(r^{15} - h^{15}) + A_{18}(r^{16} - h^{16}) \\ & A_{19}(r^{17} - h^{17}).\end{aligned} \tag{5.40}$$

Integrating Eq. (5.39) using software "**MATHEMATICA**" calculating pressure gradient as

$$\frac{dp}{dz} = -\frac{C_2}{3C_1} - \frac{2^{\frac{1}{2}}\left(-C_2{}^2 + 3C_1C_3\right)}{3C_1\left(C_5 + \sqrt{4(C_6)^3 - (C_7)^2}\right)^{\frac{1}{3}}} + \frac{\left(C_8 + \left(C_5 + \sqrt{4(C_9)^3 - (C_{10})^2}\right)^{\frac{1}{3}}\right)}{3 \times 2^{\frac{1}{3}}C_1}. \tag{5.41}$$

5.3 Entropy Generation

Entropy generation can be written as

$$S'''_{gen} = \frac{k_f}{T_\infty^2}\left(\left(\frac{\partial T}{\partial r}\right)^2 + \left(\frac{\partial T}{\partial r}\right)^2\right) + \frac{1}{T_0}\tau_{zr}\frac{\partial w}{\partial r}. \tag{5.42}$$

Dimensionless form of entropy generation can be written as

$$N_S = \frac{S'''_{gen}}{S'''_G} = \left(\frac{\partial \theta}{\partial r}\right)^2 + Br\Lambda\left(1 + m\left(We\frac{\partial w}{\partial r} - 1\right)\right)\left(\frac{\partial w}{\partial r}\right)^2, \tag{5.43}$$

$$S'''_G = \frac{k_f T_0^2}{\bar{\theta}_0^2 a^2}, \qquad \Lambda = \frac{\bar{\theta}_0}{T_0}. \tag{5.44}$$

5.4 Graphical Results

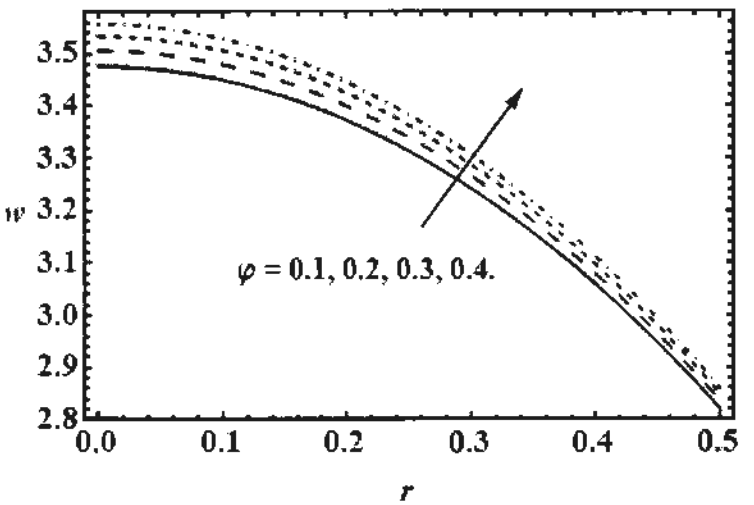

Fig. 5.2: Impact of nanoparticles volume fraction φ on axial velocity w for $M = 0.1$ and $D_a = 1$.

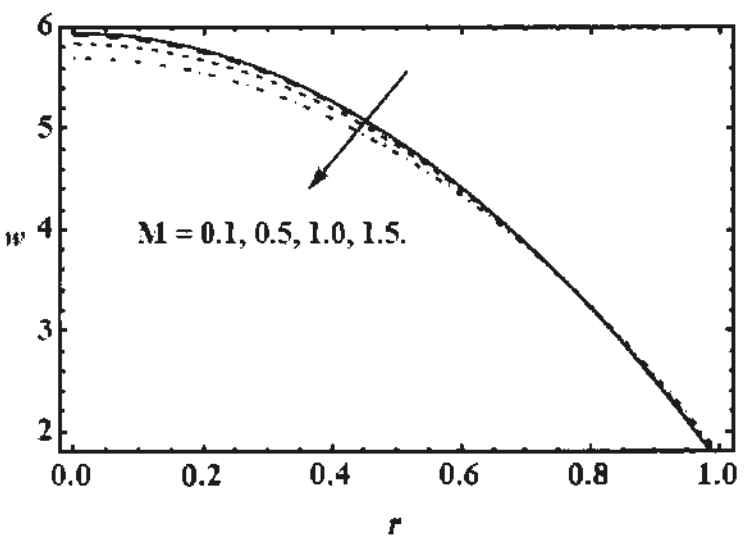

Fig. 5.3: Impact of Hartmann number M on axial velocity w for $\varphi = 0.1$ and $D_a = 1$.

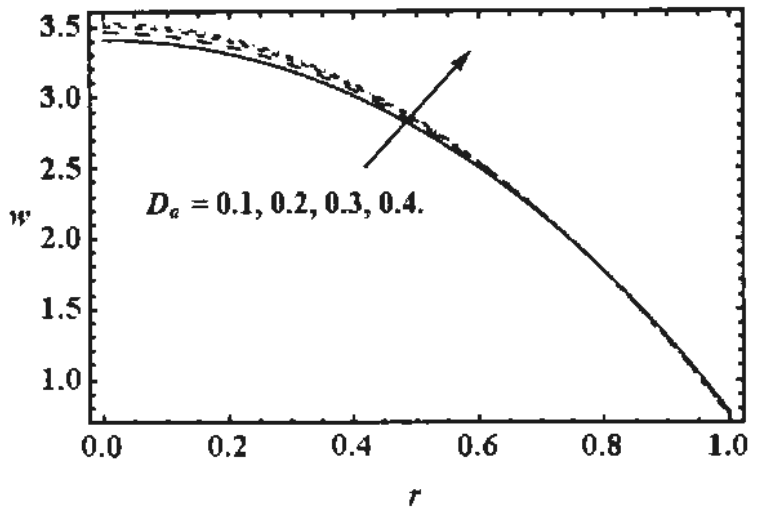

Fig. 5.4: Influence of Darcy's parameter D_a on axial velocity w for $\varphi = 0.1$ and $M = 0.1$.

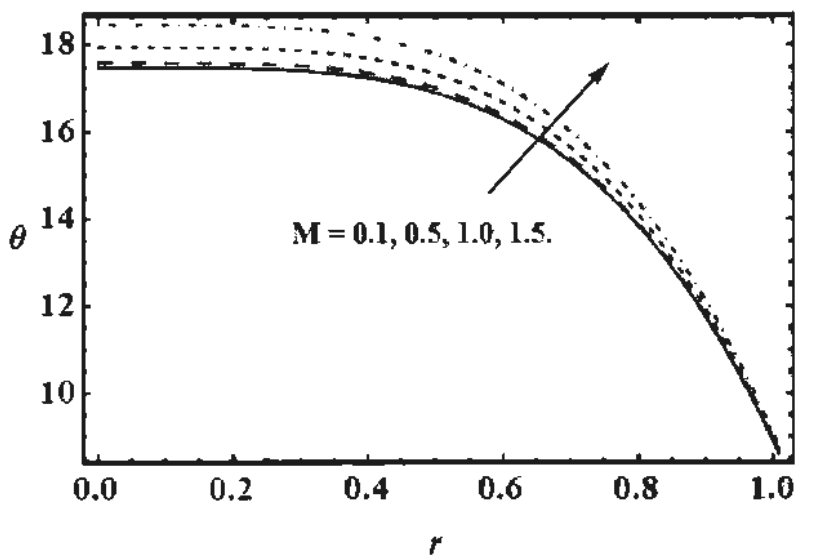

Fig. 5.5: Impact of Hartmann number M on temperature field θ for $\varphi = 0.1$ and $D_a = 1$.

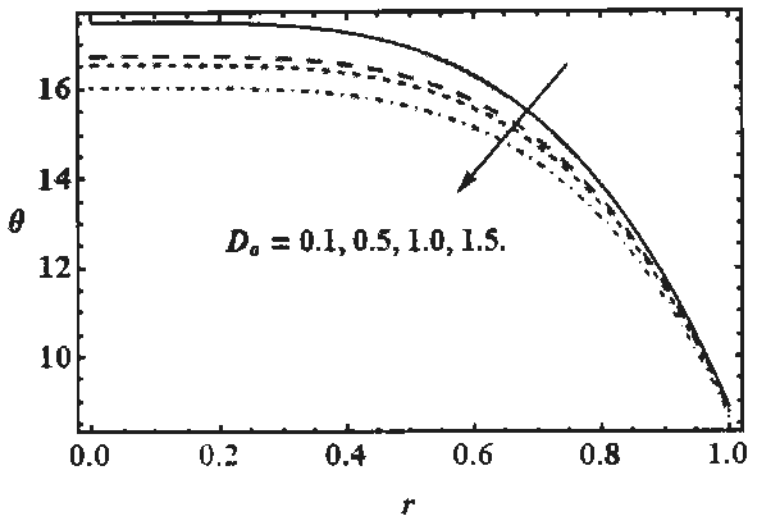

Fig. 5.6: Impact of Darcy's parameter D_a on temperature field θ for $\varphi = 0.1$ and $M = 0.1$.

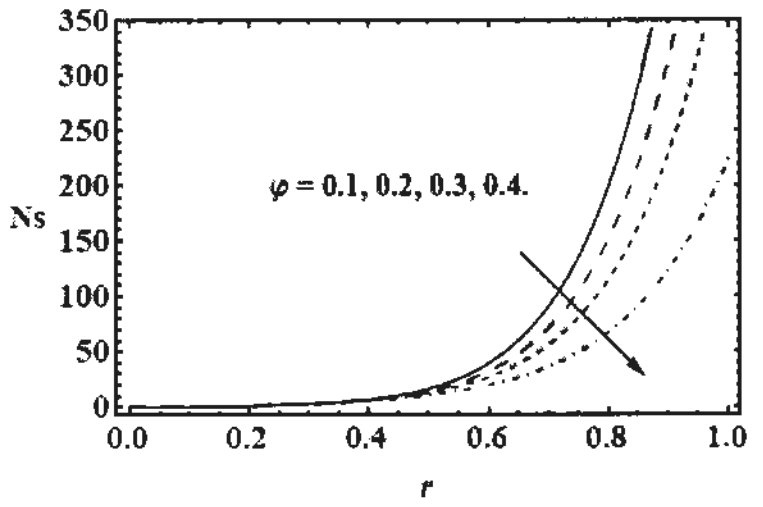

Fig. 5.7: Influence of nanoparticles volume fraction φ on entropy generation Ns for $M = 0.1$ and $D_a = 1$.

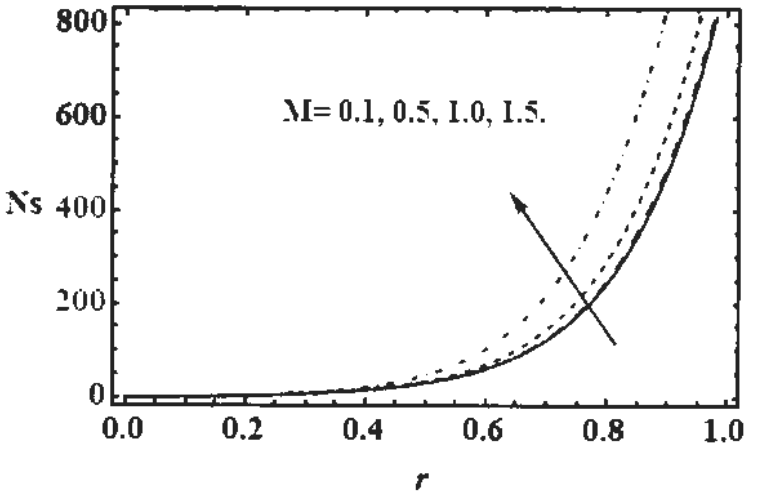

Fig. 5.8: Influence of magnetic parameter M on entropy generation Ns for $\varphi = 0.1$ and $D_a = 1$.

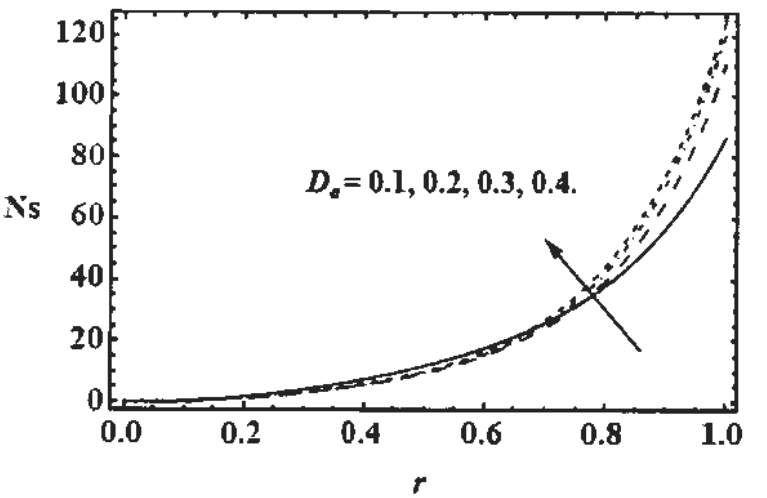

Fig. 5.9: Influence of Darcy's parameter D_a on entropy generation Ns for $\varphi = 0.1$ and $M = 0.1$.

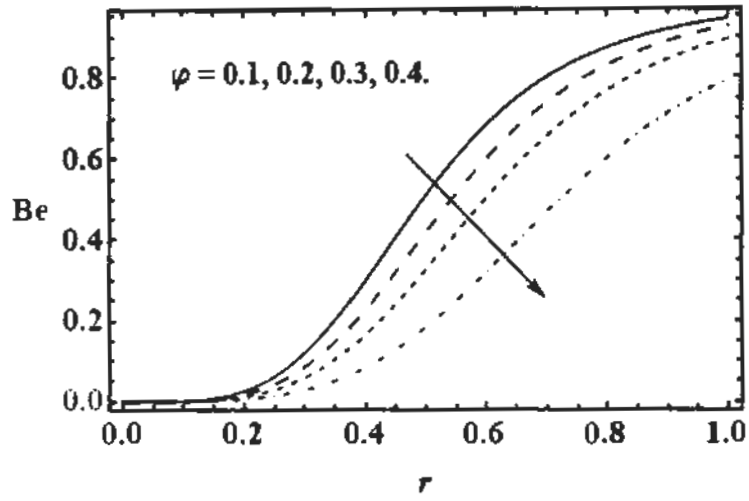

Fig. 5.10: Impact of nanoparticles volume fraction φ on Bejan number Be for $M = 0.1$ and $D_a = 1$.

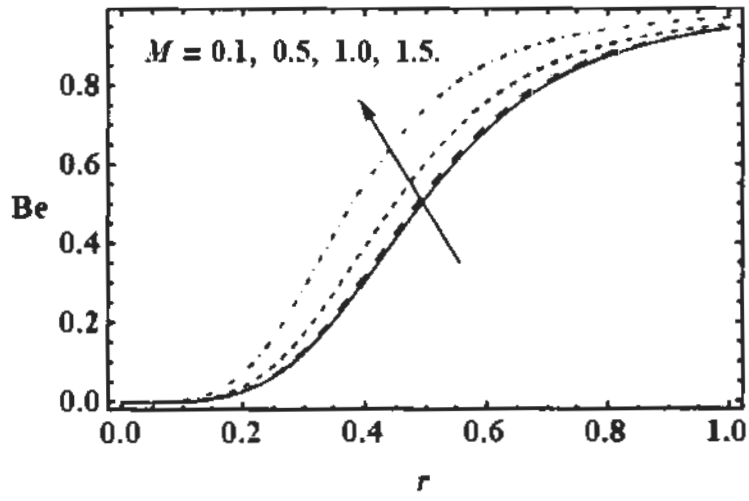

Fig. 5.11: Influence of Hartmann number M on Bejan number Be for $\varphi = 0.1$ and $D_a = 1$.

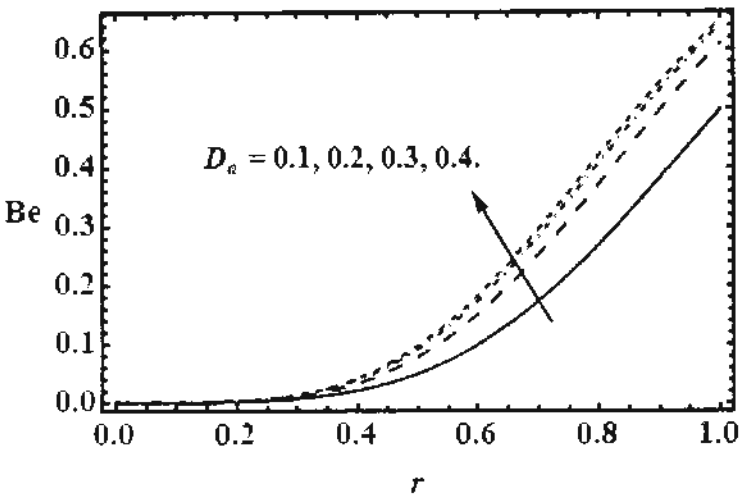

Fig. 5.12: Influence of Darcy's parameter D_a on Bejan number Be for $\varphi = 0.1$ and $M = 0.1$.

5.5 Discussion

In this section, graphical results have shown the impact of various parameters of interest. The cilia induced flow of a tangent hyperbolic nano-fluid in circular tube is investigated. The effect of emerging parameters for the entropy generation, and stream functions are observed.

Axial velocity for various values of, nanoparticle volume fraction of the fluid φ, Hartmann number M and Darcy's number D_a are observed in figures $5.2 - 5.4$. Fig. 5.2 shows that velocity increases by increasing nanoparticle volume fraction of the fluid because when nanoparticles are increased in fluid, they will move fastly enhancing the velocity of the fluid. Fig. 5.3 shows that velocity of fluid decreases by increasing Hartmann number M because Lorentz force always opposes the fluid motion and Fig. 5.4 shows that velocity increases by increasing Darcy's number velocity of fluid increases because as Darcy's number increases which means more porous is the medium and fluid permeability increases and fluid through porous layer meets little resistance.

Temperature profile for distinct values of Hartmann number M and Darcy's number D_a are observed in Figs. 5.5 – 5.6. It can be seen that temperature is maximum near the middle of tube and minimum at the boundaries where it is effected by ciliated walls. Fig. 5.5 shows that by increasing Hartmann number M temperature profile increases as some supplementary work has to be done by the fluid to drag it against Lorentz force which in result increases kinetic energy which is dissipated as heat. Fig. 5.6 shows that by increasing Darcy's number temperature profile decreases. This is due to decrease in thermal boundary layer thickness.

In Fig. 5.7 – 5.9 entropy generation for distinct values of nanoparticle volume fraction of the fluid φ, Hartmann number M, and Darcy's number D_a are observed. It can be depicted that entropy generation is maximum at the ciliated walls and minimum at the centre of tube. It is noted in Figs. 5.7 entropy generation increases by increasing nano-fluid volume fraction. As φ increases effective thermal conductivity of blood rises due to which rate of heat transfer increases and temperature decreases therefore entropy generation decreases. In Fig. 5.8, it can be seen by increasing magnetic parameter entropy generation rises. Due to increase in Hartmann number temperature of fluid rises thus entropy generation is increased. In Fig. 5.9, it is noticed that entropy generation increases by increasing Darcy's number. As by increasing Darcy's number thermal boundary layer thickness reduces therefore heat transfer increases and temperature decreases which rises entropy generation.

In Figs. 5.10 – 5.12, Bejan number for different values of nanoparticle volume fraction of the fluid φ, Hartmann number M, and Darcy's number D_a are observed. As heat transfer across a finite temperature difference is small and frictional forces are also negligible at center due to which Bejan number decreases at the middle of the tube and at the walls of tube Bejan number is maximum. It is noted in Fig. 5.10 that Bejan

number decreases with an increase in nanoparticles volume fraction φ which shows that total entropy generation in blood flow is greater than entropy generation with the help of heat transfer. From Figs. 5.11 and 5.12 it can be noted that by increasing Hartmann number M and Darcy's numher D_a Bejan number increases which shows that entropy generation due to heat transfer is greater than net entropy generation.

5.6 Conclusions

In this study, we have developed a mathematical model of forced convective flow of tangent hyperholic fluid through a ciliated axisymmetric tube in a porous medium. Effects of copper nano particles, MHD and porous media are observed for the blood flow (tangent hyperbolic fluid) in a tube. The fluid is flowing due to presence of ciliated surface which is considered as a continuous envelope obtained by the coordinated cilia. The boundary conditions are considered at the center of the tube and on the tip of cilia which is anchored in the wall of the tuhe and formed a wavy surface. The simulation shows that energy and momentum equations involves physical parameter like velocity, temperature, pressure, thermal conductivity to see the effects of nano particles, MHD and porous medium for the enhancement of heat transfer. The present study can he validated by the work of [30] if m⟶0 present model reduces to Newtonian fluid model. Following observations are highlighted in the present study.

- The large distribution of nanoparticles into the hase fluid (blood) enhance the heat transfer.
- The blood flow along the tube has been accelerated by increasing the volume fraction of nanoparticles.
- The speed of the fluid flow has been decelerated by imposing the applied magnetic field in the transverse direction whereas heat transfer has increased by applying the magnetic field.

- The blood flow requires less amount of pressure due to the presence of nano particles.
- The presence of nanoparticles in base fluid results in weak disorder which helps to reduce viscous dissipation effects.

Chapter 6

Effect of Temperature difference on Airway Mucus Clearance in Cilia Induced Flow with Inertial Forces

In this chapter, thermal analysis of cilia-induced flow of mucus clearance through an idealized two-dimensional model of the human airway is presented. The cilia motion is simulated by an elliptic wave pattern which is responsible for the mobilization of highly viscous mucus with nonzero Reynolds numbers. The mucus is analyzed with the robust Upper Convective Maxwell (UCM) viscoelastic formulation. The resulting differential equations are perturbed about wave number. Flow rate, temperature profile and velocity distribution are calculated via the regular perturbation method, pressure rise is computed with numerical integration in symbolic software "MATHEMATICA. The influence of selected parameters for prescribed values of wave number are visualized graphically.

6.1 Mathematical Modeling

The physical model for this problem is shown in **Fig. 6.1**. We consider the thermal analysis of an incompressible, Maxwell cilia induced flow. An infinite number of beating adjacent cilia are present along the internal wall surface of the tube and they collectively generate a metachronal wave which propagate in the direction of z-axis. This generates fluid motion and the sustained whip-motions propel the mucus downstream. The elliptic envelope model [76-77] is adopted for which the motion of

tips of cilia are assumed to trace elliptic paths. The continuity, momentum and energy equations may then be written as:

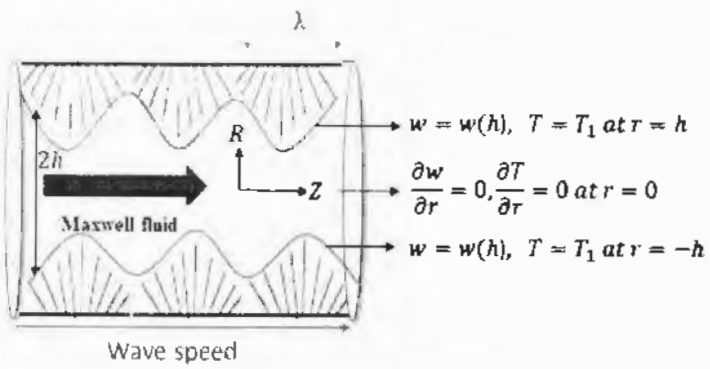

Fig. 6.1: Model for airways mucus clearance

$$\nabla . \boldsymbol{V} = 0, \tag{6.1}$$

$$\rho \frac{d\boldsymbol{V}}{Dt} = div\boldsymbol{\tau}, \tag{6.2}$$

$$\boldsymbol{\tau} = -\boldsymbol{p}\boldsymbol{I} + \boldsymbol{S}, \tag{6.3}$$

$$\rho c_p \frac{dT}{dt} = k\nabla^2 T + trace(\boldsymbol{S}.\boldsymbol{L}). \tag{6.4}$$

Here the extra stress tensors for Maxwell viscoelastic model are defined as [88 & 89]

$$\boldsymbol{S} + \boldsymbol{\lambda_1}\left(\frac{\boldsymbol{dS}}{\boldsymbol{dt}} - \boldsymbol{L}^T\boldsymbol{S} - \boldsymbol{S}\boldsymbol{L}\right) = \mu \boldsymbol{A_1}. \tag{6.5}$$

The velocity vector in Eq. (6.2) for axisymmetric flow in the ciliated tube can be chosen as follows

$$V = (u(r,z), 0, w(r,z)). \tag{6.6}$$

The component from of Eq. (6.2), can be written in the following manner

$$F_1(u) = -\frac{\partial w}{\partial z}, \tag{6.7}$$

$$\rho E(u) = G(S_{rr}) + \frac{\partial S_{rz}}{\partial z} - \frac{S_{\theta\theta}}{r} - \frac{\partial p}{\partial r}, \tag{6.8}$$

$$\rho E(w) = G(S_{rz}) + \frac{\partial S_{zz}}{\partial z} - \frac{\partial p}{\partial z}, \tag{6.9}$$

$$c_p \rho E(T) + S_{rz}\left(\frac{\partial u}{\partial z} + \frac{\partial w}{\partial r}\right) + kF_1(T) + \frac{\partial^2 T}{\partial z^2} + S_{rr}\frac{\partial u}{\partial r} + S_{zz}\frac{\partial w}{\partial z} = 0. \tag{6.10}$$

Where $G = \frac{1}{r}\frac{\partial}{\partial r}(r(.))$

Here the shear and normal stresses satisfy the following expressions:

$$S_{rr} + \lambda_1\left(E(S_{rr}) - 2\frac{\partial u}{\partial r}S_{rr} - 2\frac{\partial u}{\partial z}S_{rz}\right) = 2\eta\frac{\partial u}{\partial r}, \tag{6.11}$$

$$S_{rz} + \lambda_1\left(E(S_{rz}) - \frac{\partial u}{\partial z}S_{zz} - \frac{\partial w}{\partial z}S_{zr} - \frac{\partial u}{\partial r}S_{zr} - \frac{\partial w}{\partial r}S_{rr}\right) = \eta\frac{\partial u}{\partial z} + \eta\frac{\partial w}{\partial r}, \tag{6.12}$$

$$S_{zz} + \lambda_1\left(E(S_{zz}) - 2\frac{\partial w}{\partial r}S_{rz} - 2\frac{\partial w}{\partial z}S_{zz}\right) = 2\eta\frac{\partial w}{\partial z}. \tag{6.13}$$

With boundary conditions

$$\frac{\partial w}{\partial r} = 0, \quad \frac{\partial T}{\partial r} = 0 \qquad at\ centre\ of\ tube\ r = 0 \tag{6.14a}$$

$$w = \frac{-\left(\frac{2\pi}{\lambda}\right)\left[\epsilon a a c \sin\frac{2\pi}{\lambda}z\right]}{1 - \left(\frac{2\pi}{\lambda}\right)\left[\epsilon a \alpha \cos\frac{2\pi}{\lambda}z\right]} \tag{6.14b}$$

$$u = \frac{\left(\frac{2\pi}{\lambda}\right)\left[\epsilon a a c \sin\frac{2\pi}{\lambda}z\right]}{1 - \left(\frac{2\pi}{\lambda}\right)\left[\epsilon a \alpha \cos\frac{2\pi}{\lambda}z\right]}, T = T_1 \tag{6.14c}$$

at

$$r = h(z) = \left[a + \epsilon a a \cos\frac{2\pi}{\lambda}z\right].$$

To normalize the above equations, the following non-dimensional parameters are introduced:

$$z^* = \frac{z}{\lambda}, \quad u^* = \frac{u}{\beta c}, \quad Re = \frac{\rho a c}{\mu}, \quad p^* = \frac{a\beta}{c\mu}p, \quad S_{ij}{}^* = \frac{a}{\mu c}S_{ij},$$

$$\beta = \frac{a}{\lambda}, \quad \lambda_1{}^* = \frac{c\lambda_1}{a}, \quad r^* = \frac{r}{a}, \quad w^* = \frac{w}{c}, \theta = \frac{T - T_0}{T_1 - T_0},$$

$$h^* = \frac{h}{a}, \quad Pr = \frac{\mu c_p}{k}, Ec = \frac{c^2}{c_p(T_1 - T_0)}, \quad Br = Pr.Ec. \tag{6.15}$$

Here z^* denotes dimensionless axial coordinate, r^* denotes dimensionless radial coordinate, w^* is dimensionless axial velocity, h^* is dimensionless radius of the tube, p^* is dimensionless hydrodynamic pressure, β is dimensionless wave number, S^*_{ij} is the non-dimensional stress tensor, λ_1 is Maxwell relaxation time parameter, λ is metachronal wavelength, respectively, T_0 is the temperature at the centre of flow regime and T_1 is the temperature of the fluid adjacent to the ciliated wall. After using Eq. (6.5) and dropping the asterisk notation for dimensionless quantities, Eqs. (6.7)-(6.14) in non-dimensional form are:

$$\frac{\partial u}{\partial r} + \frac{\partial w}{\partial z} = -\frac{u}{r}, \tag{6.16}$$

$$Re\beta^3 E(u) = \beta G(S_{rr}) - \beta\frac{S_{\theta\theta}}{r} + \beta^2\frac{\partial S_{zr}}{\partial z} - \frac{\partial p}{\partial r}, \tag{6.17}$$

$$Re\beta E(w) = G(S_{zr}) + \beta\frac{\partial S_{zz}}{\partial z} - \frac{\partial p}{\partial z}, \tag{6.18}$$

$$\beta RePrE(\theta) = \left(F_1(\theta) + \beta^2\frac{\partial^2\theta}{\partial z^2}\right)$$
$$+Br\left(\beta S_{zz}\frac{\partial w}{\partial z} + \beta S_{rr}\frac{\partial u}{\partial r} + S_{zr}\frac{\partial w}{\partial r} + \beta^2 S_{rz}\frac{\partial u}{\partial z}\right). \tag{6.19}$$

$$S_{rr} + \lambda_1\beta\left[E(S_{rr}) - 2\frac{\partial u}{\partial r}S_{rr} - 2\beta\frac{\partial u}{\partial z}S_{zr}\right] = 2\beta\frac{\partial u}{\partial r}, \tag{6.20}$$

$$S_{rz} + \lambda_1\left(\beta E(S_{rz}) - \beta S_{zr}\frac{\partial w}{\partial z} - \beta S_{zr}\frac{\partial u}{\partial z}S_{zz} - \frac{\partial w}{\partial r}S_{rr}\right)$$
$$-\beta^2\frac{\partial u}{\partial z} = \frac{\partial w}{\partial r}, \tag{6.21}$$

$$S_{zz} + \beta\lambda_1 E(S_{zz}) - 2\lambda_1 \frac{\partial w}{\partial r} S_{rz} = 2\beta \frac{\partial w}{\partial z} - 2\lambda_1 \beta \frac{\partial w}{\partial z} S_{zz}. \tag{6.22}$$

along with boundary conditions

$$\frac{\partial \theta}{\partial r} = 0, \qquad \frac{\partial w}{\partial r} = 0, \qquad at \;\; r = 0 \tag{6.23a}$$

$$w = w(h) = -(1 + 2\pi\epsilon a\beta \cos(2\pi z)), \tag{6.23b}$$

$$u = u(h) = 2\pi\epsilon(\sin(2\pi z)) + \beta 2\pi\epsilon a \sin(2\pi z)\cos(2\pi z), \quad \theta = 1 \tag{6.23c}$$

at

$$r = h(z) = [a + \epsilon a a \cos(2\pi z)],$$

To reduce the unknowns, it is judicious to define following dimensional stream function

$$u = \frac{-1}{r}\frac{\partial \psi}{\partial z}, \qquad w = \frac{1}{r}\frac{\partial \psi}{\partial r}. \tag{6.24}$$

Eqs. (6.17) to (6.23) are transformed into following form

$$\beta^3\left(-\frac{1}{r^3}\left(\frac{\partial \psi}{\partial z}\right)^2 + \frac{1}{r^2}\frac{\partial \psi}{\partial z}\frac{\partial^2 \psi}{\partial z \partial r} - \frac{1}{r^2}\frac{\partial^3 \psi}{\partial r \partial z^2}\right) = \beta G(S_{rr}) - \frac{\partial p}{\partial r} + \beta^2 \frac{\partial S_{zz}}{\partial z} - \beta \frac{S_{\theta\theta}}{r}, \tag{6.25}$$

$$\beta Re\left(\frac{\partial}{\partial r}\left(\frac{1}{r}\frac{\partial \psi}{\partial r}\right)\left(\frac{-1}{r}\frac{\partial \psi}{\partial z}\right) + \frac{\partial}{\partial z}\left(\frac{1}{r}\frac{\partial \psi}{\partial z}\right)\left(\frac{1}{r}\frac{\partial \psi}{\partial r}\right)\right) = G(S_{rz}) - \frac{\partial p}{\partial z} + \beta \frac{\partial S_{zz}}{\partial z}, \tag{6.26}$$

$$\beta RePr\left[\frac{\partial \theta}{\partial r}\left(\frac{-1}{r}\frac{\partial \psi}{\partial z}\right) + \frac{\partial \theta}{\partial z}\left(\frac{1}{r}\frac{\partial \psi}{\partial r}\right)\right] = \left(F_1(\theta) + \beta^2 \frac{\partial^2 \theta}{\partial z^2}\right) + Br\left(-\beta S_{rr}\frac{\partial}{\partial r}\left(\frac{\partial \psi}{\partial z}\frac{1}{r}\right) - \frac{\beta^2}{r}S_{rz}\frac{\partial}{\partial z}\left(\frac{\partial \psi}{\partial z}\right) + S_{zr}\frac{\partial}{\partial r}\left(\frac{\partial \psi}{\partial r}\frac{1}{r}\right) + \frac{\beta}{r}S_{zz}\frac{\partial}{\partial z}\left(\frac{\partial \psi}{\partial r}\right)\right. \tag{6.27}$$

Eliminating pressure gradient from Eqs. (6.25)-(6.26), one can set following form

$$\beta^3 Re\frac{\partial}{\partial z}\left(\frac{-1}{r}\frac{\partial\psi}{\partial z}\frac{\partial}{\partial r}\left(-\frac{1}{r}\frac{\partial\psi}{\partial z}\right)+\left(\frac{1}{r}\frac{\partial\psi}{\partial r}\right)\frac{\partial}{\partial z}\left(-\frac{1}{r}\frac{\partial\psi}{\partial z}\right)\right)$$
$$-\beta Re\frac{\partial}{\partial r}\left(\frac{-1}{r}\frac{\partial\psi}{\partial z}\frac{\partial}{\partial r}\left(\frac{1}{r}\frac{\partial\psi}{\partial r}\right)+\left(\frac{1}{r}\frac{\partial\psi}{\partial r}\right)\frac{\partial}{\partial z}\left(\frac{1}{r}\frac{\partial\psi}{\partial r}\right)\right)$$
$$=\frac{\partial}{\partial z}\left(\frac{\beta}{r}\frac{\partial}{\partial r}(rS_{rr})+\beta^2\frac{\partial S_{zz}}{\partial z}-\beta\frac{S_{\theta\theta}}{r}\right) \tag{6.28}$$
$$-\frac{\partial}{\partial r}\left(\frac{1}{r}\frac{\partial}{\partial r}(rS_{rz})+\beta\frac{\partial S_{zz}}{\partial z}\right),$$

where

$$S_{rr}+\lambda_1\beta\left[\frac{1}{r}\left(-\frac{\partial\psi}{\partial z}\frac{\partial}{\partial r}+\frac{\partial\psi}{\partial r}\frac{\partial}{\partial z}\right)S_{rr}+2\beta\frac{\partial}{\partial r}\left(\frac{1}{r}\frac{\partial\psi}{\partial z}\right)S_{rr}+2\beta^2\frac{\partial}{\partial z}\left(\frac{1}{r}\frac{\partial\psi}{\partial z}\right)S_{rz}\right]$$
$$=-2\beta\frac{\partial}{\partial r}\left(\frac{1}{r}\frac{\partial\psi}{\partial z}\right), \tag{6.29}$$

$$S_{rz}+\lambda_1\beta\left[\begin{array}{c}\frac{1}{r}\left(-\frac{\partial\psi}{\partial z}\frac{\partial}{\partial r}+\frac{\partial\psi}{\partial r}\frac{\partial}{\partial z}\right)S_{rz}-\beta\left(\frac{\partial}{\partial z}\left(\frac{1}{r}\frac{\partial\psi}{\partial r}\right)-\frac{\partial}{\partial r}\left(\frac{1}{r}\frac{\partial\psi}{\partial z}\right)\right)S_{rz}\\ +\beta^2\frac{\partial}{\partial z}\left(\frac{1}{r}\frac{\partial\psi}{\partial z}\right)S_{zz}-\frac{\partial}{\partial r}\left(\frac{1}{r}\frac{\partial\psi}{\partial r}\right)S_{rr}\end{array}\right]$$
$$=\beta^2\frac{\partial}{\partial z}\left(\frac{-1}{r}\frac{\partial\psi}{\partial z}\right)+\frac{\partial}{\partial r}\left(\frac{1}{r}\frac{\partial\psi}{\partial r}\right), \tag{6.30}$$

$$S_{zz}+\lambda_1\left[\frac{\beta}{r}\left(-\frac{\partial\psi}{\partial z}\frac{\partial}{\partial r}+\frac{\partial\psi}{\partial r}\frac{\partial}{\partial z}\right)S_{zz}-2\frac{\partial}{\partial r}\left(\frac{1}{r}\frac{\partial\psi}{\partial r}\right)S_{rz}-2\beta\frac{\partial}{\partial z}\left(\frac{1}{r}\frac{\partial\psi}{\partial r}\right)S_{zz}\right]$$
$$=2\beta\frac{\partial}{\partial z}\left(\frac{1}{r}\frac{\partial\psi}{\partial r}\right). \tag{6.31}$$

The volume flow rate in the inertial frame can be written as:

$$Q(Z,t)=2\pi\int_0^h RW(R,Z,t)dR, \tag{6.32}$$

In the laboratory (wave) frame volumetric flow rate becomes:

$$q=2\pi\int_0^h rw(r,z)dr, \tag{6.33}$$

Using Eqns. (6.16), (6.32) and (6.33), we obtain:

$$Q(Z,t)=q+c\pi h^2, \tag{6.34}$$

The average volume flow rate can be defined as:

$$Q^* = \frac{1}{T}\int_0^1 Qdt = q + a^2 c\pi\left(1 + \frac{\varepsilon^2}{2}\right), \tag{6.35}$$

Defining $\bar{Q} = \frac{Q^*}{2a^2 c\pi}$ and $F = \frac{Q}{2a^2 c\pi}$ it follows that dimensionless mean-time volumetric flow rate:

$$\bar{Q} = F + \left(1 + \frac{\varepsilon^2}{2}\right). \tag{6.36}$$

Boundary conditions in terms of stream function can be written as

$$\psi = 0, \frac{\partial\theta}{\partial r} = 0, \qquad by\ convension \tag{6.37a}$$

$$\frac{\partial}{\partial r}\left(\frac{1}{r}\frac{\partial\psi}{\partial r}\right) = 0\ \ by\ \ symmetry\ \ at\ \ r = 0, \tag{6.37b}$$

$$\left(\frac{1}{r}\frac{\partial\psi}{\partial r}\right) = w(h)\ \ by\ \ no\ \ slip\ \ condition \tag{6.37c}$$

$$\psi = F, \theta = 1 \qquad at\ \ r = h. \tag{6.37d}$$

6.2 Perturbation Solution

To find the solution of BVP perturbation technique [78] is implemented so, expand the stream function ψ, pressure distribution p, stress S and flux F in power series of small parameter β (Since wave number have inverse relationship with wavelength and wave length of metachronal wave is large as compared to diameter of tube).

$$\psi = \psi_0 + \beta\psi_1 + \beta^2\psi_2 \ldots, \tag{6.38a}$$

$$p = p_0 + \beta p_1 + \beta^2 p_2 \ldots, \tag{6.38b}$$

$$S = S_0 + \beta S_1 + \beta^2 S_2 \ldots, \tag{6.38c}$$

$$F = F_0 + \beta F_1 + \beta^2 F_2 \ldots, \tag{6.38d}$$

$$\theta = \theta_0 + \beta\theta_1 + \beta^2\theta_2 \ldots. \tag{6.38e}$$

6.2.1 System of Zeroth Order

After lengthy algebraic calculations, the following boundary value problems for the stream function, pressure gradient, temperature profile and stress components can be derived.

$$\frac{\partial}{\partial r}\left(\frac{1}{r}\frac{\partial}{\partial r}\left(r\frac{\partial}{\partial r}\left(\frac{1}{r}\frac{\partial \psi_0}{\partial r}\right)\right)\right) = 0, \tag{6.39a}$$

$$\frac{\partial p_0}{\partial z} = \frac{1}{r}\frac{\partial}{\partial r}\left(r\frac{\partial}{\partial r}\left(\frac{1}{r}\frac{\partial \psi_0}{\partial r}\right)\right), \tag{6.39b}$$

$$\frac{\partial p_0}{\partial r} = 0, \tag{6.39c}$$

$$\frac{1}{r}\frac{\partial}{\partial r}\left(r\frac{\partial \theta_0}{\partial r}\right) = -Br\frac{\partial}{\partial r}\left(\frac{1}{r}\frac{\partial \psi_0}{\partial r}\right)S_{0rz}, \tag{6.39d}$$

$$S_{0rr} = 0, \tag{6.39e}$$

$$S_{0rz} = \frac{\partial}{\partial r}\left(\frac{1}{r}\frac{\partial \psi_0}{\partial r}\right), \tag{6.39f}$$

$$S_{0zz} = 2\lambda_1\frac{\partial}{\partial r}\left(\frac{1}{r}\frac{\partial \psi_0}{\partial r}\right)S_{0rz}. \tag{6.39g}$$

$$S_{0\theta\theta} = 0. \tag{6.39h}$$

The associated boundary conditions are:

$$\psi_0 = 0, \qquad \frac{\partial}{\partial r}\left(\frac{1}{r}\frac{\partial \psi_0}{\partial r}\right) = 0, \qquad \frac{\partial \theta_0}{\partial r} = 0 \qquad at\ \ r = 0, \tag{6.40a}$$

$$\psi_0 = F_0, \qquad \frac{\partial \psi_0}{\partial r} = w(h), \qquad \theta_0 = 1 \qquad at\ \ r = h. \tag{6.40b}$$

Pressure rise per wavelength can be calculated as:

$$\Delta p_{\lambda_0} = \int \frac{\partial p_0}{\partial z}dz. \tag{6.41}$$

6.2.2 System of First Order

$$Re\frac{\partial}{\partial r}\left(-\frac{1}{r}\frac{\partial\psi_0}{\partial z}\frac{\partial}{\partial r}\left(\frac{1}{r}\frac{\partial\psi_0}{\partial r}\right)+\left(\frac{1}{r}\frac{\partial\psi_0}{\partial r}\right)\frac{\partial}{\partial z}\left(\frac{1}{r}\frac{\partial\psi_0}{\partial z}\right)\right)$$
$$=\frac{\partial}{\partial z}\left(\frac{1}{r}\frac{\partial}{\partial r}(rS_{0rr})-\frac{S_{0\theta\theta}}{r}\right)-\frac{\partial}{\partial r}\left(\frac{1}{r}\frac{\partial}{\partial r}(rS_{1rz})+\frac{\partial S_{0zz}}{\partial z}\right), \tag{6.42a}$$

$$\frac{\partial p_1}{\partial z}=-Re\left(\left(\frac{-1}{r}\frac{\partial\psi_0}{\partial z}\right)\frac{\partial}{\partial r}\left(\frac{1}{r}\frac{\partial\psi_0}{\partial r}\right)+\left(\frac{1}{r}\frac{\partial\psi_0}{\partial r}\right)\frac{\partial}{\partial z}\left(\frac{1}{r}\frac{\partial\psi_0}{\partial r}\right)\right)$$
$$+\frac{1}{r}\frac{\partial}{\partial r}(rS_{1rz})+\frac{\partial S_{0zz}}{\partial z}, \tag{6.42b}$$

$$\frac{1}{r}\frac{\partial}{\partial r}\left(r\frac{\partial\theta_1}{\partial r}\right)=-\frac{\partial}{\partial r}\left(\frac{1}{r}\frac{\partial\psi_1}{\partial r}\right)S_{0rz}-\frac{\partial}{\partial r}\left(\frac{1}{r}\frac{\partial\psi_0}{\partial r}\right)S_{1rz}-\frac{\partial}{\partial r}\left(\frac{1}{r}\frac{\partial\psi_0}{\partial r}\right)S_{0zz}$$
$$+RePr\left(\left(\frac{-1}{r}\frac{\partial\psi_0}{\partial z}\right)\frac{\partial\theta_0}{\partial r}+\left(\frac{1}{r}\frac{\partial\psi_0}{\partial r}\right)\frac{\partial\theta_0}{\partial z}\right), \tag{6.42c}$$

$$\frac{\partial p_1}{\partial r}=0, \tag{6.42d}$$

$$S_{1rr}=-2\frac{\partial}{\partial r}\left(\frac{1}{r}\frac{\partial\psi_0}{\partial z}\right), \tag{6.42e}$$

$$S_{1rz}=\frac{\partial}{\partial r}\left(\frac{1}{r}\frac{\partial\psi_1}{\partial r}\right)-\lambda_1\left[\left(-\frac{1}{r}\frac{\partial\psi_0}{\partial z}\frac{\partial}{\partial r}+\frac{1}{r}\frac{\partial\psi_0}{\partial r}\frac{\partial}{\partial z}\right)\right]S_{0rz}-S_{1rr}\frac{\partial}{\partial r}\left(\frac{1}{r}\frac{\partial\psi_0}{\partial r}\right)$$
$$-\left[\frac{\partial}{\partial r}\left(\frac{1}{r}\frac{\partial\psi_0}{\partial z}\right)+\frac{\partial}{\partial z}\left(\frac{1}{r}\frac{\partial\psi_0}{\partial r}\right)\right]S_{0rz}, \tag{6.42f}$$

The relevant boundary conditions are:

$$\psi_1=0, \qquad \frac{\partial}{\partial r}\left(\frac{1}{r}\frac{\partial\psi_1}{\partial r}\right)=0, \qquad \frac{\partial\theta_1}{\partial r}=0 \qquad at\ \ r=0. \tag{6.43a}$$

$$\psi_1=F_1, \qquad \frac{1}{r}\frac{\partial\psi_1}{\partial r}=0 \quad , \qquad \theta_1=0 \qquad at\ \ r=h. \tag{6.43b}$$

Integrating Eq. (6.42b) we get pressure rise

$$\Delta p_{\lambda_1}=\int\frac{\partial p_1}{\partial z}dz. \tag{6.44}$$

6.3 Graphical Results

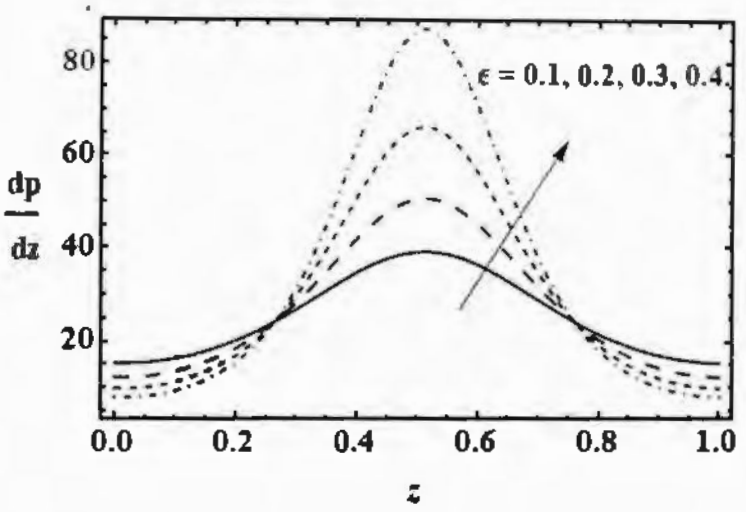

Fig. 6.2: Influence of cilia length parameter ϵ on pressure gradient $\frac{dp}{dz}$ for $Re = 0.1 \ \ and \ \ \lambda_1 = 1.$

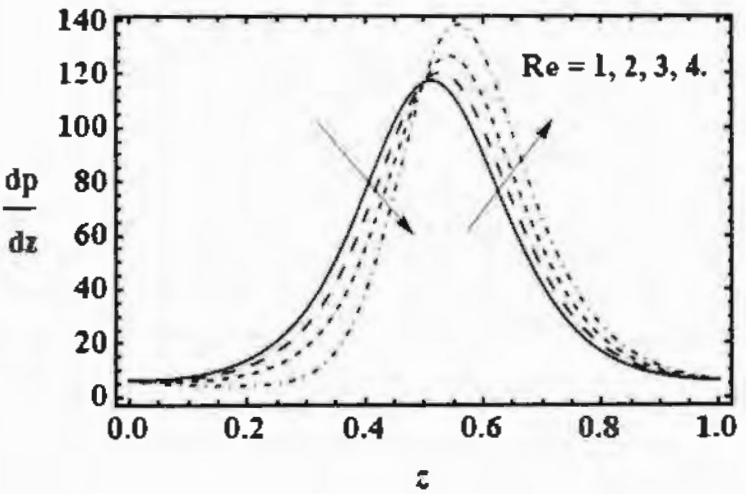

Fig. 6.3: Influence of Reynolds number Re on pressure gradient $\frac{dp}{dz}$ for $Re = 0.1 \ \ and \ \ \lambda_1 = 1.$

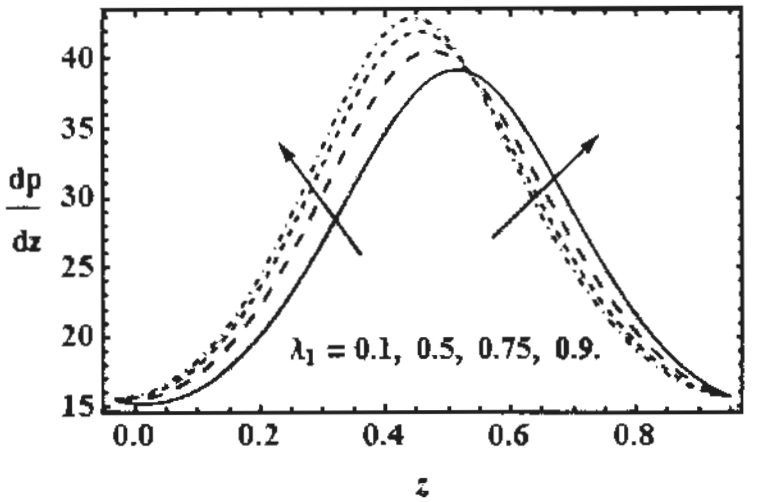

Fig. 6.4: Influence of Maxwell's parameter λ_1 on pressure gradient $\frac{dp}{dz}$ for $Re = 0.1$ and $\epsilon = 0.1$.

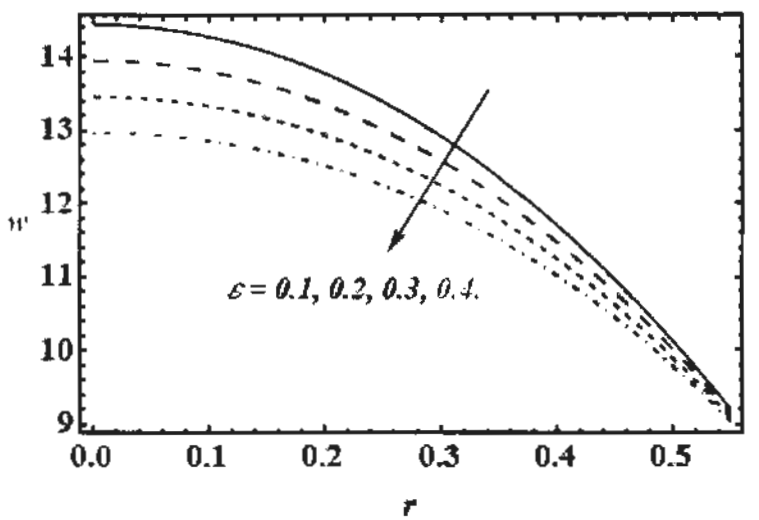

Fig. 6.5: Influence of cilia length parameter ϵ on axial velocity w for $Re = 0.1$ and $\lambda_1 = 1$.

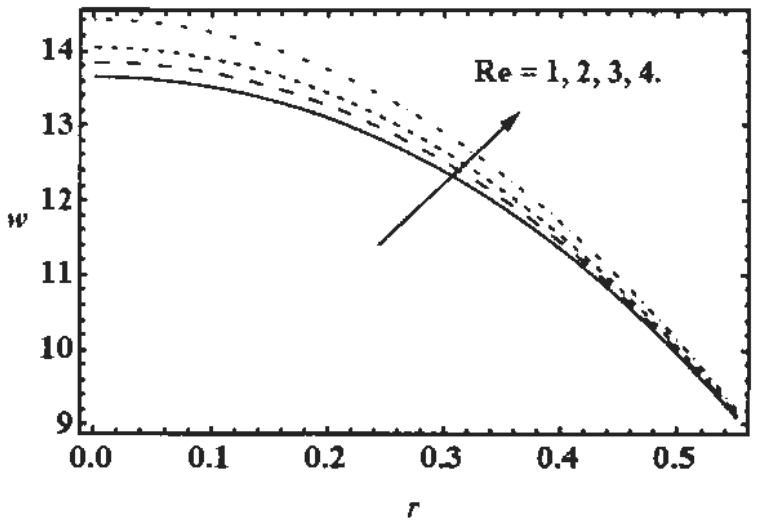

Fig. 6.6: Influence of Reynolds number Re on axial velocity w for $\epsilon = 0.1$ *and* $\lambda_1 = 1$.

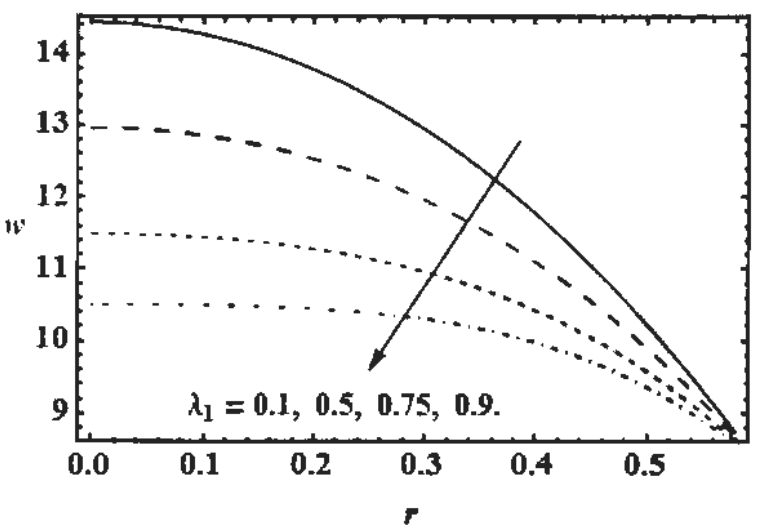

Fig. 6.7: Influence of Maxwell's parameter λ_1 on axial velocity w for $Re = 0.1$ *and* $\epsilon = 0.1$.

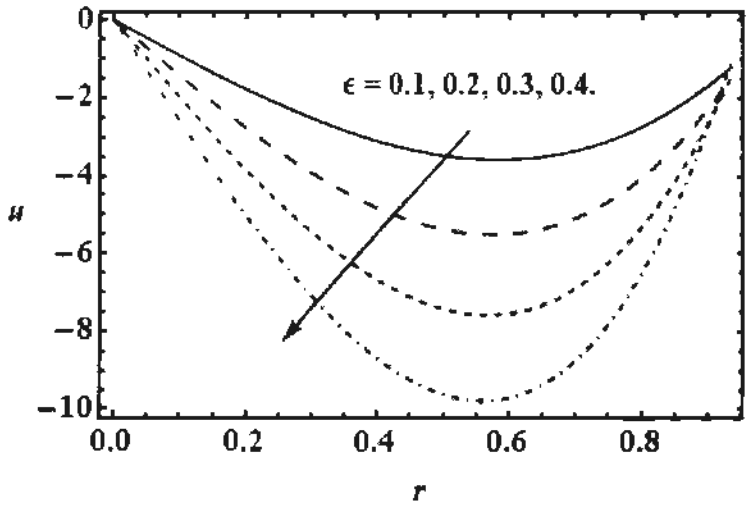

Fig. 6.8: Influence of cilia length parameter ϵ on radial velocity u for $Re = 0.1$ *and* $\lambda_1 = 1$.

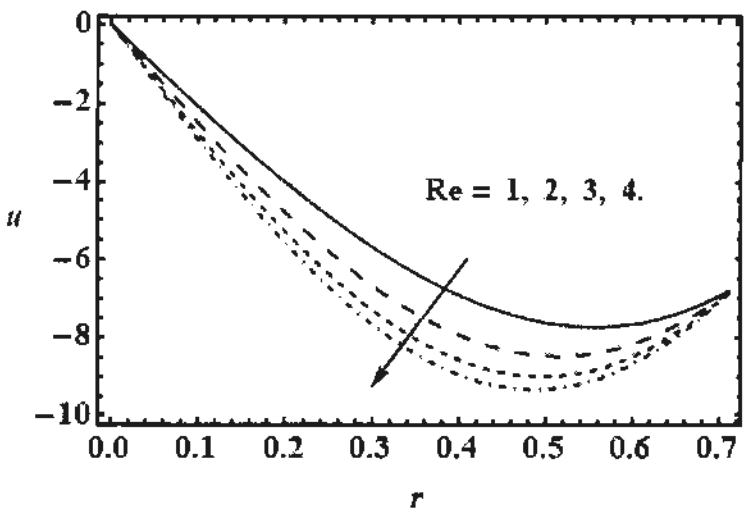

Fig. 6.9: Influence of Reynolds number Re on radial velocity u for $Re = 0.1$ *and* $\lambda_1 = 1$.

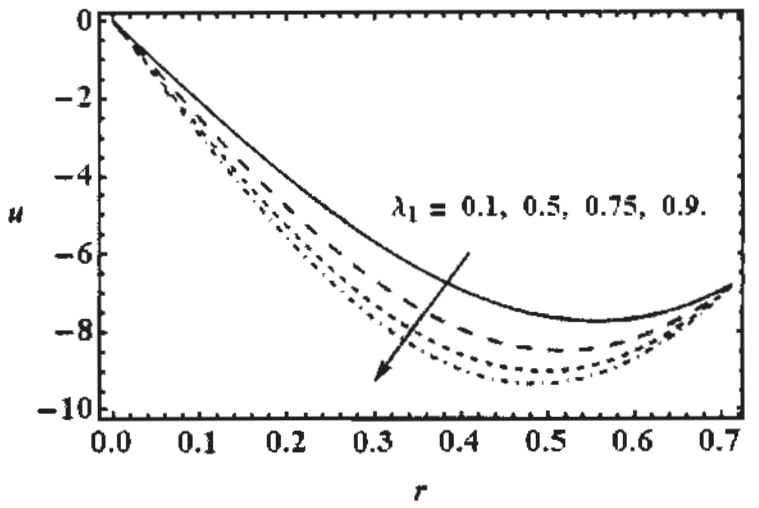

Fig. 6.10: Influence of Maxwell's parameter λ_1 on radial velocity u for $Re = 0.1$ and $\epsilon = 0.1$.

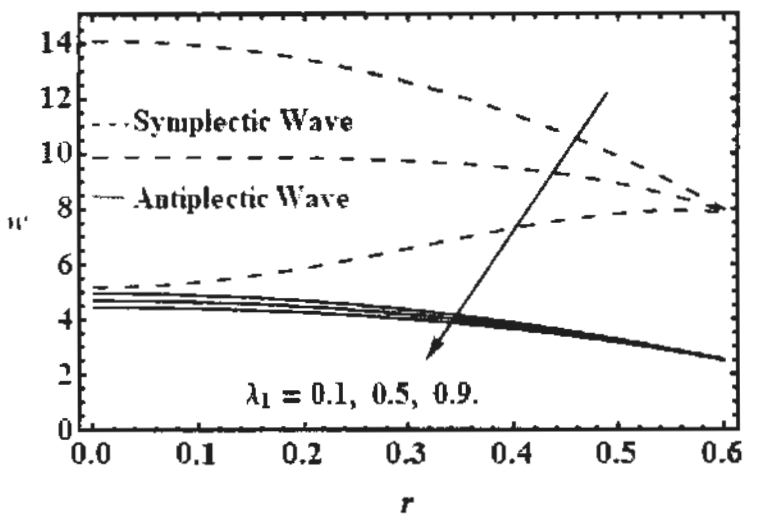

Fig. 6.11: Comparison of axial velocity profile w of mucus with symplectic and antiplectic wave pattern for $Re = 0.1$ and $\epsilon = 0.1$.

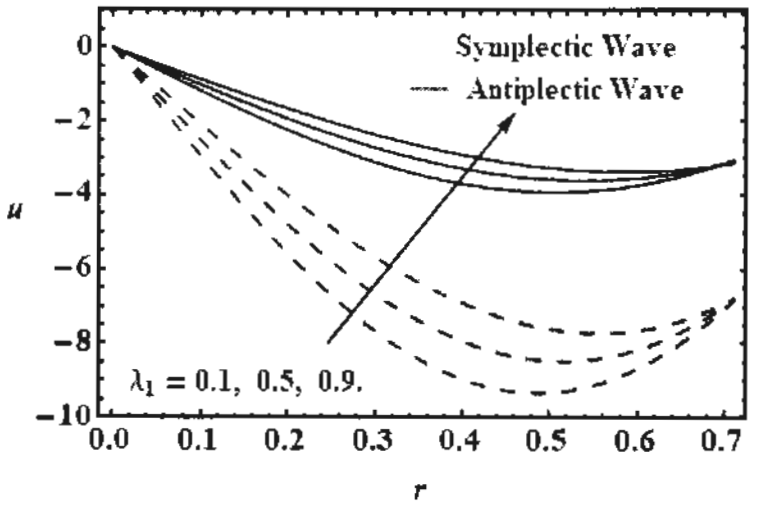

Fig. 6.12: Comparison of radial velocity u of mucus with symplectic and antiplectic wave pattern for $Re = 0.1$ *and* $\epsilon = 0.1$.

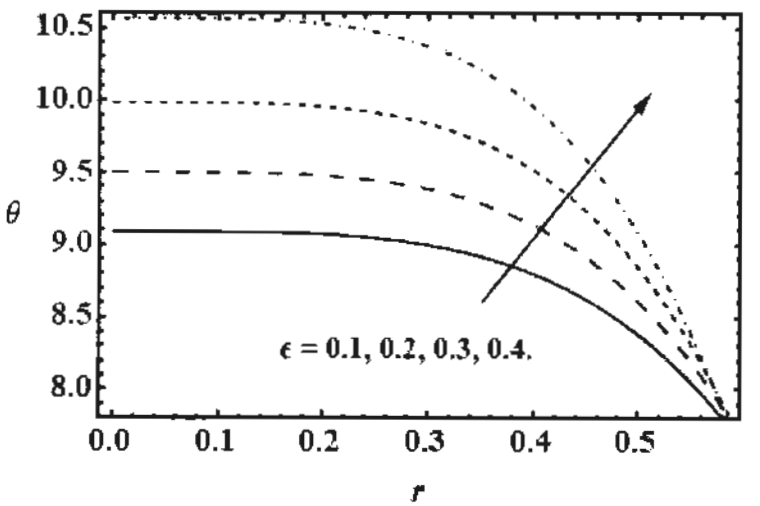

Fig. 6.13: Influence of cilia length parameter ϵ on temperature profile θ for $Re = 0.1$ *and* $\lambda_1 = 1$.

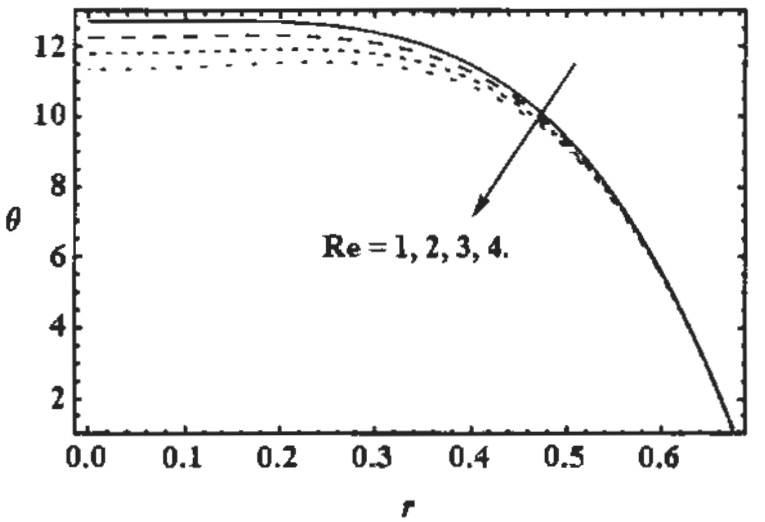

Fig. 6.14: Impact of Reynolds number Re on temperature field θ for $Re = 0.1$ *and* $\lambda_1 = 1$.

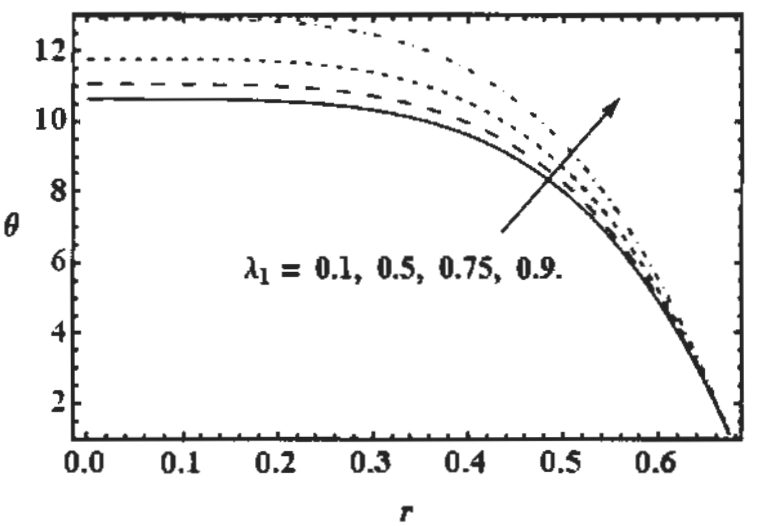

Fig. 6.15: Impact of Maxwell's parameter λ_1 on temperature field θ for $Re = 0.1$ *and* $\epsilon = 0.1$.

6.4 Discussion

Effect of temperature difference on Airway Mucus Clearance in cilia induced flow with inertial forces is governed by the energy and momentum equation. The results of pressure gradient, velocity and temperature profile is presented through graphs. For the biological relevance of the present study we have assumed $\alpha = 0.4, \beta = 0.01, z = 0.1, \varepsilon = 0.3,\ Re = 1\ \ and\ \ \lambda_1 = 0.1.$

Figs. 6.2 – 6.4 visualize the impact of cilia length parameter (ϵ), Reynolds number (Re) and relaxation time (λ_1) on axial pressure gradient distributions with axial length (z). Fig. 6.2 shows that pressure gradient rises with higher values of cilia length parameter. Fig. 6.3 shows that pressure gradient decrease with higher values of Re at the entrance of tube but it increases at the center and exit point of the tube i.e. with greater inertial forces fluid requires less amount of pressure gradient for the flow at the exit.

By increasing λ_1 there is as noted earlier, an increase in mucus elastic properties. These impede the cilia metachronal propulsion. Fig. 6.4 shows that for the initial region along the tube there is a boost in axial pressure gradient with Maxwell relaxation time, whereas with further distance along the tube the contrary response is computed. It is known based on experiments, that optimum propulsion is achieved when the concentration of glycoprotein is close to that of the gel transformation phase in mucus. Since healthy mucus contains glycoproteins (long chain polymers), viscoelastic behaviour is inevitable. However, at excessively higher concentrations of these glycoproteins, the mucus begins to morph into a gel network where elastic forces dominate rather than viscous forces. This leads to a pressure gradient rise with higher relaxation times. However, with further distance from the hydrodynamic entry zone,

the gel may achieve a relaxed state (even during metachronal propulsion) and this may lead to a reduction in axial pressure gradient as observed in Fig. 6.4.

Figs. $6.5 - 6.7$ present the radial distributions for axial velocity for distinct values (ϵ), (Re) and (λ_1). By increasing cilia length parameter radial velocity increases because cilia length assist flow in radial direction as shown in Fig. 6.5. Increasing Re increases inertial forces and reduces viscous force, so velocity of fluid increases. Weakly viscoelastic mucus generates maximum velocity magnitudes. It is also of interest that even with high relaxation time (or indeed cilia length) the flow is never reversed i.e. back flow is not induced as testified to by the consistently positive values of axial velocity in Figs. $6.5 - 6.7$. Overall it may be concluded that there is an intimate relationship between cilia length, Reynolds number, mucus viscoelasticity and optimized metachronal propulsion in healthy trachea.

Figs. $6.8 - 6.10$ present the radial component of velocity distributions for distinct values of (ϵ), (Re) and (λ_1). Increasing values of cilia length cause to increases fluid velocity in radial direction as shown in Fig. 6.8. Increasing values of Reynolds number cause to increases fluid velocity. Whereas, an increase in (λ_1) produces considerable retardation in the flow. Mucus takes longer to return to its relaxed state after deformation.

Figs. $6.11 - 6.12$ present the comparison of symplectic and antiplectic wave patterns on axial and radial velocity. It is shown that symplectic wave is more effective than antiplectic wave. Figs. $6.13 - 6.15$ visualize the effects of (ϵ), (Re) and (λ_1). Fig. 6.13 shows that by increasing cilia length parameter (ϵ) magnitude of temperature profile increases. Fig. 6.14 shows that by rising (Re) magnitude of temperature gradient decreases. Fig. 6.15 shows that by increasing Maxwell parameter

(λ_1) magnitude of temperature profile increases, with the increasing values of Maxwell parameter fluid become thick and for the heat transfer in highly viscous fluid large amount of temperature is required.

6.5 Conclusions

Motivated by providing a deeper insight into the mechanics of cilia-induced flow of mucus in the human trachea with heat transfer, a mathematical model has been developed for metachronal wave propulsion of viscoelastic mucus in an axisymmetric ciliated tube at moderate Reynolds numbers. An elliptic envelope cilia model and the Upper-Convective Maxwell (UCM) viscoelastic model have been deployed. We have considered the effect of non-zero Reynolds' number and resulting equations are perturbed about wave number. Perturbation solutions for the velocity field have been derived, numerical integration employed to compute pressure rise in the tube and temperature profile is obtained by integration. The influence of selected parameters i.e. Reynolds number (Re) and Maxwell viscoelastic material parameter i.e. relaxation time (λ_1) for prescribed values of β have been presented through graphs The study has shown following features:

- Inertial forces causes to increase axial and radial velocity
- By rising Maxwell parameter, again there is an increase in pressure gradient fall is observed in axial and radial flow.
- The computations are consistent with experimental studies in which it has been shown that undesirable high viscoelasticity inhibits efficient metachronal wave propagation of mucus in the respiratory tract due to respiratory diseases and denser, more elastic mucus constitution which cannot propel as easily with an associated reduction in cilia beat efficiency.

Chapter 7

Thermal Analysis on Power Law Fluid Flow due to Ciliary Movement under the Effect of Nanoparticles

In this chapter, we discuss the thermal and concentration analysis on the flow of power law fluid model through a ciliated tube. Exact solutions for velocity of fluid whereas, solutions for temperature and concentration profiles are calculated by using Homotopy Perturbation method. The impact of physical parameters along the characteristics of ciliary motion are presented in graphical results section.

7.1 Mathematical Model

We consider the flow of an incompressible power law fluid in a two-dimensional symmetric cylinder, whose inner walls are ciliated. We choose a cylindrical coordinate system with the Z^* −axis along the centreline of the cylinder and the R^*-axis normal to it. Due to cilia beating, an infinite symplectic metachronal wave train is produced and travels with a speed c along the walls, that is shown in Fig. 7.1.

In an axisymmetric tube the cilia tips moving in elliptical path therefore position of fluid particles is defined by the following expression

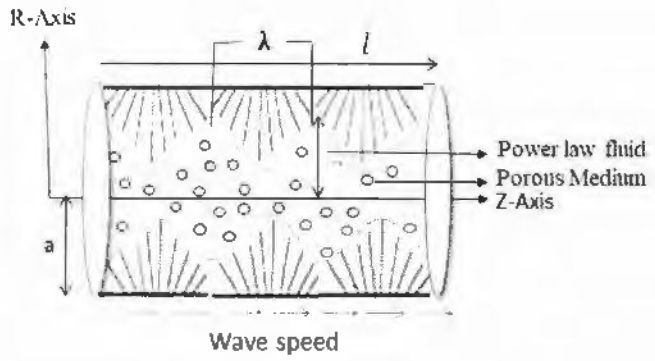

Fig. 7. 1: Schematic diagram of the ciliary flow.

The governing equations for the power law nano fluid flow through a ciliated tube with thermophoresis and Brownian effects are given as follow

$$V = [u(r,z), 0, w(r,z)], \tag{7.1}$$

$$\frac{1}{r}\frac{\partial}{\partial r}(ru) + \frac{\partial w}{\partial z} = 0, \tag{7.2}$$

$$\rho_f \frac{dV}{dt} = \nabla . \tau, \tag{7.3}$$

Where

$$\tau = pI + \mu_{eff} A_1, \tag{7.4}$$

$$(\rho c_p)_f \left(\frac{dT}{dt}\right) = k\nabla^2 T + trace(\tau . L) + (\rho c)_p (D_B \nabla C . \nabla T) + \frac{D_T}{T_0}\nabla T . \nabla T, \tag{7.5}$$

$$\frac{dC}{dt} = D_B \nabla^2 C + \frac{D_T}{T_0}\nabla^2 T, \tag{7.6}$$

$$\mu_{eff} = \eta\left(\frac{1}{2} trace A_1^2\right)^m, \tag{7.7}$$

where the boundary conditions are

$$w = w(h) = \frac{-\left(\frac{2\pi}{\lambda}\right)\left[\epsilon a \alpha c \sin\left(\frac{2\pi}{\lambda}\right) z\right]}{1 - \left(\frac{2\pi}{\lambda}\right)\left[\epsilon a \alpha \cos\left(\frac{2\pi}{\lambda}\right) z\right]}, \tag{7.8}$$

$$u = u(h) = \frac{\left(\frac{2\pi}{\lambda}\right)\left[\epsilon a a c \sin\left(\frac{2\pi}{\lambda}\right)z\right]}{1-\left(\frac{2\pi}{\lambda}\right)\left[\epsilon a a \cos\left(\frac{2\pi}{\lambda}\right)z\right]}, \tag{7.9}$$

$$T = T_0, C = C_0. \tag{7.10}$$

at

$$r = h(z) = \left[a + \epsilon a \cos\left(\frac{2\pi}{\lambda}\right)z\right].$$

The biological flows are observed by velocity, temperature and concentration that are assumed to be maximum at the center line of the ciliated tube

$$\frac{\partial w}{\partial r} = 0 \quad at \quad r = 0, \tag{7.11}$$

$$\frac{\partial T}{\partial r} = 0, \frac{\partial C}{\partial r} = 0 \quad at \quad r = 0. \tag{7.12}$$

In above equations V, τ, ρ_f, k, D_B and D_T shows the velocity profile, extra stress tensor, density of fluid, thermal conductivity, Brownian diffusion cofficient and thermospheric diffusion coefficient respectively.

To normalize the above equations, the following non-dimensional parameters are introduced:

$$z^* = \frac{z}{\lambda}, \quad u^* = \frac{u}{\beta c}, \quad r^* = \frac{r}{a}, \quad w^* = \frac{w}{c}, \quad p^* = \frac{a\beta}{c\eta}p, \quad h^* = \frac{h}{a},$$

$$\beta = \frac{a}{\lambda}, \quad S_{ij}{}^* = \frac{a}{\mu c}S_{ij}, \quad Re = \frac{\rho a c}{\mu}, \quad Pr = \frac{\eta c_p}{k}, \quad Br = \frac{\eta c^2}{k(T_1 - T_0)}$$

$$\theta = \frac{T - T_0}{T_1 - T_0}, \phi = \frac{C - C_0}{C_1 - C_0}, Nb = \frac{(\rho c)_p D_B (C_1 - C_0)}{(\rho c)_f \alpha_f}, Nt = \frac{(\rho c)_p D_T (C_1 - C_0)}{(\rho c)_f \alpha_f}. \tag{7.13}$$

Using Eq. (7.13) into Eq. (7.1)-(7.12), one can obtain the following form of equations after dropping the asterisk

$$\frac{1}{r}\frac{\partial}{\partial r}(ru) + \frac{\partial w}{\partial z} = 0, \tag{7.14}$$

$$Re\beta E(w) = F_1(S_{rz}) + \beta^2 \frac{\partial S_{zz}}{\partial z} - \frac{\partial p}{\partial z}, \tag{7.15}$$

$$Re\beta^2 E(u) = \beta F_1(S_{rr}) + \beta^2 \frac{\partial S_{zr}}{\partial z} - \frac{\partial p}{\partial r}, \tag{7.16}$$

$$\begin{aligned} \beta E(\theta) = F_1(\theta) + \beta^2 \frac{\partial^2 \theta}{\partial z^2} + Nb\left(\frac{\partial \theta}{\partial r}\frac{\partial \phi}{\partial r} + \beta^2 \frac{\partial \theta}{\partial z}\frac{\partial \phi}{\partial z}\right) \\ + Nt\left(\left(\frac{\partial \theta}{\partial r}\right)^2 + \beta^2\left(\frac{\partial \theta}{\partial z}\right)^2\right) + Br\frac{\partial w}{\partial r}S_{rz}, \end{aligned} \tag{7.17}$$

$$\beta E(\phi) = F_1\left(\phi + \frac{Nt}{Nb}\theta\right) + \beta^2 \frac{\partial^2 \phi}{\partial z^2}, \tag{7.18}$$

where

$$S_{rz} = \left(2\beta^2\left(\frac{\partial u}{\partial z}\right)^2 + \beta^2\left(\frac{\partial u}{\partial z} + \frac{\partial w}{\partial r}\right)^2 + 2\beta^2\left(\frac{\partial w}{\partial z}\right)^2\right)^m \left(\beta^2 \frac{\partial u}{\partial z} + \frac{\partial w}{\partial r}\right), \tag{7.19}$$

with boundary conditions

$$w = w(h) = -(1 + 2\pi\epsilon\alpha\beta\cos(2\pi z)), \tag{7.20}$$

$$u = u(h) = 2\pi\epsilon(\sin(2\pi z)) + \beta 2\pi\epsilon\alpha \sin(2\pi z)\cos(2\pi z), \tag{7.21}$$

at

$$\begin{aligned} r = h(z) = a + \epsilon\alpha a\cos(2\pi z), \\ \frac{\partial w}{\partial r} = \frac{\partial \theta}{\partial r} = \frac{\partial \phi}{\partial r} = 0 \qquad at\ \ r = 0. \end{aligned} \tag{7.22}$$

Incorporating the approximation of long wave length and small Reynolds number ($\lambda \to \infty,\ Re \to 0$)

$$\left(F_1(w)\right)^{2m+1} = \frac{dp}{dz}, \tag{7.23}$$

$$\frac{dp}{dr} = 0, \tag{7.24}$$

$$F_1(\theta) = \frac{\partial \theta}{\partial r}\left(Nb\frac{\partial \phi}{\partial r} + Nt\frac{\partial \theta}{\partial r}\right) - Br\left(\frac{\partial w}{\partial r}\right)^{2m+2}, \tag{7.25}$$

$$F_1\left(\phi - \frac{Nt}{Nb}\theta\right) = 0. \tag{7.26}$$

with boundary conditions

$$w = w(h) = -1 - 2\pi\epsilon\alpha\beta\cos(2\pi z), \theta = 0, \phi = 0, at \;\; r = h, \tag{7.27}$$

$$\frac{\partial w}{\partial r} = \frac{\partial \theta}{\partial r} = \frac{\partial \phi}{\partial r} = 0 \qquad at \;\; r = 0. \tag{7.28}$$

In bionic biological systems, volume flow rate is a key design quantity. The instantaneous volumetric flow rate in a fixed frame is given by

$$q = 2\int_0^h rwdr, \tag{7.29}$$

using the formula of transformation (fixed to wave), we get

$$Q = 2\int_0^l rwdr = 2\int_0^l r(w+1)dr = q + h^2. \tag{7.30}$$

The time-mean flow over a period t is defined as

$$\bar{Q} = \frac{1}{t}\int_0^t Qdt^* = q + 1 + 0.5\epsilon^2. \tag{7.31}$$

7.2 Homotopy Perturbation Solution

Integrating Eq. (7.23) w.r.t r and using the boundary conditions in Eq. (7.27) & (7.28) the following exact solution of velocity profile is obtained

$$w = w(h) + \left(\frac{1}{2}\frac{dp}{dz}\right)^{\frac{1}{2m+1}}\frac{2m+2}{2m+1}\left(r^{\frac{2m+2}{2m+1}} - h^{\frac{2m+2}{2m+1}}\right). \tag{7.32}$$

To obtain the solution of Eq. (7.25) and (7.26) we define the homotopy equation which can be written as

$$\mathcal{H}(j,\theta) = (1-j)[\mathcal{L}(\theta) - \mathcal{L}(\theta_0)] + j\left(\begin{array}{c}\mathcal{L}(\theta) - \frac{\partial\theta}{\partial r}\left(Nb\frac{\partial\phi}{\partial r} + Nt\frac{\partial\theta}{\partial r}\right) \\ +Br\left(\frac{\partial w}{\partial r}\right)^{2m+2}\end{array}\right), \tag{7.33}$$

$$\mathcal{H}(j,\phi) = (1-j)[\mathcal{L}(\phi) - \mathcal{L}(\phi_0)] + j\left(\mathcal{L}(\phi) - \frac{Nt}{Nb}\left(\frac{\partial^2\theta}{\partial r^2} + \frac{1}{r}\frac{\partial\theta}{\partial r}\right)\right). \tag{7.34}$$

We choose linear operator and initial guesses as

$$\mathcal{L} = \left(\frac{\partial^2}{\partial r^2} + \frac{1}{r}\frac{\partial}{\partial r}\right), \tag{7.35}$$

$$\theta_0 = \frac{r^2 - h^2}{4}, \phi_0 = \frac{r^2 - h^2}{4}. \tag{7.36}$$

Homotopy perturbation method suggest the following relations

$$\theta = \theta_0 + j\theta_1 + j^2\theta_2 + \cdots, \tag{7.37}$$

$$\theta = \phi_0 + j\phi_1 + j^2\phi_2 + \cdots, \tag{7.38}$$

where $j \in [0,1]$ is the embedding parameter and $j = 0$ provides initial approximation and $j = 1$ provides the final solution. With the help of Eqs. (7.33) & (7.34), One can obtain the second order solution for the temperature and concentration profile which are given as

$$\begin{aligned}\theta = {} & \frac{1}{16}\left(\frac{Nb}{2} - \frac{Nt}{2}\right)(r^4 - h^4) + \frac{1}{36}\left(\frac{Nb^2}{32} + \frac{3NbNt}{32} + \frac{Nt^2}{16}\right)(r^6 - h^6) \\ & - \frac{Br(1+2m)^2\left(2^{\frac{1}{-2-2m}}p^{\frac{1}{1+2m}}\right)^{2(1+m)}}{(4+6m)^2}\left(r^{\frac{4+6m}{1+2m}} - h^{\frac{4+6m}{1+2m}}\right) \\ & + \left(\frac{2^{\frac{-4(1+m)}{1+2m}}Br(1+2m)(Nb+2Nt)p^{\frac{2}{1+2m}}\left(2^{\frac{1}{-1-2m}}p^{\frac{1}{1+2m}}\right)^{2m}}{2+3m}\right) \\ & \times \left(\frac{1+2m}{6+10m}\right)^2\left(r^{\frac{4+6m}{1+2m}} - h^{\frac{4+6m}{1+2m}}\right),\end{aligned} \tag{7.39}$$

$$\begin{aligned}\phi = {} & \frac{Nt}{4Nb}(r^2 - h^2) - \frac{\left(\frac{Nb}{4} - \frac{Nt}{4}\right)Nt}{16Nb}(r^4 - h^4) \\ & - \frac{Nt}{Nb}\left(-4^{\frac{1}{-1-2m}}Brp^{\frac{2}{1+2m}}\right)\left(2^{\frac{1}{-2-2m}}p^{\frac{1}{1+2m}}\right)^{2(1+m)} \\ & \times \left(\frac{1+2m}{4+6m}\right)^2\left(r^{\frac{4+6m}{1+2m}} - h^{\frac{4+6m}{1+2m}}\right).\end{aligned} \tag{7.40}$$

Integrating Eq. (7.32), pressure gradient can be written as

(7.41)

$$\frac{dp}{dz} = \left(-\frac{2^{1+\frac{1}{2m+1}} h^{-\frac{2(3m+2)}{2m+1}} (2 + 5m + 3m^2)\left(\bar{Q} - h^2 w(h)\right)}{(1 + 3m + 2m^2)} \right)^{2m+1}.$$

7.3 Graphical Results

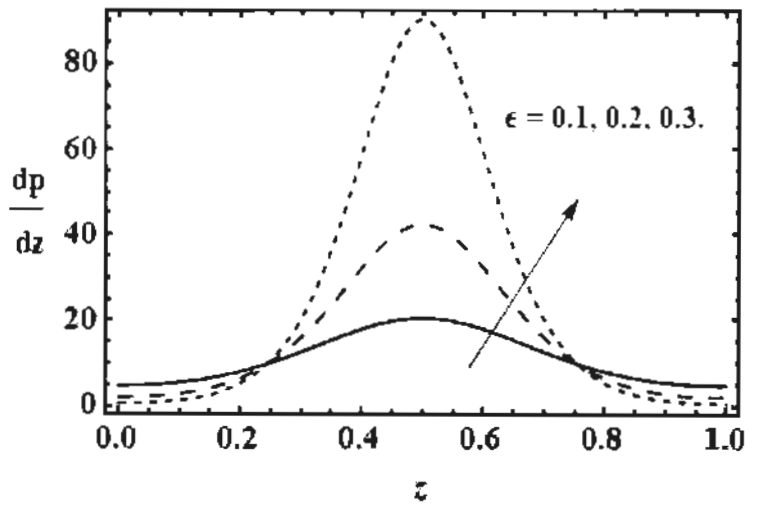

Fig. 7.2: Influence of cilia length parameter ϵ on pressure gradient $\frac{dp}{dz}$ for $m = 0.01$.

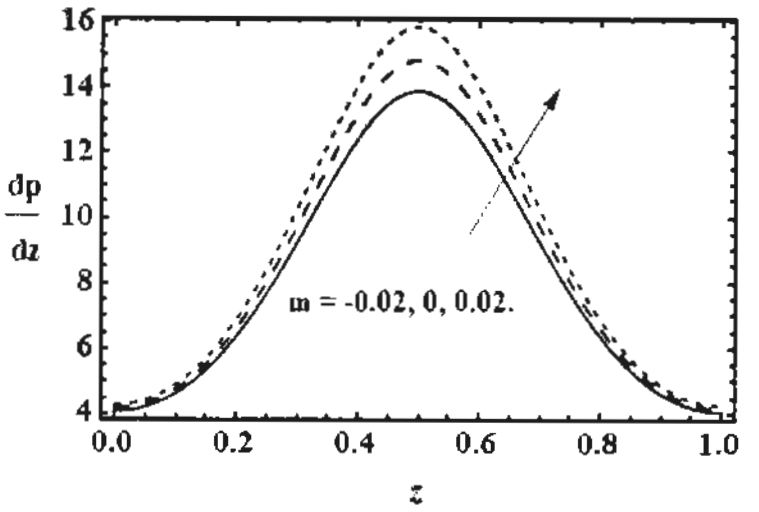

Fig. 7.3: Influence of power law index m on pressure gradient $\frac{dp}{dz}$ for $\epsilon = 0.1$.

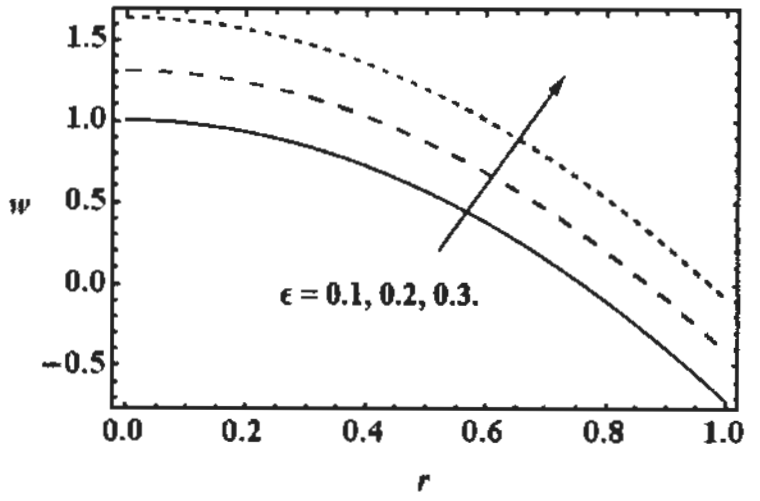

Fig. 7.4: Impact of cilia length parameter ϵ on axial velocity w for $m = 0.01$.

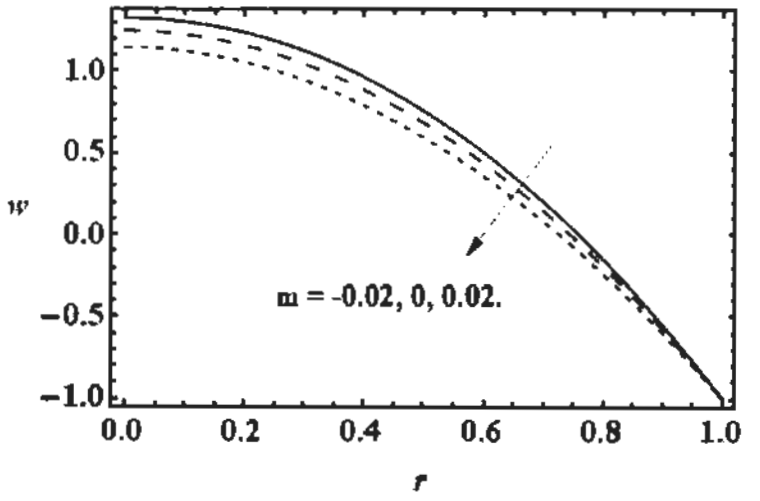

Fig. 7.5: Impact of power law index m on axial velocity w for $\epsilon = 0.1$.

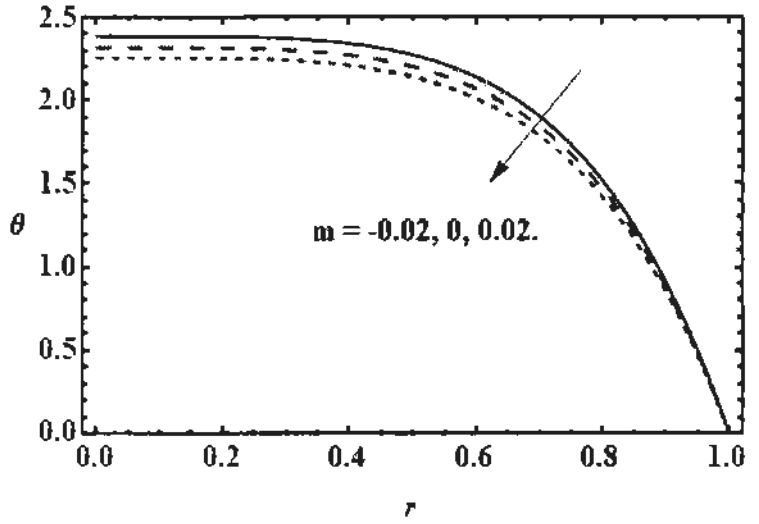

Fig. 7.6: Impact of power law index m on temperature field θ for $Br = 4, Nb = 1$ and $Nt = 1$.

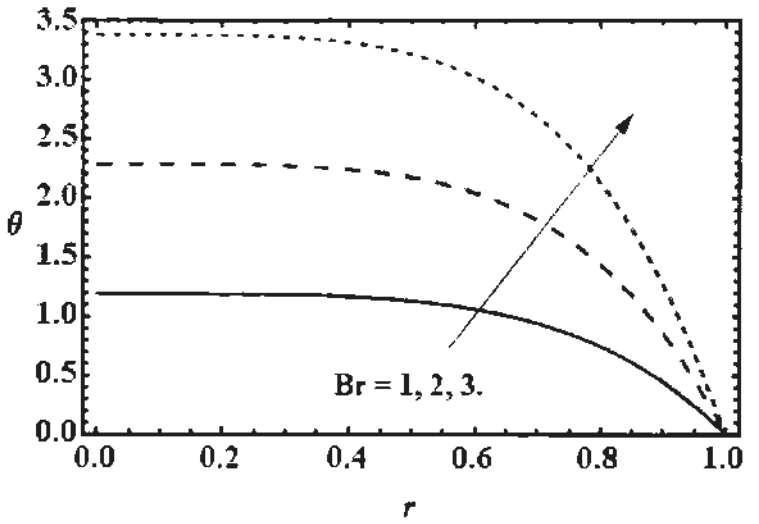

Fig. 7.7: Impact of Brinkman number Br on temperature profile θ for $m = 0.01$, $Nb = 1$ and $Nt = 1$.

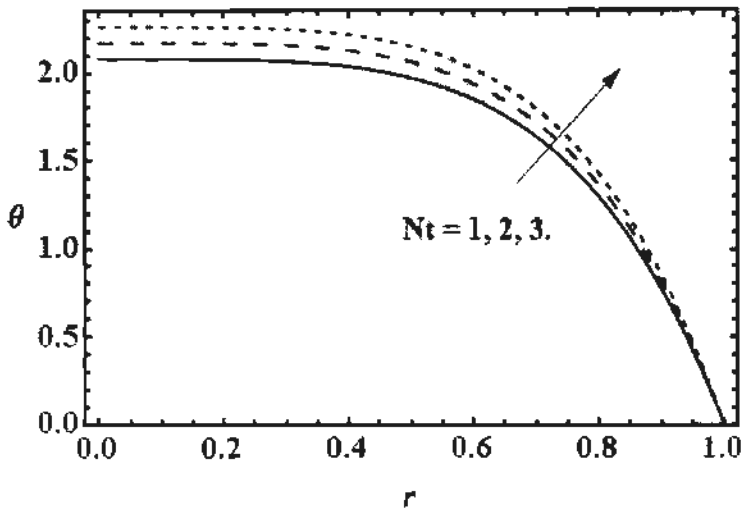

Fig. 7.8: Impact of thermophoretic parameter Nt on temperature field θ for $Br = 4$, $Nb = 1$ and $m = 0.01$.

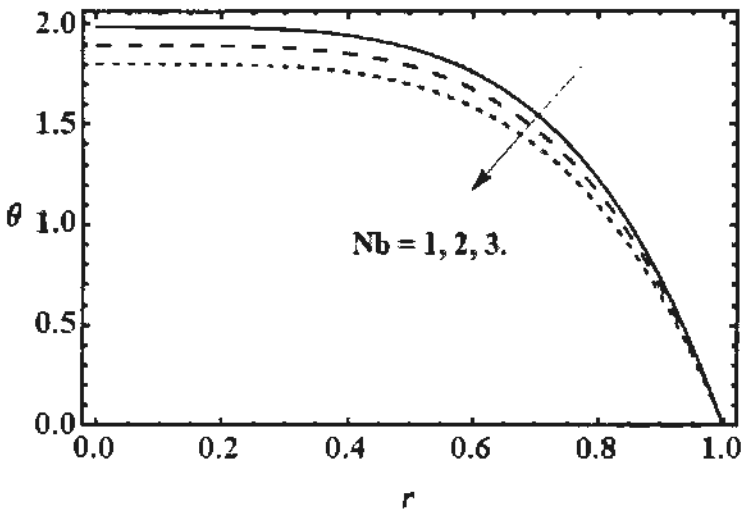

Fig. 7.9: Impact of Brownian motion parameter Nb on temperature field θ for $Br = 4$, $m = 0.01$ and $Nt = 1$.

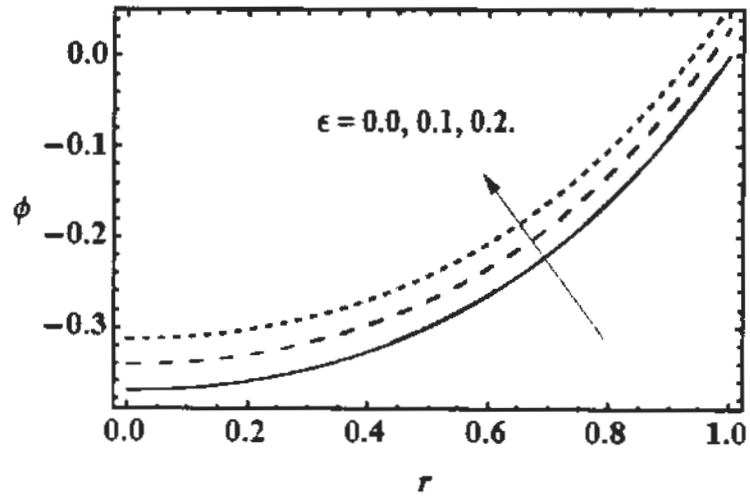

Fig. 7.10: Impact of cilia length parameter ϵ on concentration field ϕ for $m = 0.01$, $Nb = 1$ and $Nt = 1$.

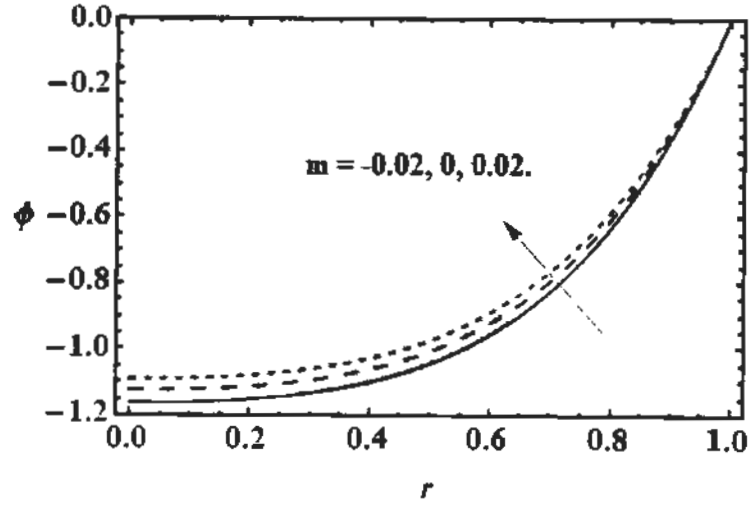

Fig. 7.11: Influence of power law index m on concentration profile ϕ for $\epsilon = 0.1$, $Nb = 1$ and $Nt = 1$.

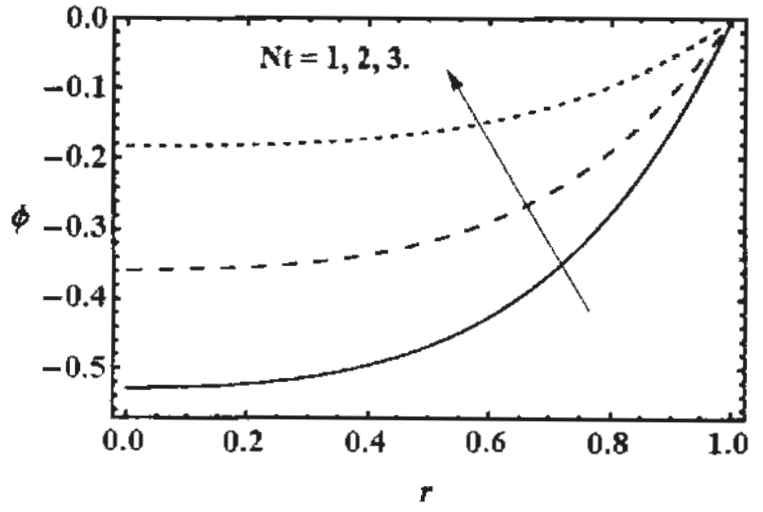

Fig. 7.12: Impact of Thermophoretic parameter Nt on concentration field ϕ for $\epsilon = 0.1$, $Nb = 1$ and $m = 0.01$.

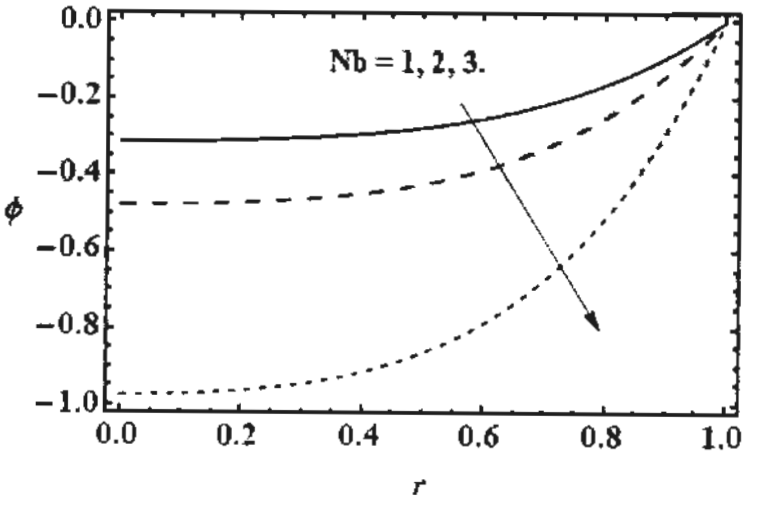

Fig. 7.13: Impact of Brownian motion parameter Nb on concentration field ϕ for $\varepsilon = 0.1$, $Nt = 1$ and $m = 0.01$.

7.4 Discussion

This section compromises a detailed discussion on the graphs of pressure gradient, velocity, temperature and concentration distribution. Figs. $7.2-7.3$ show the impact of interested parameters on the pressure gradient . The consequence of interested parameters on the velocity profile can be depicted from Figs. 7.4 &7.5. Figs. $7.6-7.9$ presents the influence of interested parameters on temperature profile and Figs. $7.10-7.13$ present the impact of different parameters on temperature profile. These graphs are plotted by fixing the parameters as $\alpha = 0.2, \beta = 0.2 \ and \ z = 0.25$.

The variation of cilia length ϵ and flow behavior index m has been displayed in Figs. 7.2 & 7.3 for pressure gradient. It can be seen that pressure gradient rises by increasing the values of cilia length parameter ϵ. By increasing the values of power law index m pressure deviation for the ciliary flow rises because of increase in viscosity of the fluid flow.

Figs. 7.4 & 7.5 indicate that by increasing values of cilia length parameter ϵ axial velocity of fluid increases.It is noticed that flow behavior index m also accelerates the fluid flow.

Figs. $7.6-7.9$ depict the significance change in temperature profile θ for growing values of various parameters. The trend of temperature profile is same as velocity profile attains its peak at center of tube (i.e $r = 0$). These figures display that rise in flow behavior index m, thermophoretic parameter Nt and Brownian motion parameter Nb results to decrease in temperature profile whereas it is observed that Brinkman number Br enhances the temperature profile.

Figs. $7.10-7.13$ show the significance change in magnitude of concentration profile ϕ for increasing values of various parameters. The trend of concentration profile is also same as velocity and temperature profiles attains their peaks at center of tube (i.e $r =$

0). These figures display that rise in cilia length ϵ and thermophoretic parameter Nt results to decrease in magnitude of concentration profile whereas it is observed that flow behavior index m and Brownian motion parameter Nb enhances the magnitude of concentration profile.

7.5 Conclusions

In this study we have studied a mathematical model of forced convective flow of power law nano fluid through a ciliated axisymmetric tube. The fluid is flowing due to ciliary motion which creates a continuous envelop called metachronal wave. The boundary conditions are considered at the center of the tube and on the tip of cilia which is anchored in the wall of the tube and formed a wavy surface. The simulation shows that energy, momentum and concentration equations involve physical parameter like velocity, temperature, pressure, concentration to see the effects of nano particles for the enhancement of heat and mass transfer. The present study can be validated by the work of [30] if m→0 i.e. Power law index is zero. Following observations are highlighted in the present study.

- Velocity profile reduces with the cilia length parameter ϵ whereas it rises with flow behavior index m.
- Pressure gradient decreases for larger values of cilia length constant ϵ and flow behavior index m.
- Temperature profile diminishes by increasing cilia length ϵ, flow behavior index m and Brownian motion parameter Nb and enhances by increasing Brinkman number Br and thermophoretic parameter Nt.

- Temperature profile diminishes by increasing cilia length ϵ, flow behaviour index m and Brownian motion parameter Nb and enhances by increasing Brinkman number Br and thermophoretic parameter Nt.
- Magnitude of concentration profile diminishes by increasing cilia length parameter ϵ, thermophoretic parameter Nt and flow behavior index m, but magnitude of concentration profile enhances with increasing Brownian motion parameter Nb.

Chapter 8

Thermal and Concentration Analysis of PTT Fluid Flow due to Ciliary Movement in a Peripheral Layer

In this chapter, we discuss the thermal and diffusion effects in peripheral layer due to ciliary movement. The fluid flow is modeled using the linear Phan-Thien-Tanner (PTT) fluid model. After incorporating long wavelength and low Reynolds number approximations, the resulting equations are then solved. Exact solution for velocity, temperature and concentration fields are obtained. The influence of various parameters along the characteristics of ciliary motion are illustrated by the graphs and discussed in graphical results section.

8.1 Mathematical Modeling

We have considered two-dimensional flow of PTT fluids with distinct densities, viscosities, thermal conductivities and diffusion parameters in two immiscible fluid layers, i.e. central and peripheral layers in a channel. The X-axis is considered along the direction of metachronal wave and Y-axis is normal to it that is shown in Fig. **8.1**. In an axisymmetric tube the cilia tips moving in elliptical path therefore position of fluid particles is defined by the following expression

$$X^* = g(X^*, X_0^*, t^*) = X_0^* + a\epsilon\alpha \sin\left(2\pi\left(\frac{X^* - ct^*}{\lambda}\right)\right), \tag{8.1}$$

$$Y^* = f(X^*, t^*) = a + a\epsilon \cos\left(2\pi\left(\frac{X^* - ct^*}{\lambda}\right)\right), \tag{8.2}$$

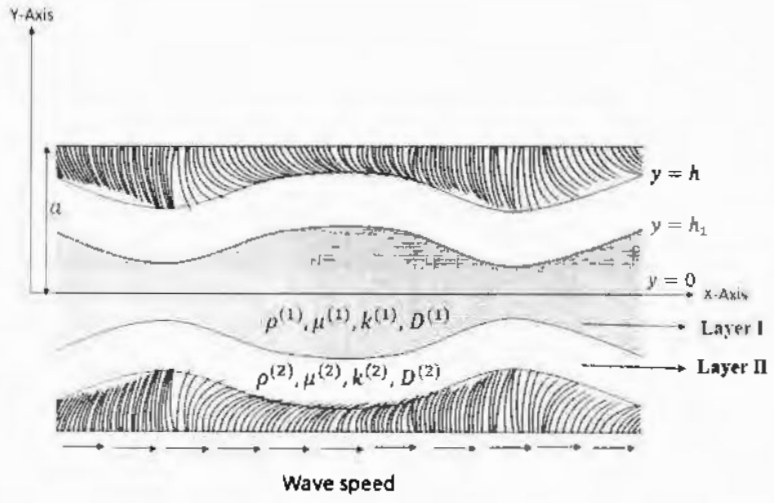

Figure 8.1: Geometry of the problem

After using no slip condition X^* and Y^* components of velocity are given as follows

$$U^* = \dot{X}^*|_{X^*=X^*_0} = \dot{G} + G'\dot{X}^* = \dot{G} + G'U, \tag{8.3}$$

$$V^* = \dot{Y}^*|_{X^*=X^*_0} = \dot{F} + F'\dot{X}^* = \dot{F} + F'U^*, \tag{8.4}$$

where (.) represents the derivative $w.r.t\ t^*$ and ($'$) represents the derivative $w.r.t\ X^*$.

Using Eqs. (8.1)-(8.2) in Eqs. (8.3)-(8.4), we arrive at

$$U^* = \frac{-\left(\frac{2\pi}{\lambda}\right)\left[\epsilon\alpha ac\cos\left(2\pi\left(\frac{X^*-ct^*}{\lambda}\right)\right)\right]}{1-\left(\frac{2\pi}{\lambda}\right)\left[\epsilon\alpha a\cos\left(2\pi\left(\frac{X^*-ct^*}{\lambda}\right)\right)\right]}, \tag{8.5}$$

and

$$V^* = \frac{-\left(\frac{2\pi}{\lambda}\right)\left[\epsilon\alpha ac\sin\left(2\pi\left(\frac{X^*-ct^*}{\lambda}\right)\right)\right]}{1-\left(\frac{2\pi}{\lambda}\right)\left[\epsilon\alpha a\cos\left(2\pi\left(\frac{X^*-ct^*}{\lambda}\right)\right)\right]}. \tag{8.6}$$

The wave frame and fixed frame are related by the following transformation

$$x^* = X^* - ct^*, y^* = Y^*, u^* = U^* - c, v^* = V^*, p^*(x,y) = P^*(X^*,Y^*,T), \tag{8.7}$$

For the transportation of two immiscible mucus layers in the airways, the continuity, momentum, heat and concentration equations can be written as

$$\nabla . V^{(i)} = 0, \qquad i = 1,2 \tag{8.8}$$

and

$$\rho^{(i)} \frac{dV^{(i)}}{dt} = div\tau^{(i)}, \qquad i = 1,2 \tag{8.9}$$

$$\rho^{(i)} c_p^{(i)} \frac{dT^{(i)}}{dt} = \kappa^{(i)} \nabla^2 T^{(i)} + \tau^{(i)} . L^{(i)}, \qquad i = 1,2 \tag{8.10}$$

$$\frac{dC^{(i)}}{dt} = \frac{D_{kT}}{T_0} \nabla^2 T^{(i)} + D^{(i)} \nabla^2 C^{(i)}, \qquad i = 1,2. \tag{8.11}$$

Where

$$V^{(i)} = \left[u^{(i)}(x,y), v^{(i)}(x,y)\right], \tag{8.12}$$

Stress tensor for PTT fluid model is given by [90]

$$f\left(trace\left(\tau^{(i)}\right)\right)\tau^{(i)} + \lambda^{(i)} \hat{\tau}^{(i)} = 2\eta^{(i)} A_1^{(i)}, \tag{8.13}$$

where $\eta^{(i)}, \lambda^{(i)}, \tau^{(i)}, A_1^{(i)}$ represent the coefficient of viscosity, relaxation time, stress tensor and deformation rate of both fluid and shear stress is defined as follows

$$\hat{\tau}^{(i)} = \frac{d\tau^{(i)}}{dt} - \tau^{(i)} . L^{(i)} - \left(L^{(i)}\right)^T . \tau^{(i)}, \tag{8.14}$$

$$f\left(trace\left(\tau^{(i)}\right)\right) = 1 + \frac{\varepsilon^{(i)} \lambda^{(i)}}{\eta^{(i)}} trace\left(\tau^{(i)}\right), \tag{8.15}$$

where superscript i denotes the two fluids, $i = 1$ shows the fluid in first layer and the fluid in second layer is represented by $i = 2$. $\varepsilon^{(i)}$ denotes the elongation behavior parameter and $\lambda^{(i)}$ denotes the material parameters.

In the muco ciliary pumping, velocity, pressure and shear stress need to be analyzed, therefore continuity, momentum, heat and concentration equation together with the stress and strain relationship are expressed in the following manner

$$\frac{\partial u^{(i)}}{\partial x} + \frac{\partial v^{(i)}}{\partial y} = 0, \tag{8.16}$$

$$\rho^{(i)} F^{(i)}\left(u^{(i)}\right) = \frac{\partial \tau_{xy}^{(i)}}{\partial y} + \frac{\partial \tau_{xx}^{(i)}}{\partial x} - \frac{\partial p}{\partial x}, \tag{8.17}$$

$$\rho^{(i)}F^{(i)}\left(v^{(i)}\right)=\frac{\partial\tau_{yy}^{(i)}}{\partial y}+\frac{\partial\tau_{yx}^{(i)}}{\partial x}-\frac{\partial p}{\partial y}, \tag{8.18}$$

$$\rho^{(i)}c_p^{(i)}F^{(i)}\left(T^{(i)}\right)=trace\left(\boldsymbol{\tau}^{(i)}.\boldsymbol{L}^{(i)}\right)+\kappa^{(i)}\left(\frac{\partial^2T^{(i)}}{\partial x^2}+\frac{\partial^2T^{(i)}}{\partial y^2}\right), \tag{8.19}$$

$$F^{(i)}\left(C^{(i)}\right)=\frac{D_{KT}}{(T_1-T_0)}\left(\frac{\partial^2T^{(i)}}{\partial x^2}+\frac{\partial^2T^{(i)}}{\partial y^2}\right)+D^{(i)}\left(\frac{\partial^2C^{(i)}}{\partial x^2}+\frac{\partial^2C^{(i)}}{\partial y^2}\right), \tag{8.20}$$

where $F^{(i)}=u^{(i)}\frac{\partial}{\partial x}+v^{(i)}\frac{\partial}{\partial y}$ and stress tensors can be written as

$$\left(1+\frac{\varepsilon^{(i)}\lambda^{(i)}}{\eta^{(i)}}trace\left(\boldsymbol{\tau}^{(i)}\right)\right)\tau_{xx}^{(i)}+\lambda^{(i)}G^{(i)}\tau_{xx}^{(i)}$$

$$-2\lambda^{(i)}\left(\tau_{xx}^{(i)}\frac{\partial u^{(i)}}{\partial x}+\tau_{xy}^{(i)}\frac{\partial v^{(i)}}{\partial x}\right)=2\eta^{(i)}\frac{\partial u^{(i)}}{\partial x}, \tag{8.21}$$

$$\left(1+\frac{\varepsilon^{(i)}\lambda^{(i)}}{\eta^{(i)}}trace\left(\boldsymbol{\tau}^{(i)}\right)\right)\tau_{xy}^{(i)}+\lambda^{(i)}G^{(i)}\tau_{xy}^{(i)}$$

$$-2\lambda^{(i)}\left(\tau_{xx}^{(i)}\frac{\partial u^{(i)}}{\partial y}+\tau_{xy}^{(i)}\frac{\partial v^{(i)}}{\partial y}+\tau_{xy}^{(i)}\frac{\partial u^{(i)}}{\partial x}+\tau_{yy}^{(i)}\frac{\partial v^{(i)}}{\partial x}\right)=\eta^{(i)}\left(\frac{\partial u^{(i)}}{\partial y}+\frac{\partial v^{(i)}}{\partial x}\right) \tag{8.22}$$

$$\left(1+\frac{\varepsilon^{(i)}\lambda^{(i)}}{\eta^{i}}trace\left(\boldsymbol{\tau}^{(i)}\right)\right)\tau_{yy}^{(i)}+\lambda^{(i)}G^{(i)}\tau_{yy}^{(i)}$$

$$-2\lambda^{(i)}\left(\tau_{xy}^{(i)}\frac{\partial u^{(i)}}{\partial y}+\tau_{yy}^{(i)}\frac{\partial v^{(i)}}{\partial y}\right)=2\eta^{(i)}\frac{\partial u^{(i)}}{\partial y}, \tag{8.23}$$

where $G^{(i)}=u^{(i)}\frac{\partial u^{(i)}}{\partial x}+v^{(i)}\frac{\partial v^{(i)}}{\partial y}$.

The biological flows are observed by velocity, temperature and concentration that are assumed to be maximum at the center line of the ciliated tube whereas at the interface shear stresses and velocities of fluids are equal as considered in Ref. [91], therefore boundary conditions for velocities and shear stress can be written as

$$\tau_{xy}^{(1)}=0 \quad at \quad y=0, \tag{8.24a}$$

$$\tau_{xy}^{(1)} = \tau_{xy}^{(2)} \quad at \quad y = h_1, \tag{8.24b}$$

$$u^{(1)} = u^{(2)} \quad at \quad y = h_1, \tag{8.24c}$$

$$u^{(2)} = \frac{-\left(\frac{2\pi}{\lambda}\right)\left[\epsilon aac \sin\left(\frac{2\pi}{\lambda}\right)x\right]}{1-\left(\frac{2\pi}{\lambda}\right)\left[\epsilon aa \cos\left(\frac{2\pi}{\lambda}\right)x\right]} \quad at \quad y = h, \tag{8.24d}$$

$$v^{(2)} = \frac{\left(\frac{2\pi}{\lambda}\right)\left[\epsilon aac \sin\left(\frac{2\pi}{\lambda}\right)z\right]}{1-\left(\frac{2\pi}{\lambda}\right)\left[\epsilon aa \cos\left(\frac{2\pi}{\lambda}\right)z\right]} \quad at \quad y = h. \tag{8.24e}$$

Similarly boundary conditions for temperature and concentration profile can be written as:

$$\frac{\partial T^{(1)}}{\partial y} = 0 \quad at \quad y = 0, \tag{8.25a}$$

$$\kappa^{(1)}\frac{\partial T^{(1)}}{\partial y} = \kappa^{(2)}\frac{\partial T^{(2)}}{\partial y} \quad at \quad y = h_1, \tag{8.25b}$$

$$T^{(1)} = T^{(2)} \quad at \quad y = h_1, \tag{8.25c}$$

$$T^{(2)} = T_0 \quad at \quad y = h. \tag{8.25d}$$

$$\frac{\partial C^{(1)}}{\partial y} = 0 \quad at \quad y = 0, \tag{8.26a}$$

$$D^{(1)}\frac{\partial C^{(1)}}{\partial y} = D^{(2)}\frac{\partial C^{(2)}}{\partial y} \quad at \quad y = h_1, \tag{8.26b}$$

$$C^{(1)} = C^{(2)} \quad at \quad y = h_1, \tag{8.26c}$$

$$C^{(2)} = C_0 \quad at \quad y = h. \tag{8.26d}$$

where

$$h(x) = \left[a + \epsilon a\left(\frac{2\pi}{\lambda}\right)x\right],$$

$$h_1(x) = \left[a_1 + \epsilon a_1\left(\frac{2\pi}{\lambda}\right)x\right].$$

For the mathematical computation following non-dimensional quantities are required

$$x^* = \frac{x}{\lambda}, \quad y^* = \frac{y}{a}, \quad u^{*(i)} = \frac{u^{(i)}}{c}, \quad v^{*(i)} = \frac{v^{(i)}}{\beta c}, \quad h^* = \frac{h}{a}, \quad h_1^* = \frac{h_1}{a},$$

$$p^* = \frac{a\beta}{c\eta^{(1)}}p, \beta = \frac{a}{\lambda}, \qquad {\tau_{ij}}^{*(i)} = \frac{a}{\eta^{(1)}c}{\tau^{(i)}}_{ij}, \qquad Re = \frac{\rho ac}{\eta^{(1)}}, \qquad Pr = \frac{\eta^{(1)}c_p}{\kappa^{(1)}}, \qquad Br = \frac{\eta^{(1)}c^2}{\kappa^{(1)}(T_1 - T_0)},$$
$$\theta^{(i)} = \frac{T^{(i)} - T_0}{T_1 - T_0}, \phi^{(i)} = \frac{C^{(i)} - C_0}{C_1 - C_0}, \qquad S_H = \frac{\eta^{(1)}}{D^{(1)}\rho^{(1)}},$$
$$S_T = \frac{\rho^{(1)}D_{KT}}{\eta^{(1)}(C_1 - C_0)}, \quad \rho^{*(i)} = \frac{\rho^{*(i)}}{\rho^{(1)}}, \delta = \frac{a_1}{a},$$
$$\eta^{*(i)} = \frac{\eta^{*(i)}}{\eta^{(1)}}, \qquad \kappa^{*(i)} = \frac{\kappa^{*(i)}}{\kappa^{(1)}}, \qquad D^{*(i)} = \frac{D^{*(i)}}{D^{(1)}}. \tag{8.27}$$

After dropping * non-dimensional form of Eqs. (8.16)-(8.26) are given as follow

$$\frac{\partial u^{(k)}}{\partial x} + \frac{\partial v^{(k)}}{\partial y} = 0, \tag{8.28}$$

$$ReF^{(i)}\left(u^{(i)}\right) = \beta^2\frac{\partial \tau_{xx}^{(i)}}{\partial x} + \frac{\partial \tau_{xy}^{(i)}}{\partial y} - \frac{\partial p}{\partial x}, \tag{8.29}$$

$$Re\beta^2F^{(i)}\left(v^{(i)}\right) = \beta^2\frac{\partial \tau_{yx}^{(i)}}{\partial x} + \beta\frac{\partial \tau_{yy}^{(i)}}{\partial y} - \frac{\partial p}{\partial y}, \tag{8.30}$$

$$\beta RePrF^{(i)}\left(\theta^{(i)}\right) = \frac{\partial^2\theta^{(i)}}{\partial y^2} + \frac{Br}{\kappa^{(i)}}\tau_{yx}^{(i)}\frac{\partial u^{(i)}}{\partial y}, \tag{8.31}$$

$$\beta ReS_HF^{(i)}\left(\phi^{(i)}\right) = \frac{\partial^2\phi^{(i)}}{\partial y^2} + \frac{S_HS_T}{D^{(i)}}\frac{\partial^2\theta^{(i)}}{\partial y^2}, \tag{8.32}$$

where stress tensors can be written as

$$\left(1 + \frac{\varepsilon^{(i)}\lambda^{(i)}}{\eta^{(i)}}trace\left(\boldsymbol{\tau}^{(i)}\right)\right)\tau_{xx}^{(i)} + \lambda^{(i)}\left(\beta u^{(i)}\frac{\partial u^{(i)}}{\partial x} + \beta^2 v^{(i)}\frac{\partial v^{(i)}}{\partial y}\right)\tau_{xx}^{(i)}$$
$$-2\lambda^{(i)}\left(\beta\tau_{xx}^{(i)}\frac{\partial u^{(i)}}{\partial x} + \beta^2\tau_{xy}^{(i)}\frac{\partial v^{(i)}}{\partial x}\right) = 2\beta\eta^{(i)}\frac{\partial u^{(i)}}{\partial x}, \tag{8.33}$$
$$\left(1 + \frac{\varepsilon^{(i)}\lambda^{(i)}}{\eta^{(i)}}trace\left(\boldsymbol{\tau}^{(i)}\right)\right)\tau_{xy}^{(k)} + \lambda^{(i)}\left(\beta u^{(i)}\frac{\partial u^{(i)}}{\partial x} + \beta^2 v^{(i)}\frac{\partial v^{(i)}}{\partial y}\right)\tau_{xy}^{(i)}$$

$$-2\lambda^{(i)}\left(\tau_{xx}^{(i)}\frac{\partial u^{(i)}}{\partial y}+\beta^2\tau_{xy}^{(i)}\frac{\partial v^{(i)}}{\partial y}+\beta\tau_{xy}^{(i)}\frac{\partial u^{(i)}}{\partial x}+\beta^2\tau_{yy}^{(i)}\frac{\partial v^{(i)}}{\partial x}\right)$$
$$=\eta^{(i)}\left(\frac{\partial u^{(i)}}{\partial y}+\beta^2\frac{\partial v^{(i)}}{\partial x}\right), \tag{8.34}$$

$$\left(1+\frac{\varepsilon^{(i)}\lambda^{(i)}}{\eta^{(i)}}trace(\boldsymbol{\tau}^{(i)})\right)\tau_{yy}^{(i)}+\lambda^{(i)}\left(\beta u^{(i)}\frac{\partial u^{(i)}}{\partial x}+\beta^2 v^{(i)}\frac{\partial v^{(i)}}{\partial y}\right)\tau_{yy}^{(i)}$$
$$-2\lambda^{(i)}\left(\tau_{xy}^{(i)}\frac{\partial u^{(i)}}{\partial y}+\beta\tau_{yy}^{(i)}\frac{\partial v^{(i)}}{\partial y}\right)=2\eta^{(i)}\frac{\partial u^{(i)}}{\partial y}. \tag{8.35}$$

Also boundary conditions for velocity, stress, temperature and concentration are given as follow

$$\tau_{xy}^{(1)}=0 \quad at \quad y=0, \tag{8.36a}$$
$$\tau_{xy}^{(1)}=\tau_{xy}^{(2)} \quad at \quad y=h_1, \tag{8.36b}$$
$$u^{(1)}=u^{(2)} \quad at \quad y=h_1, \tag{8.36c}$$
$$u^{(2)}=-1-2\pi\epsilon a\beta\cos(2\pi x) \quad at \quad y=h, \tag{8.36d}$$
$$v^{(2)}=\pm 2\pi\epsilon(\sin(2\pi x)+2\pi\epsilon a\beta\sin(2\pi x)\cos(2\pi x)) \quad at \quad y=h. \tag{8.36e}$$

$$\frac{\partial\theta^{(1)}}{\partial y}=0 \quad at \quad y=0, \tag{8.37a}$$
$$\kappa^{(1)}\frac{\partial\theta^{(1)}}{\partial y}=\kappa^{(2)}\frac{\partial\theta^{(2)}}{\partial y} \quad at \quad y=h_1, \tag{8.37b}$$
$$\theta^{(1)}=\theta^{(2)} \quad at \quad y=h_1, \tag{8.37c}$$
$$\theta^{(2)}=0 \quad at \quad y=h. \tag{8.37d}$$

$$\frac{\partial\phi^{(1)}}{\partial y}=0 \quad at \quad y=0, \tag{8.38a}$$
$$D^{(1)}\frac{\partial\phi^{(1)}}{\partial y}=D^{(2)}\frac{\partial\phi^{(2)}}{\partial y} \quad at \quad y=h_1, \tag{8.38b}$$
$$\phi^{(1)}=\phi^{(2)} \quad at \quad y=h_1, \tag{8.38c}$$

$$\phi^{(2)} = 0 \qquad at \;\; y = h. \tag{8.38d}$$

where

$$h(x) = [1 + \epsilon \cos x],$$
$$h_1(x) = [\delta + \delta\epsilon \cos x].$$

Using long wavelength and small Reynolds' number approximation in Eqs. (6.28-6.38), one can get the following form

$$\frac{\partial p}{\partial x} = \frac{\partial \tau_{xy}^{(i)}}{\partial y}, \tag{8.39}$$

$$\frac{\partial p}{\partial y} = 0, \tag{8.40}$$

$$\frac{\partial^2 \theta^{(i)}}{\partial y^2} = -\frac{Br}{\kappa^{(i)}} \tau_{yx}^{(i)} \frac{\partial u^{(i)}}{\partial y}, \tag{8.41}$$

$$\frac{\partial^2 \phi^{(i)}}{\partial y^2} = -\frac{S_H S_T}{D^{(i)}} \frac{\partial^2 \theta^{(i)}}{\partial y^2}. \tag{8.42}$$

After using long wavelength approximation and solving Eqs. (8.33-8.35), one can write following expressions

$$\tau_{xx}^{(i)} = 0, \tag{8.43}$$

$$\tau_{yy}^{(i)} = \frac{2\lambda^{(i)}}{\eta^{(i)}} \tau_{xy}^{2(i)}, \tag{8.44}$$

$$\tau_{xy}^{(i)} + 2\frac{\varepsilon^{(i)}\lambda^{2(i)}}{\eta^{2(i)}} \tau_{xy}^{3(i)} = \eta^{(i)} \frac{\partial u^{(i)}}{\partial y}. \tag{8.45}$$

with boundary conditions

$$\tau_{xy}^{(1)} = 0 \;\; at \;\; y = 0, \tag{8.46a}$$
$$\tau_{xy}^{(1)} = \tau_{xy}^{(2)} \quad at \;\; y = h_1, \tag{8.46b}$$
$$u^{(1)} = u^{(2)} \quad at \;\; y = h_1, \tag{8.46c}$$
$$u^{(2)} = -1 - 2\pi\epsilon\alpha\beta \cos(2\pi x) \quad at \;\; y = h, \tag{8.46d}$$
$$v^{(2)} = 2\pi\epsilon(\sin(2\pi x) + 2\pi\epsilon\alpha\beta \sin(2\pi x)\cos(2\pi x)) \;\; at \;\; y = h. \tag{8.46e}$$

$$\frac{\partial \theta^{(1)}}{\partial y} = 0 \qquad at \;\; y = 0, \tag{8.47a}$$

$$\kappa^{(1)} \frac{\partial \theta^{(1)}}{\partial y} = \kappa^{(2)} \frac{\partial \theta^{(2)}}{\partial y} \qquad at \;\; y = h_1, \tag{8.47b}$$

$$\theta^{(1)} = \theta^{(2)} \qquad at \;\; y = h_1, \tag{8.47c}$$

$$\theta^{(2)} = 0 \qquad at \;\; y = h. \tag{8.47d}$$

$$\frac{\partial \phi^{(1)}}{\partial y} = 0 \qquad at \;\; y = 0, \tag{8.48a}$$

$$D^{(1)} \frac{\partial \phi^{(1)}}{\partial y} = D^{(2)} \frac{\partial \phi^{(2)}}{\partial y} \qquad at \;\; y = h_1, \tag{8.48b}$$

$$\phi^{(1)} = \phi^{(2)} \qquad at \;\; y = h_1, \tag{8.48c}$$

$$\phi^{(2)} = 0 \qquad at \;\; y = h \tag{8.48d}$$

where

$$h(x) = [1 + \epsilon \cos x],$$
$$h_1(x) = [\delta + \delta\epsilon \cos x].$$

8.2 Solution of the Problem

To find the following stresses, one can make the integration of Eq. (8.39) w.r.t "y"

$$\tau_{xy}^{(i)} = \frac{\partial p}{\partial x} y + A_1^{(i)}, \qquad i = 1,2. \tag{8.49}$$

where $A_1^{(i)}$ are constants of integration.

Using conditions mentioned in Eq. (8.45a) into the above equation for $= 1$, one can find $A_1^{(1)} = 0$.

$$\tau_{xy}^{(1)} = \frac{\partial p}{\partial x} y, \qquad 0 \le y \le h_1 \tag{8.50}$$

Similarly we use Eq. (8.45b) in Eq. (8.49) for $i = 2$ and find that $A_1^{(2)} = 0$

$$\tau_{xy}^{(2)} = \frac{\partial p}{\partial x} y, \qquad h_1 \le y \le h \tag{8.51}$$

Expressions in Eq. (8.50) and Eq. (8.51) clearly show that stresses $\tau_{xy}^{(i)}$ in both

regions are same.

$$\tau_{xy}^{(i)} = \frac{\partial p}{\partial x} y, \tag{8.52}$$

Substituting the Eq. (8.52) in Eq. (8.43), one can write the following form

$$\tau_{yy}^{(i)} = \frac{2\lambda^{(i)}}{\eta^{(i)}} \left(\frac{\partial p}{\partial x}\right)^2 y^2. \tag{8.53}$$

After using the Eq. (8.52) and Eq. (8.44), one can find the following form of velocity

$$\frac{\partial u^{(i)}}{\partial y} = c^{(i)} y^3 + \frac{\partial p}{\partial x} \frac{y}{\eta^{(i)}}, \tag{8.54}$$

Integration of above equation yields the following form

$$u^{(i)} = c^{(i)} \frac{y^4}{2} + \frac{\partial p}{\partial x} \frac{y^2}{2\eta^{(i)}} + B^{(i)}, \tag{8.55}$$

where $c^{(i)} = 2 \frac{\varepsilon^{(i)} \lambda^{2(i)}}{\eta^{3(i)}} \left(\frac{\partial p}{\partial x}\right)^3$

Using boundary conditions given in Eqs. (8.45a) - Eq. (8.45e) in above equation, one can get the following velocity profiles in two regions.

$$u^{(1)} = u(h) + \frac{\partial p}{\partial x} \frac{1}{2\eta^{(1)}} (y^2 - h_1^2) + \frac{\varepsilon^{(1)} \lambda^{2(1)}}{2\eta^{3(1)}} \left(\frac{\partial p}{\partial x}\right)^3 (y^4 - h_1^4) + \frac{\partial p}{\partial x} \frac{1}{2\eta^{(2)}} (h_1^2 - h^2) + \frac{\varepsilon^{(1)} \lambda^{2(1)}}{2\eta^{3(1)}} \left(\frac{\partial p}{\partial x}\right)^3 (h_1^4 - h^4). \tag{8.56}$$

$$u^{(2)} = u(h) + \frac{\partial p}{\partial x} \frac{1}{2\eta^{(2)}} (y^2 - h^2) + \frac{\varepsilon^{(2)} \lambda^{2(2)}}{2\eta^{3(2)}} \left(\frac{\partial p}{\partial x}\right)^3 (y^4 - h^4). \tag{8.57}$$

After integrating Eq. (8.41) and using boundary conditions given in Eq. $8.47(a-d)$ one can get following temperature profiles

$$\theta^{(1)} = -\frac{Br}{12\kappa^{(1)}\eta^{(1)}} \left(\frac{\partial p}{\partial x}\right)^2 (y^4 - h_1^4) - \frac{2Br\varepsilon^{(1)}\lambda^{2(1)}}{30\kappa^{(1)}\eta^{3(1)}} \left(\frac{\partial p}{\partial x}\right)^4 (y^6 - h_1^6) - \frac{Br}{12\kappa^{(2)}\eta^{(2)}} \left(\frac{\partial p}{\partial x}\right)^2 (h_1^4 - h^4) - \frac{2Br\varepsilon^{(2)}\lambda^{2(2)}}{30\kappa^{(2)}\eta^{3(2)}} \left(\frac{\partial p}{\partial x}\right)^4 (h_1^6 - h^6) + \left(-\frac{Br}{3\eta^{(1)}} \left(\frac{\partial p}{\partial x}\right)^2 h_1^3 - \frac{2Br\varepsilon^{(1)}\lambda^{2(1)}}{5\eta^{3(1)}} \left(\frac{\partial p}{\partial x}\right)^4 h_1^5\right) (h_1 - h)$$

$$+\left(-\frac{Br}{3\eta^{(2)}}\left(\frac{\partial p}{\partial x}\right)^2 h_1^3-\frac{2Br\varepsilon^{(2)}\lambda^{2(2)}}{5\eta^{3(2)}}\left(\frac{\partial p}{\partial x}\right)^4 h_1^5\right)(h_1-h), \tag{8.58}$$

$$\theta^{(2)}=-\frac{Br}{12\kappa^{(2)}\eta^{(2)}}\left(\frac{\partial p}{\partial x}\right)^2 (y^4-h^4)-\frac{2Br\varepsilon^{(2)}\lambda^{2(2)}}{30\kappa^{(2)}\eta^{3(2)}}\left(\frac{\partial p}{\partial x}\right)^4 (y^6-h^6)$$
$$+\left(-\frac{Br}{3\eta^{(1)}}\left(\frac{\partial p}{\partial x}\right)^2 h_1^3-\frac{2Br\varepsilon^{(1)}\lambda^{2(1)}}{5\eta^{3(1)}}\left(\frac{\partial p}{\partial x}\right)^4 h_1^5\right)\left(\frac{1}{\eta^{(2)}}-\frac{1}{\eta^{(1)}}\right)(y-h). \tag{8.59}$$

Similarly, Eq. (8.42) can be written as follows

$$\phi^{(1)}=\frac{Sh*St*Br}{12D^{(1)}\kappa^{(1)}\eta^{(1)}}\left(\frac{\partial p}{\partial x}\right)^2 (y^4-h_1^4)+\frac{2Sh*St*Br\varepsilon^{(1)}\lambda^{2(1)}}{30D^{(1)}\kappa^{(1)}\eta^{3(1)}}\left(\frac{\partial p}{\partial x}\right)^4 (y^6-h_1^6$$
$$+\frac{Sh*St*Br}{12D^{(2)}\kappa^{(2)}\eta^{(2)}}\left(\frac{\partial p}{\partial x}\right)^2 (h_1^4-h^4)+\frac{2Sh*St*Br\varepsilon^{(2)}\lambda^{2(2)}}{30D^{(2)}\kappa^{(2)}\eta^{3(2)}}\left(\frac{\partial p}{\partial x}\right)^4 (h_1^6-$$
$$+\left(\frac{Sh*St*Br}{3\kappa^{(1)}\eta^{(1)}}\left(\frac{\partial p}{\partial x}\right)^2 h_1^3+\frac{2Sh*St*Br\varepsilon^{(1)}\lambda^{2(1)}}{30\kappa^{(1)}\eta^{3(1)}}\left(\frac{\partial p}{\partial x}\right)^4 h_1^5\right)(h_1-h)$$
$$-\left(\frac{Sh*St*Br}{3\kappa^{(2)}\eta^{(2)}}\left(\frac{\partial p}{\partial x}\right)^2 h_1^3+\frac{2Sh*St*Br\varepsilon^{(2)}\lambda^{2(2)}}{30\kappa^{(2)}\eta^{3(2)}}\left(\frac{\partial p}{\partial x}\right)^4 h_1^5\right)(h_1-h), \tag{8.60}$$

$$\phi^{(2)}=\frac{Sh*St*Br}{12D^{(2)}\kappa^{(2)}\eta^{(2)}}\left(\frac{\partial p}{\partial x}\right)^2 (y^4-h^4)$$
$$+\frac{2Sh*St*Br\varepsilon^{(2)}\lambda^{2(2)}}{30D^{(2)}\kappa^{(2)}\eta^{3(2)}}\left(\frac{\partial p}{\partial x}\right)^4 (y^6-h^6)$$
$$+\left(\frac{Sh*St*Br}{3\kappa^{(1)}\eta^{(1)}}\left(\frac{\partial p}{\partial x}\right)^2 h_1^3+\frac{2Sh*St*Br\varepsilon^{(1)}\lambda^{2(1)}}{30\kappa^{(1)}\eta^{3(1)}}\left(\frac{\partial p}{\partial x}\right)^4 h_1^5\right)(y-h) \tag{8.61}$$
$$-\left(\frac{Sh*St*Br}{3\kappa^{(2)}\eta^{(2)}}\left(\frac{\partial p}{\partial x}\right)^2 h_1^3+\frac{2Sh*St*Br\varepsilon^{(2)}\lambda^{2(2)}}{30\kappa^{(2)}\eta^{3(2)}}\left(\frac{\partial p}{\partial x}\right)^4 h_1^5\right)(y-h).$$

The total volumetric flow rate Q in dimensionless form is given by the following equation

$$Q=Q^{(1)}+Q^{(2)}, \tag{8.62}$$

$$Q=2hu(h)+\left(\frac{h^3}{6\eta^{(1)}}-\frac{hh_1^2}{2\eta^{(1)}}-\frac{5h^3}{6\eta^{(2)}}+\frac{hh_1^2}{2\eta^{(2)}}\right)\frac{\partial p}{\partial x}$$

$$+\left(\frac{h^5\varepsilon^{(1)}\lambda^{2(1)}}{10\eta^{3(1)}}-\frac{hh_1^4\varepsilon^{(1)}\lambda^{2(1)}}{2\eta^{3(1)}}-\frac{9h^5\varepsilon^{(2)}\lambda^{2(2)}}{10\eta^{3(2)}}+\frac{hh_1^4\varepsilon^{(2)}\lambda^{2(2)}}{2\eta^{3(2)}}\right)\left(\frac{\partial p}{\partial x}\right)^3. \tag{8.63}$$

8.3 Graphical Results

In this section the effects of involved parameters appearing in the immiscible PTT fluid flow induced by cilia motion are displayed through graphs. The effect of emerging parameters are observed on the pressure rise, velocity, temperature and concentration profile by fixing $a = 0.2, \beta = 0.2, \eta^{(1)} = 0.1, \eta^{(2)} = 0.5, \varepsilon^{(1)} = 0.1, \varepsilon^{(2)} = 0.5, \lambda^{(1)} = 0.1, \lambda^{(2)} = 0.5, x = 0.25,\ \epsilon = 0.25, p = 2,\ \delta = 0.5, \kappa^{(1)} = 0.1, \kappa^{(2)} = 0.5, Br = 1, D^{(1)} = 0.1, D^{(2)} = 0.5, S_H = 1\ \ and\ \ S_T = 1.$

Figs. $8.2 - 8.7$ show the effects of different parameters on pressure rise for two immiscible fluids. These graphs show that with the increasing values of viscosities $(\eta^{(1)}, \eta^{(2)})$ elongation parameters $(\lambda^{(1)}, \lambda^{(2)})$ and $(\varepsilon^{(1)}, \varepsilon^{(2)})$, pressure rise increases in pumping region and reduces in co pumping region. Figs. $8.8 - 8.13$ show the effects of various parameters on velocity profiles for two immiscible fluids. These graphs show that velocity is maximum at the center of the tube and continuity is clearly shown in graphs at the interface of two fluids i.e $(x = 0.5)$.

Figure (8.8) demonstrate the effect of distinct values of $\eta^{(1)}$ on the velocities of the fluids. It is observed that three curves in graph overlapped in the region of fluid phase II. It is also clearly indicated by equation (8.57) that the expression $u^{(2)}$ does not involve the coefficient of viscosity $\eta^{(1)}$ of phase I fluid in it and therefore the values of $\eta^{(1)}$ does not affect velocity of the fluid in phase II. However, the expressions (8.46) involve both parameters of viscosity, and velocities of both fluids and are affected by varying the value of $\eta^{(2)}$ as shown in figure (8.9). It is observed that with the increasing values of $\eta^{(2)}$ the velocity profiles of the fluids appear to be deliberate.

Figs. $8.10 - 8.11$ show the effect of elongation parameters $\varepsilon^{(1)}$ *and* $\varepsilon^{(2)}$ on velocity profile in both regions. By increasing elongation parameters $\varepsilon^{(1)}$ fluid decelerates in first region whereas it has no effect in second region and by increasing $\varepsilon^{(2)}$ fluid velocity decreases in both regions which shows that it has important application in ciliary flow.

Figs. $8.12 - 8.13$ show the effect of material parameters $\lambda^{(1)}$ *and* $\lambda^{(2)}$ on velocity profile in both regions. By increasing material parameters $\lambda^{(1)}$ fluid decelerates in first region whereas it has no effect in second region and by increasing $\lambda^{(2)}$ fluid velocity decreases in both the regions.

Figs. $8.14 - 8.22$ show the effects of various parameters on temperature profiles for two immiscible fluids. It can be seen from figures $8.14 - 8.19$ by increasing viscosities $(\eta^{(1)}, \eta^{(2)})$ elongation parameters $(\lambda^{(1)}, \lambda^{(2)})$ and $(\varepsilon^{(1)}, \varepsilon^{(2)})$ temperature profile decreases. Fig. (8.20) shows that by growing thermal conductivity $\kappa^{(1)}$ heat transfer decreases in first region but it does not have any effect in second region but $\kappa^{(2)}$ has the significant effect on both the regions i.e. heat transfer decreases by increasing $\kappa^{(2)}$ which can be seen in Fig. (8.21). Fig. (8.22) shows that by increasing Brinkman number Br temperature profile decreases.

Figs. $8.23 - 8.32$ show the effects of various parameters on concentration profiles for two immiscible fluids. It can be seen from figures $8.23 - 8.28$ by increasing viscosities $(\eta^{(1)}, \eta^{(2)})$ elongation parameters $(\lambda^{(1)}, \lambda^{(2)})$ and $(\varepsilon^{(1)}, \varepsilon^{(2)})$ concentration profile decreases. Fig. (8.29) shows that by increasing thermal conductivity $D^{(1)}$ concentration profile decreases in first region but it does not have significant effect in second region but $D^{(2)}$ has the noteworthy effect on both the regions i.e. concentration profile decreases by increasing $D^{(2)}$ which can be seen in

Fig. (8.30). Figs. 8.31 & 8.32 show that by increasing S_H *and* S_T concentration profile decreases.

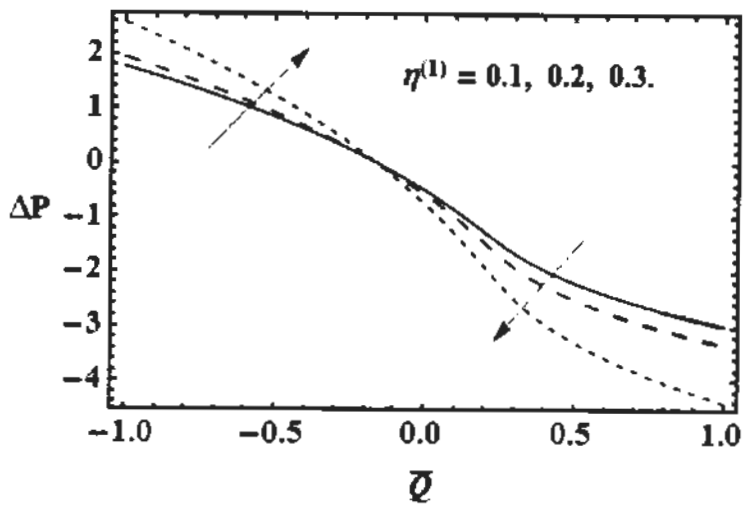

Fig. 8.2: Influence of viscosity $\eta^{(1)}$ on pressure rise ΔP for $\eta^{(2)} = 0.5, \varepsilon^{(1)} = 0.1, \varepsilon^{(2)} = 0.5, \lambda^{(1)} = 0.1$ *and* $\lambda^{(2)} = 0.5$.

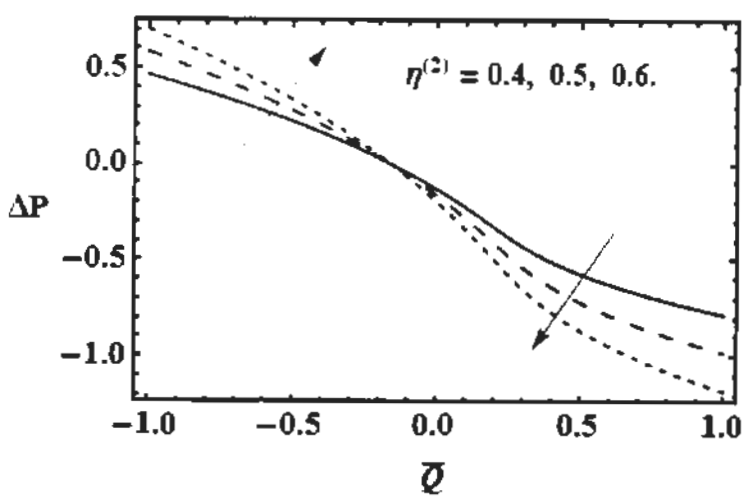

Fig. 8.3: Influence of viscosity $\eta^{(2)}$ on pressure rise ΔP for $\eta^{(1)} = 0.1, \varepsilon^{(1)} = 0.1, \varepsilon^{(2)} = 0.5, \lambda^{(1)} = 0.1$ *and* $\lambda^{(2)} = 0.5$.

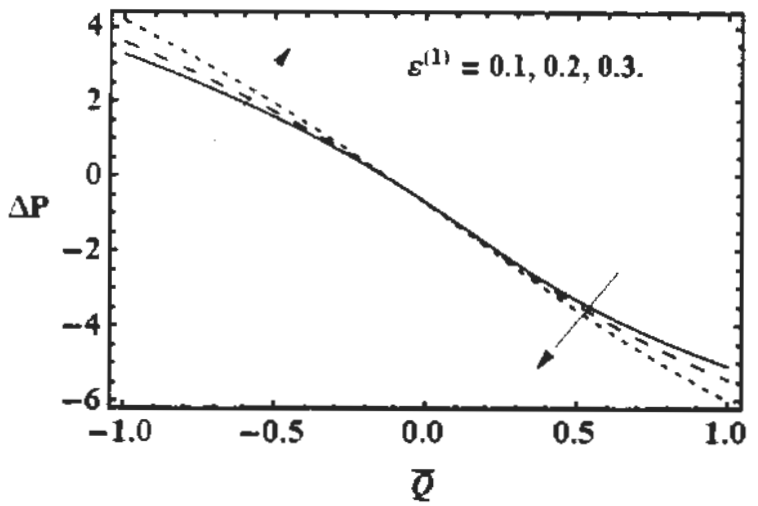

Fig. 8.4: Impact of elongation parameter $\varepsilon^{(1)}$ on pressure rise ΔP for $\eta^{(1)} = 0.1$, $\eta^{(2)} = 0.5, \varepsilon^{(2)} = 0.5, \lambda^{(1)} = 0.1$ *and* $\lambda^{(2)} = 0.5$.

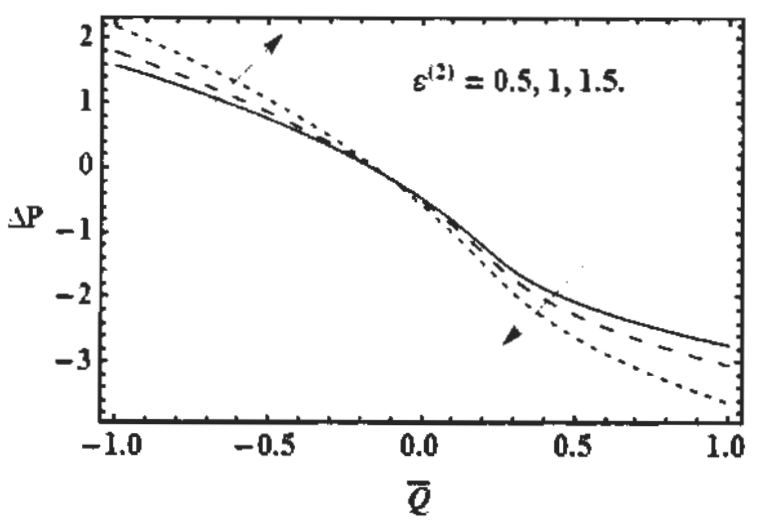

Fig. 8.5: Impact of elongation parameter $\varepsilon^{(2)}$ on pressure rise ΔP for $\eta^{(1)} = 0.1$, $\eta^{(2)} = 0.5, \varepsilon^{(1)} = 0.1, \lambda^{(1)} = 0.1$ *and* $\lambda^{(2)} = 0.5$.

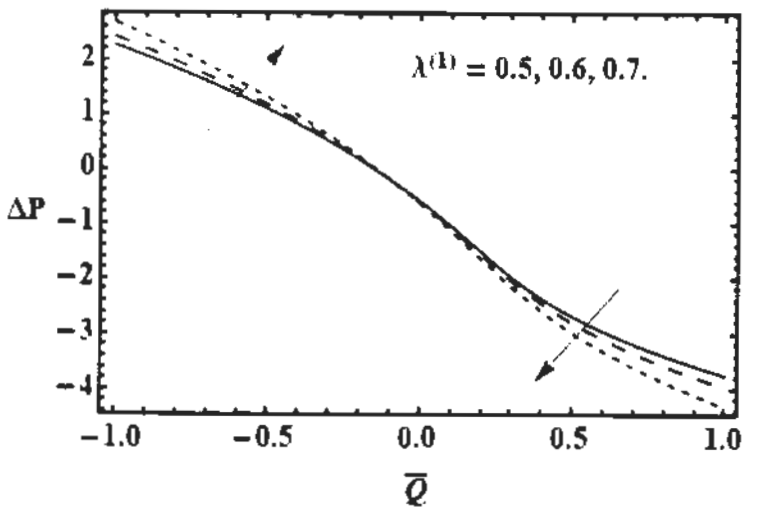

Fig. 8.6: Influence of material parameter $\lambda^{(1)}$ on pressure rise ΔP for $\eta^{(1)} = 0.1$, $\eta^{(2)} = 0.5, \varepsilon^{(1)} = 0.1, \varepsilon^{(2)} = 0.5$ *and* $\lambda^{(2)} = 0.5$.

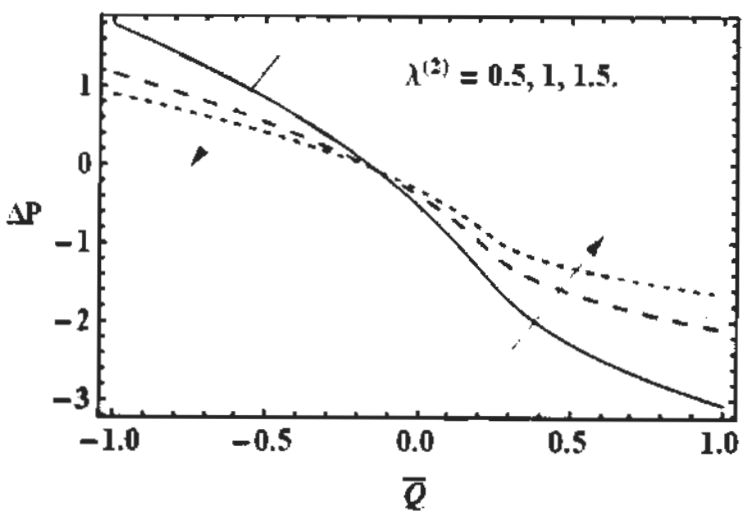

Fig. 8.7: Influence of material parameter $\lambda^{(2)}$ on pressure rise ΔP for $\eta^{(1)} = 0.1$, $\eta^{(2)} = 0.5, \varepsilon^{(1)} = 0.1, \varepsilon^{(2)} = 0.5$ *and* $\lambda^{(1)} = 0.1$.

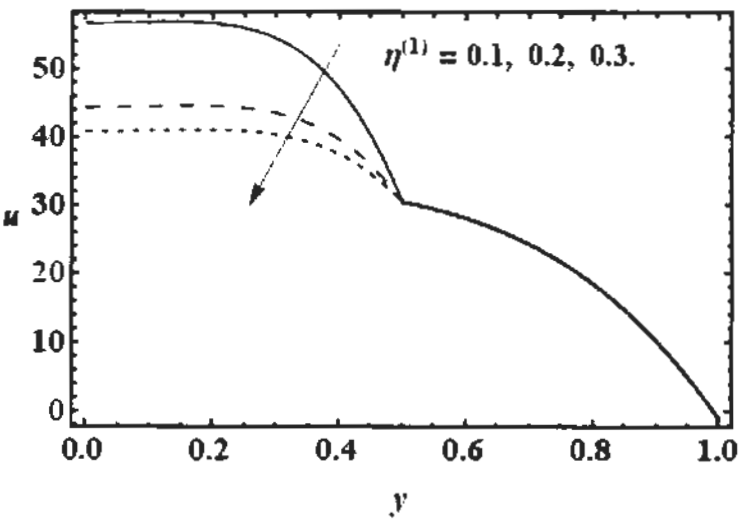

Fig. 8.8: Influence of viscosity $\eta^{(1)}$ on longitudinal velocity u for $\eta^{(2)} = 0.5$, $\varepsilon^{(1)} = 0.1, \varepsilon^{(2)} = 0.5, \lambda^{(1)} = 0.1$ *and* $\lambda^{(2)} = 0.5$.

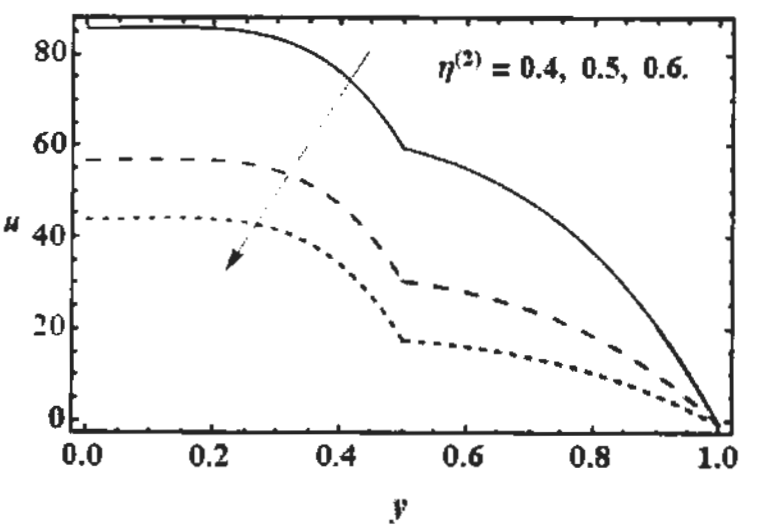

Fig. 8.9: Influence of viscosity $\eta^{(2)}$ on longitudinal velocity u for $\eta^{(1)} = 0.1$, $\varepsilon^{(1)} = 0.1, \varepsilon^{(2)} = 0.5, \lambda^{(1)} = 0.1$ *and* $\lambda^{(2)} = 0.5$.

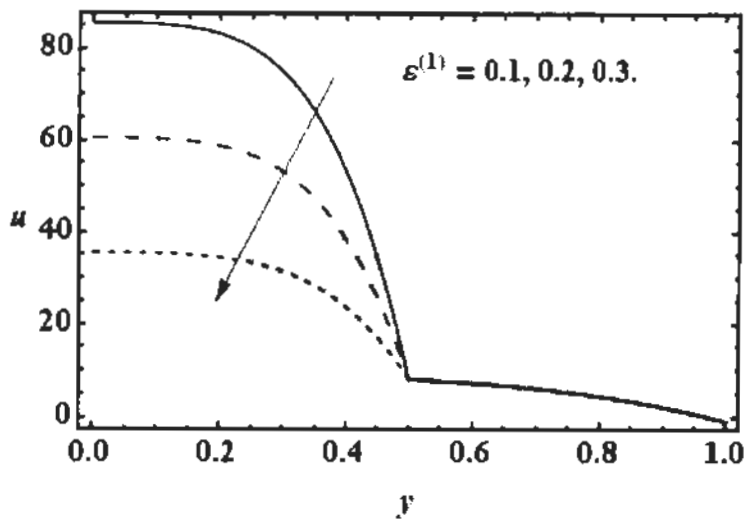

Fig. 8.10: Influence of elongation parameter $\varepsilon^{(1)}$ on longitudinal velocity u for $\eta^{(1)} = 0.1, \eta^{(2)} = 0.5, \varepsilon^{(2)} = 0.5, \lambda^{(1)} = 0.1$ *and* $\lambda^{(2)} = 0.5$.

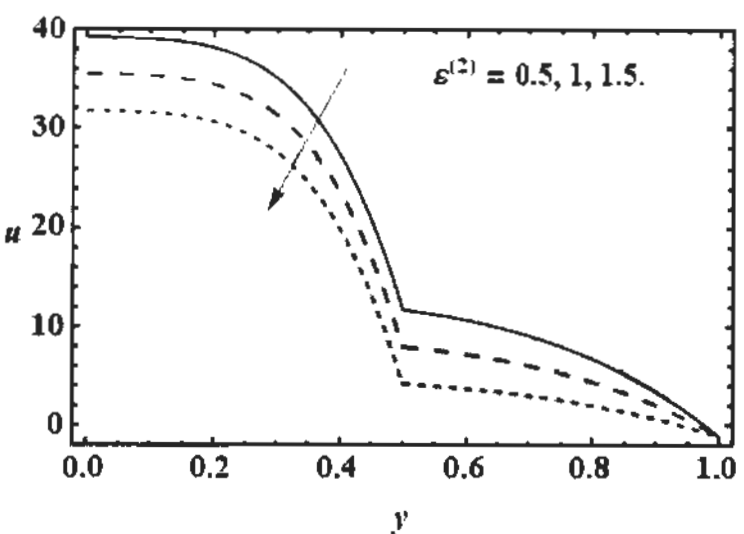

Fig. 8.11: Impact of elongation parameter $\varepsilon^{(2)}$ on longitudinal velocity u for $\eta^{(1)} = 0.1, \eta^{(2)} = 0.5, \varepsilon^{(1)} = 0.1, \lambda^{(1)} = 0.1$ *and* $\lambda^{(2)} = 0.5$.

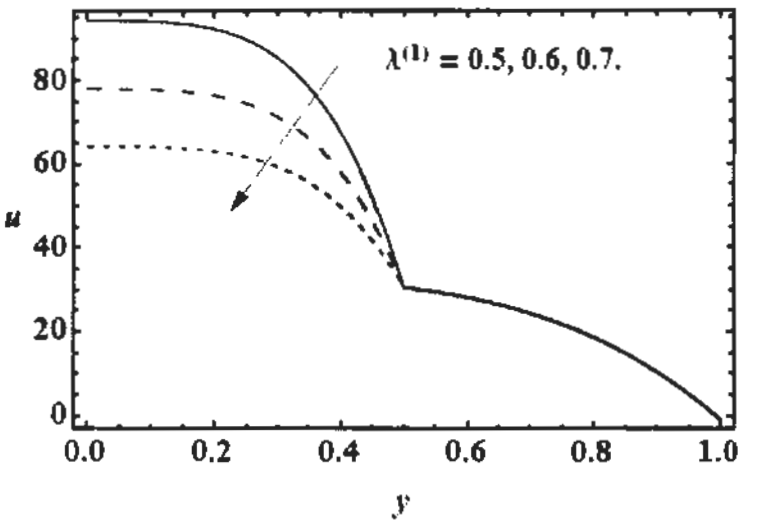

Fig. 8.12: Influence of material parameter $\lambda^{(1)}$ on longitudinal velocity u for $\eta^{(1)} = 0.1, \eta^{(2)} = 0.5, \varepsilon^{(1)} = 0.1, \varepsilon^{(2)} = 0.5$ *and* $\lambda^{(2)} = 0.5$.

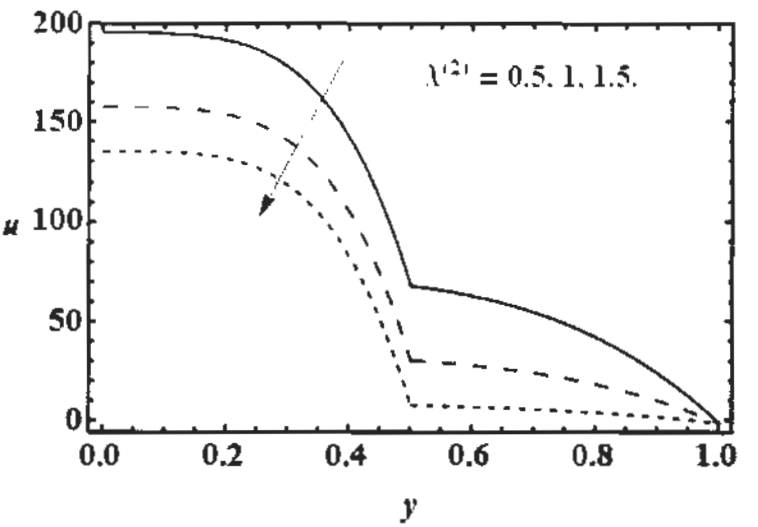

Fig. 8.13: Influence of material parameter $\lambda^{(1)}$ on longitudinal velocity u for $\eta^{(1)} = 0.1, \eta^{(2)} = 0.5, \varepsilon^{(1)} = 0.1, \varepsilon^{(2)} = 0.5$ *and* $\lambda^{(1)} = 0.1$.

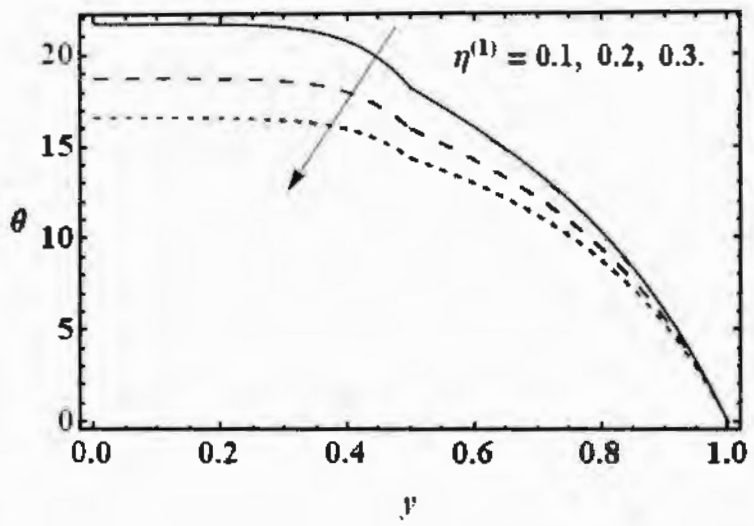

Fig. 8.14: Influence of viscosity $\eta^{(1)}$ on temperature profile θ for $\eta^{(2)} = 0.5$, $\varepsilon^{(1)} = 0.1, \varepsilon^{(2)} = 0.5, \lambda^{(1)} = 0.1, \lambda^{(2)} = 0.5,\ \kappa^{(1)} = 0.1,$ $\kappa^{(2)} = 0.5$ *and* $Br = 1$.

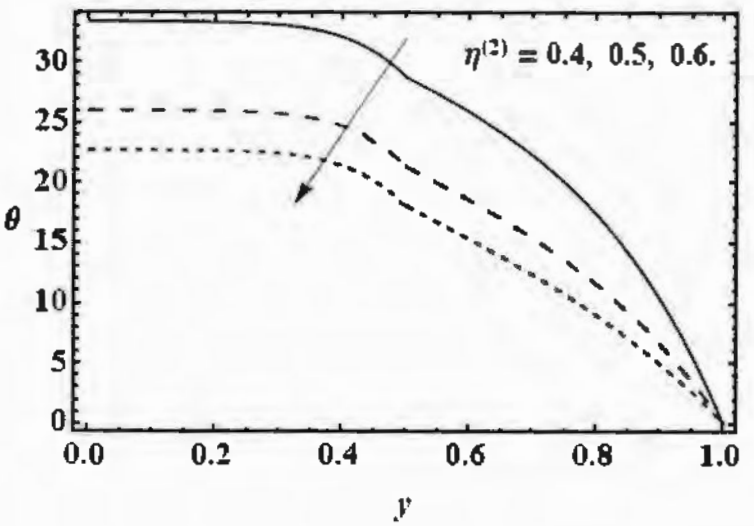

Fig. 8.15:.Influence of viscosity $\eta^{(1)}$ on temperature profile θ for $\eta^{(1)} = 0.1$, $\varepsilon^{(1)} = 0.1, \varepsilon^{(2)} = 0.5, \lambda^{(1)} = 0.1, \lambda^{(2)} = 0.5,\ \kappa^{(1)} = 0.1,$ $\kappa^{(2)} = 0.5$ *and* $Br = 1$.

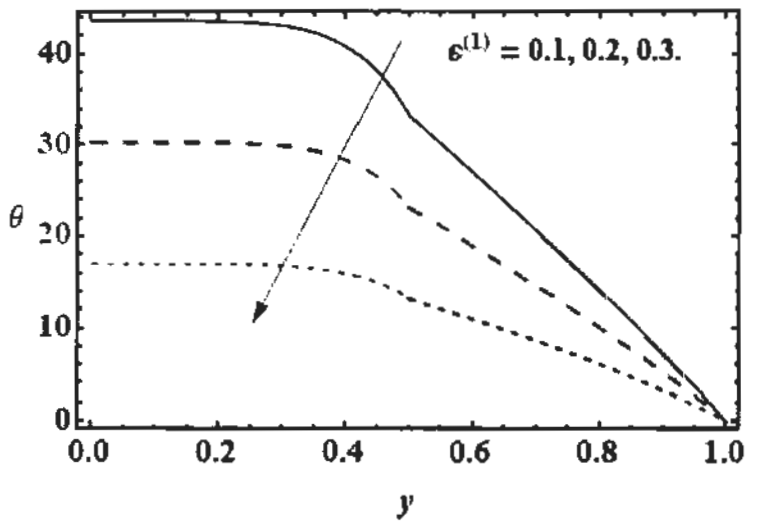

Fig. 8.16: Impact of elongation parameter $\varepsilon^{(1)}$ on temperature field θ for $\eta^{(1)} = 0.1,\ \eta^{(2)} = 0.5, \varepsilon^{(2)} = 0.5, \lambda^{(1)} = 0.1, \lambda^{(2)} = 0.5,\ \kappa^{(1)} = 0.1,$ $\kappa^{(2)} = 0.5$ *and* $Br = 1.$

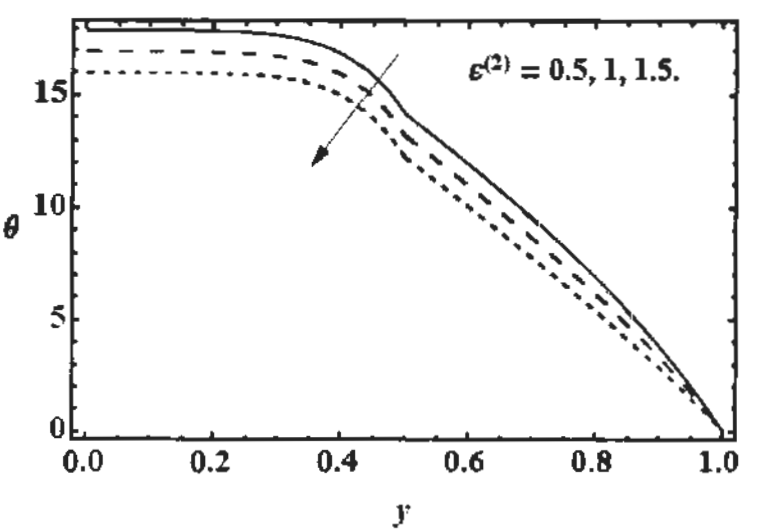

Fig. 8.17: Impact of elongation parameter $\varepsilon^{(2)}$ on temperature field θ for $\eta^{(1)} = 0.1,\ \eta^{(2)} = 0.5, \varepsilon^{(1)} = 0.1, \lambda^{(1)} = 0.1, \lambda^{(2)} = 0.5,\ \kappa^{(1)} = 0.1,$ $\kappa^{(2)} = 0.5$ *and* $Br = 1.$

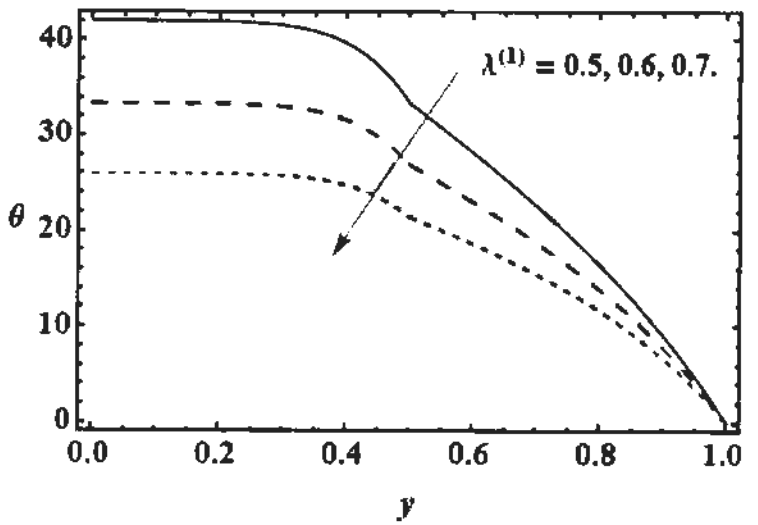

Fig. 8.18: Impact of material parameter $\lambda^{(1)}$ on temperature field θ for $\eta^{(1)} = 0.1$, $\eta^{(2)} = 0.5, \varepsilon^{(1)} = 0.1, \varepsilon^{(2)} = 0.5, \lambda^{(2)} = 0.5$, $\kappa^{(1)} = 0.1$, $\kappa^{(2)} = 0.5$ *and* $Br = 1$.

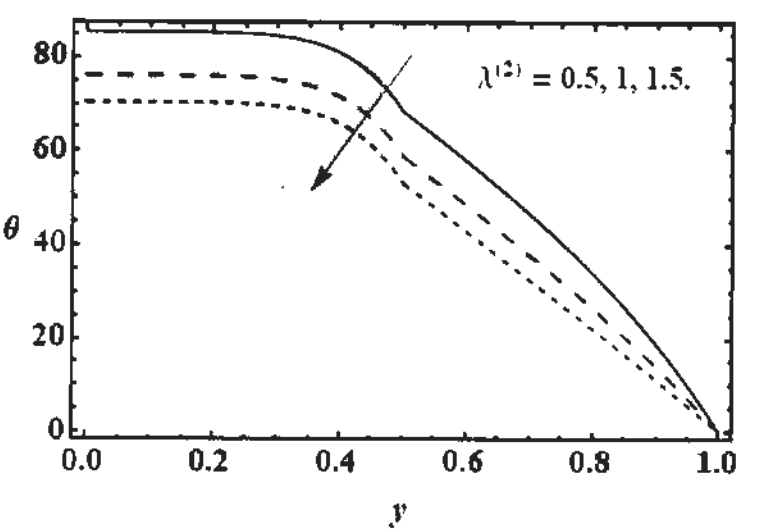

Fig. 8.19: Impact of material parameter $\lambda^{(2)}$ on temperature field θ for $\eta^{(1)} = 0.1$, $\eta^{(2)} = 0.5, \varepsilon^{(1)} = 0.1, \varepsilon^{(2)} = 0.5, \lambda^{(1)} = 0.1$, $\kappa^{(1)} = 0.1$, $\kappa^{(2)} = 0.5$ *and* $Br = 1$.

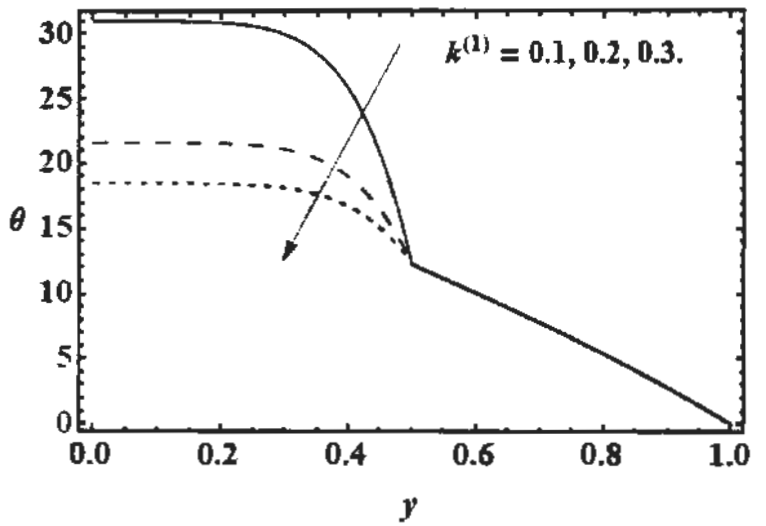

Fig. 8.20: Influence of thermal conductivity $\kappa^{(1)}$ on temperature profile θ for $\eta^{(1)} = 0.1, \eta^{(2)} = 0.5, \varepsilon^{(1)} = 0.1, \varepsilon^{(2)} = 0.5, \lambda^{(1)} = 0.1,\ \lambda^{(2)} = 0.5,$ $\kappa^{(2)} = 0.5\ \ and\ \ Br = 1.$

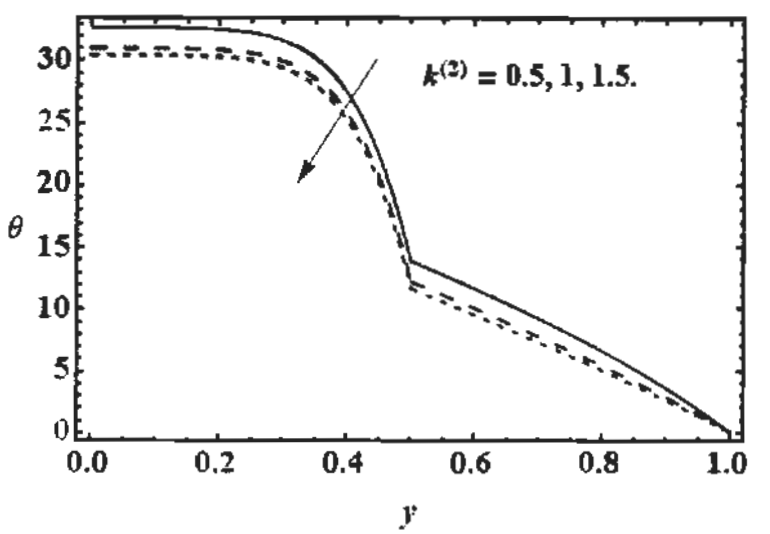

Fig. 8.21: Impact of thermal conductivity $\kappa^{(2)}$ on temperature field θ for $\eta^{(1)} = 0.1, \eta^{(2)} = 0.5, \varepsilon^{(1)} = 0.1, \varepsilon^{(2)} = 0.5, \lambda^{(1)} = 0.1,\ \lambda^{(2)} = 0.5,$ $\kappa^{(1)} = 0.1\ \ and\ \ Br = 1.$

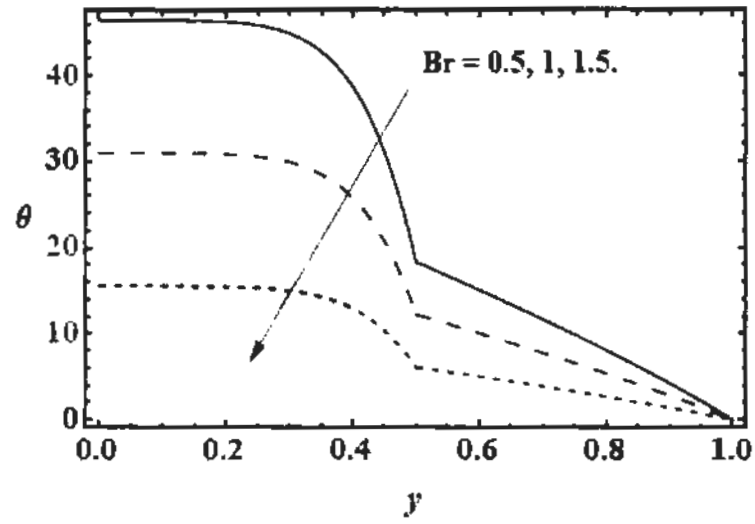

Fig. 8.22: Influence of Brinkman Br on temperature profile θ for $\eta^{(1)} = 0.1$, $\eta^{(2)} = 0.5, \varepsilon^{(1)} = 0.1, \varepsilon^{(2)} = 0.5, \lambda^{(1)} = 0.1, \ \lambda^{(2)} = 0.5,$ $\kappa^{(1)} = 0.1 \ and \ \kappa^{(2)} = 0.5.$

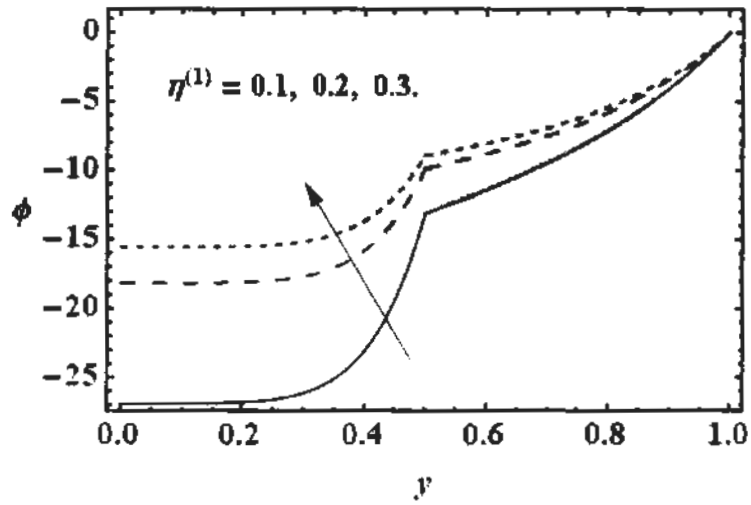

Fig. 8.23: Influence of viscosity $\eta^{(1)}$ on concentration profile ϕ for $\eta^{(2)} = 0.5$, $\varepsilon^{(1)} = 0.1, \varepsilon^{(2)} = 0.5, \lambda^{(1)} = 0.1, \lambda^{(2)} = 0.5, \ D^{(1)} = 0.1, D^{(2)} = 0.5,$ $S_H = 1 \ and \ S_T = 1.$

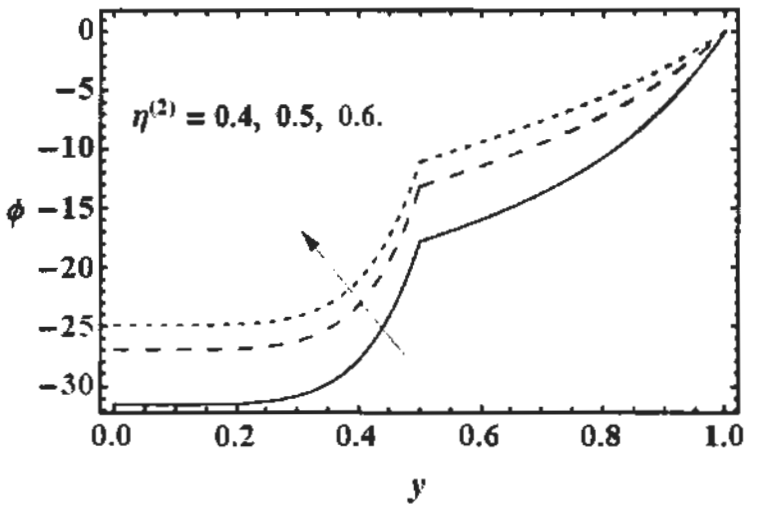

Fig. 8.24: Influence of viscosity $\eta^{(2)}$ on concentration profile ϕ for $\eta^{(1)} = 0.1$, $\varepsilon^{(1)} = 0.1, \varepsilon^{(2)} = 0.5, \lambda^{(1)} = 0.1, \lambda^{(2)} = 0.5,\ D^{(1)} = 0.1, \mathrm{D}^{(2)} = 0.5,$ $S_H = 1$ *and* $S_T = 1$.

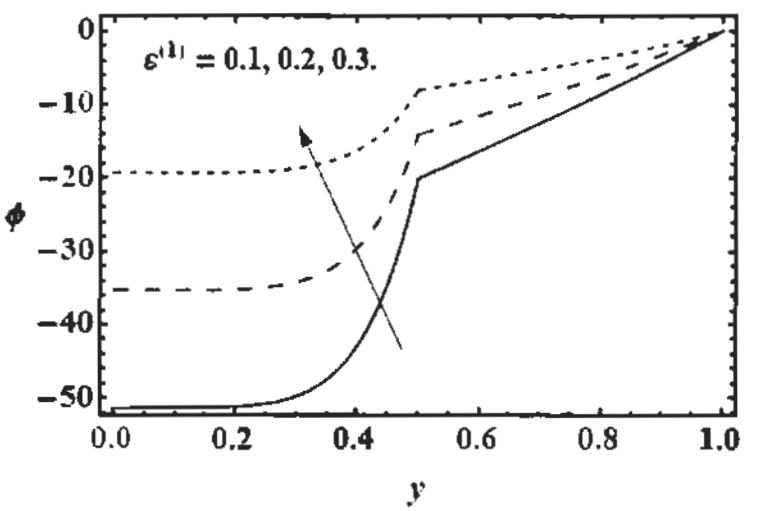

Fig. 8.25: Influence of elongation parameter $\varepsilon^{(1)}$ on concentration profile ϕ for $\eta^{(1)} = 0.1, \eta^{(2)} = 0.5, \varepsilon^{(2)} = 0.5, \lambda^{(1)} = 0.1, \lambda^{(2)} = 0.5,$ $D^{(1)} = 0.1, \mathrm{D}^{(2)} = 0.5,\quad S_H = 1$ *and* $S_T = 1$.

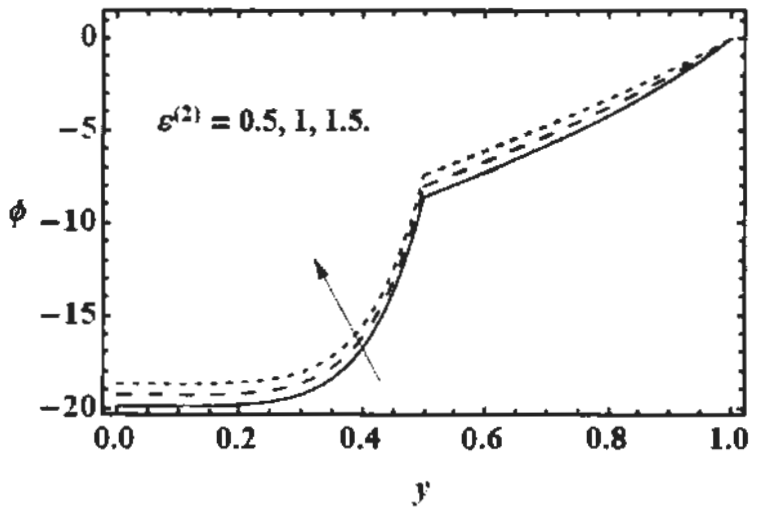

Fig. 8.26: Influence of elongation parameter $\varepsilon^{(2)}$ on concentration profile ϕ for

$\eta^{(1)} = 0.1, \eta^{(2)} = 0.5, \varepsilon^{(1)} = 0.1, \lambda^{(1)} = 0.1, \lambda^{(2)} = 0.5,$

$D^{(1)} = 0.1, \mathrm{D}^{(2)} = 0.5, \quad S_H = 1 \ \ and \ \ S_T = 1.$

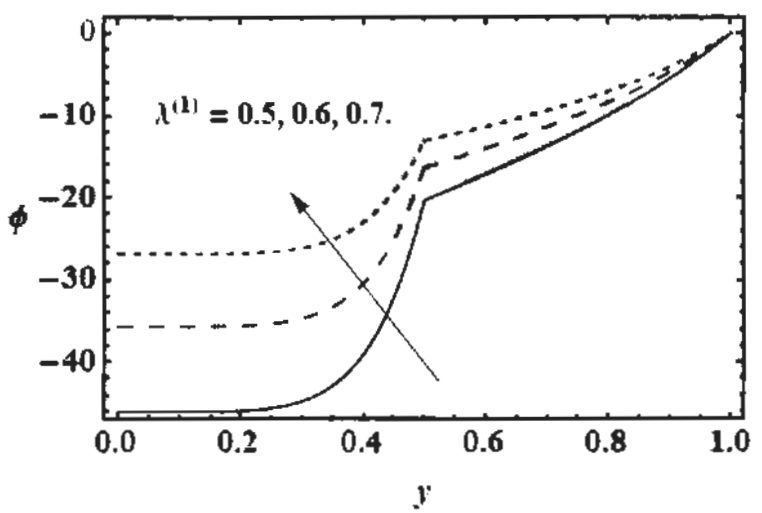

Fig. 8.27: Influence of material parameter $\lambda^{(1)}$ on concentration profile ϕ for

$\eta^{(1)} = 0.1, \eta^{(2)} = 0.5, \varepsilon^{(1)} = 0.1, \varepsilon^{(2)} = 0.5, \lambda^{(2)} = 0.5,$

$D^{(1)} = 0.1, \mathrm{D}^{(2)} = 0.5, \quad S_H = 1 \ \ and \ \ S_T = 1.$

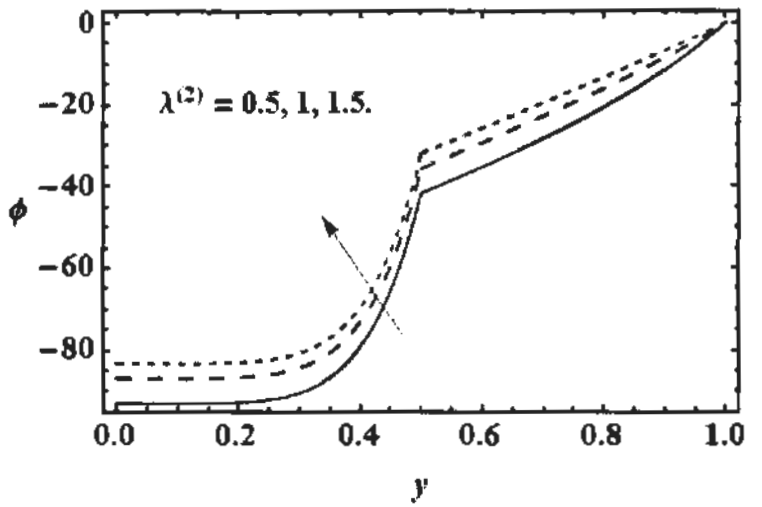

Fig. 8.28: Influence of material parameter $\lambda^{(2)}$ on concentration profile ϕ for $\eta^{(1)} = 0.1, \eta^{(2)} = 0.5, \varepsilon^{(1)} = 0.1, \varepsilon^{(2)} = 0.5, \lambda^{(1)} = 0.1,$ $D^{(1)} = 0.1, D^{(2)} = 0.5, \quad S_H = 1 \ and \ S_T = 1.$

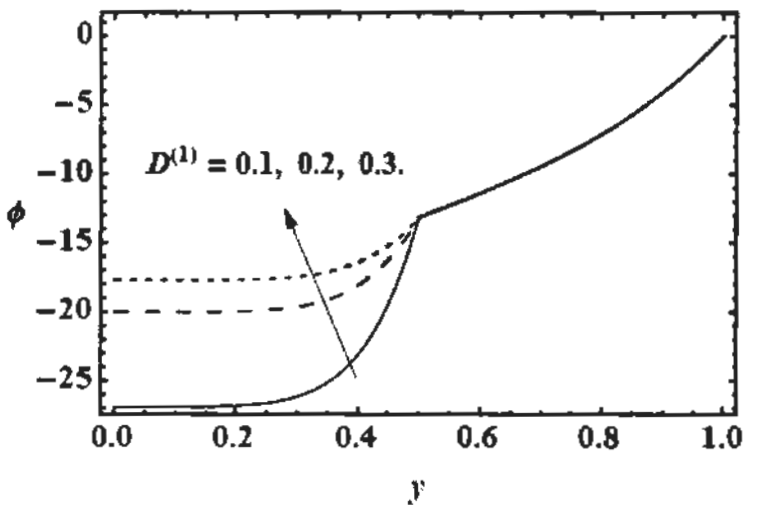

Fig. 8.29: Impact of diffusion parameter $D^{(1)}$ on concentration field ϕ for $\eta^{(1)} = 0.1,$ $\eta^{(2)} = 0.5, \varepsilon^{(1)} = 0.1, \varepsilon^{(2)} = 0.5, \lambda^{(1)} = 0.1, \ \lambda^{(2)} = 0.5, D^{(2)} = 0.5,$ $S_H = 1 \ and \ S_T = 1.$

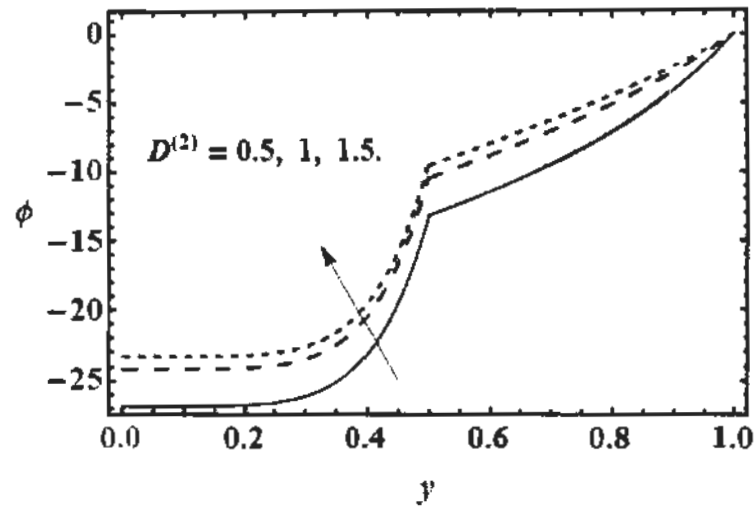

Fig. 8.30: Influence of diffusion parameter $D^{(2)}$ on concentration profile ϕ for $\eta^{(1)} = 0.1, \eta^{(2)} = 0.5, \varepsilon^{(1)} = 0.1, \varepsilon^{(2)} = 0.5, \lambda^{(1)} = 0.1,$ $\lambda^{(2)} = 0.5, \mathrm{D}^{(1)} = 0.1, S_H = 1$ *and* $S_T = 1.$

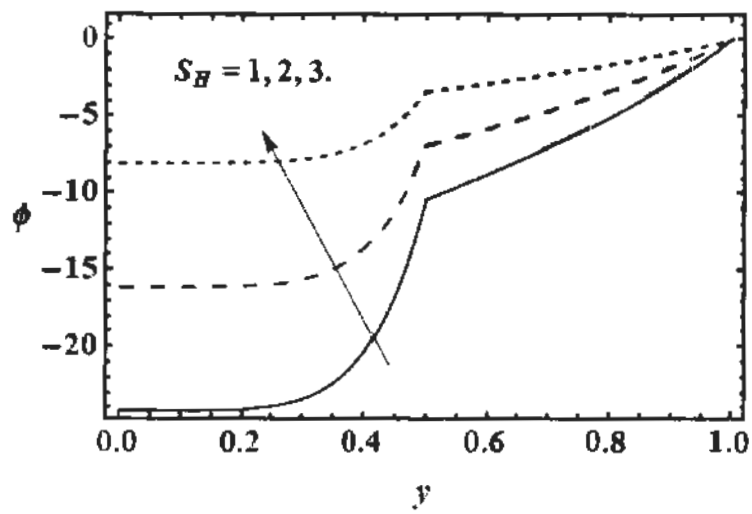

Fig. 8.31: Influence of Schmidt number S_H on concentration profile ϕ for $\eta^{(1)} = 0.1, \eta^{(2)} = 0.5, \varepsilon^{(1)} = 0.1, \varepsilon^{(2)} = 0.5, \lambda^{(1)} = 0.1,\ \lambda^{(2)} = 0.5, \mathrm{D}^{(1)} = 0.1,$ $\mathrm{D}^{(2)} = 0.5$ *and* $S_T = 1.$

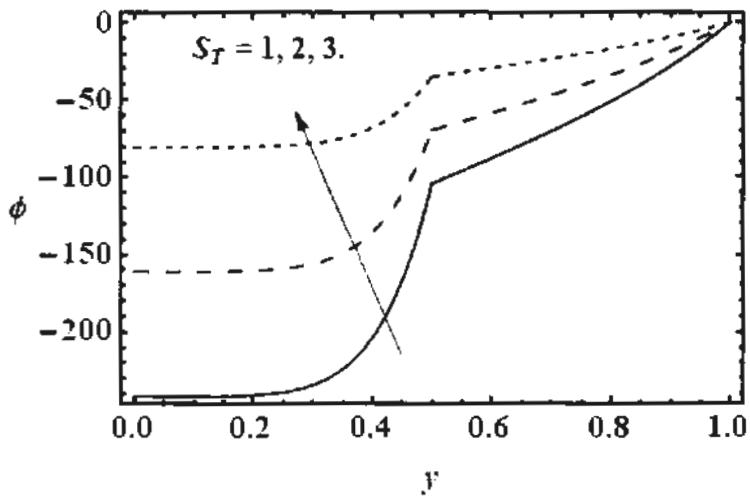

Fig. 8.32: Influence of Soret number S_T on concentration profile ϕ for $\eta^{(1)} = 0.1$, $\eta^{(2)} = 0.5, \varepsilon^{(1)} = 0.1, \varepsilon^{(2)} = 0.5, \lambda^{(1)} = 0.1$, $\lambda^{(2)} = 0.5, D^{(1)} = 0.1$, $D^{(2)} = 0.5$ *and* $S_H = 1$.

8.4 Conclusions

The mathematical analysis of ciliary flow in peripheral layer model has been discussed in this chapter. The diffusive convective heat and mass transfer of ciliary flow in two layer flow (liquid-liquid) is modelled with the help of mass, momentum, energy and concentration laws using linear PTT fluid model. The momentum, energy and concentration equations are simplified under the lubrication approach. Exact solutions for velocity, temperature and concentration have been constructed and graphical results are found with the help of software "MATHEMATICA". The flow features e.g pressure rise, velocity of fluid, temperature and concentration profiles are analyzed for different values of involved parameters and following observations are noted.

- Shear stress are independent of material constants whereas normal stresses depend on material constants.
- Pressure rise surges in pumping region and falls in co pumping region by increasing the values of various parameters.

- Continuity of velocities, temperature and concentration profile exists at the interface.
- Graphical results shows that velocity of fluid can be controlled by adjusting suitable values of different parameters
- Heat and diffusion rate can also be controlled by adjusting various values of involved parameters.

Chapter 9

Conclusions

This thesis presents the thermal and diffusion effects in cilia induced flow through channel and tube. It is found that heat and diffusion rate in the fluid can be enhanced by the ciliary movement.

In chapter 1, introduction to ciliary structure, basic laws of fluid mechanics and literature review are discussed in detail

In chapter 2, convective flow and mixing induced by cilia present in the bronchial airways under the effect of microscopic temperature gradient and magnetic field are discussed. The ciliary flow is modeled by the symplectic and antiplectic pattern that forms the metachronal wave. It is noted that the magnitude of concentration level can be increased with the help of magnetic field and thermophoretic effect but heat transfer and axial flow can be increased with the high length cilia and porous medium.

Chapter 3 is the study of thermal and concentration field analysis of cilia induced flow for Jeffrey's fluid model. It is investigated that Buoyancy force due to temperature difference causes to decrease the pressure gradient, temperature and axial velocity and buoyancy force due to concentration difference causes to increase the pressure gradient and temperature profile but it helps to reduce the axial velocity.

Effect of nanoparticles and entropy generation on tangent hyperbolic fluid due to ciliary movement is discussed in chapter 4. It is concluded that axial velocity and thermal conductivity of the fluid increases by inserting nanoparticles and entropy generation due to nanoparticles decrease the viscosity on the wall of tube and blood will flow with less/normal pressure.

In chapter 5, analysis of tangent hyperbolic nano fluid flow through a ciliated tube is discussed with effects of magnetic field. The presence of nanoparticles in base fluid results in weak disorder which helps to reduce viscous dissipation effects and nanoparticles increases the thermal conductivity of fluid.

In chapter 6, mathematical modeling of ciliary transport of inertial flow of Maxwell's fluid model is discussed in a two dimensional cylinder. It is investigated that larger inertial forces increases the velocity of flow and decreases the rate of heat transfer.

In chapter 7, mathematical modeling of ciliary flow of Power law nanofluid model is discussed in a ciliated tube. It is investigated that thermal and concentration gradient significantly accelerated the cilia induced flow. Also nanoparticles enhances the thermal conductivity of fluid and Browniam motion causes to increase concentration gradient.

In chapter 8, the impact of heat and mass transfer is discussed on the cilia induced flow of PTT fluid trough two layers with different viscosities. It is concluded that magnitude of velocity, heat and mass transfer is maximum in the central layer and minimum at the peripheral layer i.e. near the boundary of tube.

Finally, it is concluded that the temperature and concentration profile can be enhanced by cilia induced flow. This study will provide remarkable applications in medical sciences, bioengineering and medical equipment, such as cilia based micro devices for the removal of fluid from viruses, bacteria and dust particle.

Appendix

$$A_1 = -\frac{Gr_T h^2}{4} - \frac{BrGr_T h^2}{32}\left(\frac{dp}{dz}\right)^2 - \frac{3}{64}\left(M^2 + \frac{1}{D_a}\right)^2 h^4\left(-Gr_T - Gr_C + \left(M^2 + \frac{1}{D_a}\right)^2 \frac{dp}{dz}\right)$$
$$+ \frac{1}{4} Gr_C h^2 S_H S_T - \frac{1}{4}\left(M^2 + \frac{1}{D_a}\right) h^2 (1 + w(h))$$

$$A_2 = \frac{Gr_T}{4} - \frac{1}{16}\left(M^2 + \frac{1}{D_a}\right)^2 h^2\left(-Gr_T - Gr_C + \left(M^2 + \frac{1}{D_a}\right)^2 \frac{dp}{dz}\right) - \frac{1}{4} Gr_C S_H S_T$$
$$+\frac{1}{4}\left(M^2 + \frac{1}{D_a}\right) h^2 (1 + w(h))$$

$$A_3 = \frac{BrGr_T}{32}\left(\frac{dp}{dz}\right)^2 + \frac{1}{64}\left(M^2 + \frac{1}{D_a}\right)^2\left(-Gr_T - Gr_C + \left(M^2 + \frac{1}{D_a}\right)^2 \frac{dp}{dz}\right)$$

$$A_4 = \frac{-1}{2} Br \frac{dp}{dz} - \frac{h^2}{8}\left(-Gr_T - Gr_C + \frac{dp}{dz}\right) + \frac{1}{2}\left(M^2 + \frac{1}{D_a}\right)^2 (1 + w(h))$$

$$A_5 = \frac{-1}{32} Br \frac{dp}{dz}\left(-Gr_T - Gr_C + \left(M^2 + \frac{1}{D_a}\right)^2 \frac{dp}{dz}\right)$$

$$A_6 = S_H S_T$$

$$A_7 = \frac{1}{2} Br \left(\frac{dp}{dz}\right)^2 S_H S_T$$

$$A_8 = \frac{5BrGr_T h^8}{1536}$$

$$A_9 = \frac{-384h^4 - 224\left(M^2 + \frac{1}{D_a}\right)^2 h^6 + 25\left(M^2 + \frac{1}{D_a}\right)^4 h^4}{3072}$$

$$A_{10} = h^2 w(h) + \frac{1}{3072}\left(288Gr_T h^6 - 25\left(M^2 + \frac{1}{D_a}\right)^2 (Gr_T + Gr_C) h^8 + 32Gr_C h^6 (7 - 2S_H S_T)\right)$$

$$\frac{1}{3072}\left(-384\left(M^2+\frac{1}{D_a}\right)^2 h^4(1+w(h))+64\left(M^2+\frac{1}{D_a}\right)^4 h^6(1+w(h))\right)$$

$$A_{11}=\frac{-1}{18432}\left(M^2+\frac{1}{D_a}\right)^2 Gr_C-\left(M^2+\frac{1}{D_a}\right)^2 Gr_T+\left(M^2+\frac{1}{D_a}\right)^2\frac{dp}{dz}$$
$$+2BrGr_T\left(\frac{dp}{dz}\right)^2$$

$$A_{12}=\frac{12}{18432}\left(M^2+\frac{1}{D_a}\right)^2 h^2(Gr_T+Gr_C)+48\left(M^2+\frac{1}{D_a}\right)^2\frac{dp}{dz}-12\left(M^2+\frac{1}{D_a}\right)^4 h^2$$
$$-48Gr_C(1+S_HS_T)+48\left(M^2+\frac{1}{D_a}\right)^4(1+w(h))$$

$$A_{13}=\frac{1}{18432}1152\left(M^2+\frac{1}{D_a}\right)^2+54\left(M^2+\frac{1}{D_a}\right)^2 h^4(Gr_T+Gr_C)+1152\frac{dp}{dz}$$
$$288\left(M^2+\frac{1}{D_a}\right)^2 h^2\frac{dp}{dz}-54\left(M^2+\frac{1}{D_a}\right)^4 h^4\frac{dp}{dz}-36BrGr_Th^4\left(\frac{dp}{dz}\right)^2$$
$$288Gr_Ch^2(1+S_HS_T)+1152\left(M^2+\frac{1}{D_a}\right)^2 w(h)$$
$$-288\left(M^2+\frac{1}{D_a}\right)^2 h^2(1+w(h))$$

$$A_{14}=\frac{1}{18432}-2304\left(M^2+\frac{1}{D_a}\right)^2 h^2+864Gr_Th^4-140\left(M^2+\frac{1}{D_a}\right)^2 h^6(Gr_T+Gr_C)$$
$$-2304h^2\frac{dp}{dz}-432\left(M^2+\frac{1}{D_a}\right)^2 h^4\frac{dp}{dz}+140\left(M^2+\frac{1}{D_a}\right)^4 h^6\frac{dp}{dz}$$
$$+64BrGr_Th^6\left(\frac{dp}{dz}\right)^2-432Gr_Ch^4(-1+S_HS_T)+9216w(h)$$
$$-2304\left(M^2+\frac{1}{D_a}\right)^2 h^2w(h)+432\left(M^2+\frac{1}{D_a}\right)^4 h^4(1+w(h))$$

$$A_{15}=-1-2\pi\varepsilon\alpha\beta\cos(2\pi z)$$

$$A_{16}=\frac{Gr_Th^4Nb^2(1+\lambda_1)+16Gr_Ch^2Nt(1+\lambda_1)}{256Nb}$$
$$\frac{64\left(\frac{dp}{dz}+4\right)(1+\lambda_1)+16Gr_Ch^2(2+\lambda_1)}{256}$$

$$\frac{Gr_T(-16h^2\lambda_1 + h^4)(1+\lambda_1)\left(Nt - Br\left(\frac{dp}{dz}\right)^2\right)(1+\lambda_1)}{256}$$

$$A_{17} = \frac{(2Gr_T Nb - Gr_C Nt)(1+\lambda_1)}{64Nb}$$

$$A_{18} = \frac{Gr_T(1+\lambda_1)\left(Nb + Nt - Br\left(\frac{dp}{dz}\right)^2(1+\lambda_1)\right)}{2304}$$

$$A_{19} = \frac{1}{4}$$

$$A_{20} = \frac{1}{16}\left(\frac{Nb}{4} - \frac{Nb+Nt}{4}\right) + \frac{Nt}{4} + \frac{1}{16}Br(Gr_T + Gr_C)h^2\frac{dp}{dz}(1+\lambda_1)$$
$$-\frac{1}{64}\left(-Nb - Nt + Br\left(\frac{dp}{dz}\right)^2(1+\lambda_1)\right)$$

$$A_{21} = \frac{1}{36}\left(\frac{1}{32}Br(Gr_T + Gr_C)\frac{dp}{dz}(1+\lambda_1) + \frac{1}{32}(Nb + Nt)\left(Nb + Nt - Br\left(\frac{dp}{dz}\right)^2(1+\lambda_1)\right)\right)$$

$$A_{22} = \frac{1}{4} + \frac{Nt}{4Nb} + \frac{(Nb+Nt)}{4Nb}$$

$$A_{23} = \frac{Nt\left(Nb - Nt + Br\left(\frac{dp}{dz}\right)^2(1+\lambda_1)\right)}{64Nb}$$

$$A_{24} = \frac{-1}{8}h^4(1+\lambda_1)$$

$$A_{25} = \frac{5BrGr_T h^8\left((1+\lambda_1)\right)^2}{3072}$$

$$A_{26} = h^2 \frac{-3072Nbw(h) + 5Gr_T h^6 Nb^2(1+\lambda_1) + 5Gr_T h^6 NbNt(1+\lambda_1)}{3072Nb}$$

$$h^2 \frac{64Gr_C h^4(2Nb+Nt)(1+\lambda_1)}{3072Nb}$$

$$A_{27} = \frac{(1-\varphi)^{2.5}}{4(1-m)}$$

$$A_{28} = \frac{mWe(1-\varphi)^5}{12(1-m)^3}$$

$$A_{29} = \frac{-3h^5}{5} A_{28}$$

$$A_{30} = \frac{h^4}{2} A_{27}$$

$$A_{31} = q - h^2 w(h)$$

$$A_{32} = -\frac{(1-m)Br\left(\frac{dp}{dz}\right)^2(1-\varphi)^5}{4(1-m)^2}$$

$$A_{33} = \frac{mBrWe\left(\frac{dp}{dz}\right)^3(1-\varphi)^{7.5}}{4(1-m)^3} + \frac{mBrWe\left(\frac{dp}{dz}\right)^3(1-\varphi)^{7.5}}{8(1-m)^3}$$

$$A_{34} = \frac{mBrWe^2\left(\frac{dp}{dz}\right)^4(1-\varphi)^{10}}{4(1-m)^5} + \frac{3m^2BrWe^2\left(\frac{dp}{dz}\right)^4(1-\varphi)^{10}}{16(1-m)^5}$$

$$A_{35} = \frac{3m^3BrWe^3\left(\frac{dp}{dz}\right)^5(1-\varphi)^{12.5}}{32(1-m)^3}$$

$$A_{36} = \frac{m^4BrWe^4\left(\frac{dp}{dz}\right)^6(1-\varphi)^{15}}{64(1-m)^3}$$

References

[1] Wilson EB. 1925. The cell in development and heredity. New York, Macmilla.

[2] Gray J. 1928. Ciliary Motion. Cambridge University press.

[3] Taylor G. 1951. Analysis of the swimming of microscopic organisms. Proc R Soc Lond A. 209(1099): 447-461.

[4] Porter KR. 1955. The submicroscopic morphology of protoplasm. Harvey Lectures. 51:175.

[5] Satir P. 1962. On the evolutionary stability of the 9+ 2 pattern. J Cell Bio. 12(1): 181.

[6] Sleigh MA. 1962. The biology of cilia and flagella. Int Ser Monographs Pure Appl Bio.12.1-252.

[7] Blake JR. 1971. A spherical envelope approach to ciliary propulsion. J Fluid Mech. 46(1): 199-208.

[8] Blake JR. 1971. Infinite models for ciliary propulsion. Journal of Fluid Mechanics. 49(2): 209-222.

[9] Katz, David F. 1972. On the biophysics of in vivo sperm transport. Doctoral dissertation, University of California. Berkeley.

[10] Lardner TJ, Shack WJ. 1972. Cilia transport. Bullet Math Bio. 34(3): 325-335.

[11] Blake JR. 1973. Flow in tubules due to ciliary activity. Bullet Math Bio. 35: 513-523.

[12] Brennen C. 1974. An oscillating-boundary-layer theory for ciliary propulsion. J Fluid Mech. 65(4): 799-824.

[13] Brennen C. 1975. Hydromechanics of propulsion for ciliated micro-organisms. ISBN 0306370883: 235-253.

[14] Sanderson MJ, Sleigh MA. 1982. The Function of Respiratory Tract Cilia. In Lung Envir Springer US. 81-120.

[15] Agrawal HL, Anawaruddin. 1984. Cilia transport of bio-fluid with variable viscosity. In J Pure Appl Math. 15(10): 1128-1139.

[16] Fulford GR, Blake JR. 1986. Muco-ciliary transport in the lung. J Theo Bio. 121(4): 381-402.

[17] Sleigh MA. 1989. Adaptations of ciliary systems for the propulsion of water and mucus. Comp Biochem Phy Part A: Phy. 94(2): 359-364.

[18] Gueron S, Liron N. 1992. Ciliary motion modeling, and dynamic multicilia interactions. Biophy J. 63(4): 1045-1058.

[19] Pazour GJ , Witman GB. 2003. The vertebrate primary cilium is a sensory organelle. Curr Opinion Cell Bio. 15(1): 105-110.

[20] Dillon RH, Fauci LJ, Omoto C, Yang X. 2007. Fluid dynamic models of flagellar and ciliary beating. Ann New York Acad Sci. 1101(1): 494-505.

[21] Siddiqui AM, Haroon T, Rani M, Ansari AR. 2010. An analysis of the flow of a power law fluid due to ciliary motion in an infinite channel. J Biorheo. 24(2): 56-69.

[22] Mills ZG, Aziz B and Alexeev A. 2012. Beating synthetic cilia enhance heat transport in microfluidic channels. Soft Matter. 8(45): 11508-11513.

[23] Akbar NS, Butt AW, Noor FM. 2014. Heat transfer analysis on transport of copper nanofluids due to metachronal waves of cilia. Curr Nanosci. 10(6): 807-815.

[24] Smith DJ, Gaffney EA, Blake JR. 2008. Modelling mucociliary clearance. Resp Physiol Neurobi. 163:178-188.

[25] Bottier M., Fernández MP, Pelle G, Isabey D, Louis B, Grotberg JB, Filoche, M. 2017. A new index for characterizing micro-bead motion in a flow induced by ciliary beating: Part II, modeling. *PLoS* Compt Bio. 13(7): e1005605.

[26] Gallagher, J. T., & Richardson, P. S. (1982). Respiratory mucus: structure, metabolism and control of secretion. In *Mucus in Health and Disease—II* (pp. 335-350). Springer, Boston, MA.

[27] Ashraf H, Siddiqui AM, Rana MA. 2018. Fallopian tube analysis of the peristaltic-ciliary flow of third grade fluid in a finite narrow tube. Chin J Phy, 56(2): 605-621.

[28] Ashraf H. Siddiqui AM, Rana MA. 2018. Analysis of the peristaltic-ciliary flow of Johnson–Segalman fluid induced by peristalsis-cilia of the human fallopian tube. Math Biosci.300: 64-75.

[29] Halbert, S. A., Patton, D. L., Zarutskie, P. W., & Soules, M. R. (1997). Function and structure of cilia in the fallopian tube of an infertile woman witb Kartagener's syndrome. *Human reproduction*, *12*(1): 55-58.

[30] Siddiqui AM, Farooq AA, Rana MA. 2014. Hydromagnetic flow of Newtonian fluid due to ciliary motion in the channel. Magnetohydrodynamics 50: 109-122.

[31] Haroon T, Ansari AR, Imran A, Siddiqui AM. 2012. On the ciliary transport of an axisymmetric power law fluid through a tube. Math Eng Sci Aerospace .3(2), 131–142.

[32] Handling AC. 1943. The role of ciliaryaction in production of pulmonary atelectasis, vacuum in the paranasal sinuses and in otitis media. Ann Otol Rhinol Laryngol. 52: 3-19.

[33] Lee WL, Jayathilake PG, Tan Z, Le DV, Lee HP, Khoo BC. 2011. Muco-ciliary transport: effect of mucus viscosity, cilia beat frequency and cilia density. Comp & Fluids. 49(1), 214-221.

[34] Maqbool K, Shaheen S, Mann AB. (2016). Exact solution of cilia induced flow of a Jeffrey fluid in an inclined tube. SpringerPlus. 5(1): 1-16.

[35] Siddiqui AM, Sohail A, Maqbool K. (2017). Analysis of a channel and tube flow induced by cilia. Appl Math Compt. 309: 133-141.

[36] Maqbool K, Mann AB, Siddiqui AM, Shaheen S. 2017. Fractional generalized Burgers' fluid flow due to metachronal waves of cilia in an inclined tube. Adv Mech Eng. 9(8): 1687814017715565.

[37] Shaheen S, Maqbool K, Ellahi R, Sait SM. 2021. Metachronal propulsion of non-Newtonian viscoelastic mucus in an axisymmetric tube with ciliated walls. Comm Theo Phy 73(3):035006.

[38] Mann AB, Shaheen S, Maqbool K, Poncet S. 2019. Fractional Burgers fluid flow due to metachronal ciliary motion in an inclined tube. Front. Phys. 10: 588.

[39] Maqbool K, Manzoor N, Ellahi R, Sait SM. 2021. Influence of heat transfer on MHD Carreau fluid flow due to motile cilia in a channel. J Therm Anal Calorim.: 144(6). 2317-2326.

[40] Siddiqui AM, Manzoor N, Maqbool K, Mann AB, Shaheen S. 2019. Magnetohydrodynamic flow induced by ciliary movement: An application to lower respiratory tract diseases. J Mag Magn Mater. 480: 164-170.

[41] Shaheen S, Maqbool K, Siddiqui AM. 2020. Analytical model of magnetically actuated mucociliary pumping in a bronchial tube. Phy Script. 95(4): 045211.

[42] Elnaqeeb T, Mekheimer KS, Alghamdi F. 2016. Cu-blood flow model through a catheterized mild stenotic artery with a thrombosis. Math Biosci. 282: 135-146.

[43] Elnaqeeb T, Shah NA, Mekheimer KS. 2019. Hemodynamic Characteristics of Gold Nanoparticle Blood Flow Through a Tapered Stenosed Vessel with Variable Nanofluid Viscosity. BioNanoScience. 9(2): 245-255.

[44] Infante JA, Ivorra B, Ramos AM, Rey JM. 2009. On the modelling and simulation of high pressure processes and inactivation of enzymes in food engineering, Math Mod Meth Appl Sci. 19: 2203-2229.

[45] Karampatzakis A, Samaras T. 2010. Numerical model of heat transfer in the human eye with consideration of fluid dynamics of the aqueous humour. Phys Med Biol. 55: 5653-5678.

[46] Hsu CP, Jewell-Larsen NE, Krichtafovitch IA, Mamishev AV. 2008. Heat-transfer-enhancement measurement for microfabricated electrostatic fluid accelerators. J Microelectromech Sys. 18(1):111-8.

[47] Dessiatoun SV. 2009. Compact heat exchanging device based on microfabricated heat transfer surfaces. United States patent US. 7: 571-618.

[48] Tse O, Pinnau R, Siedow N. 2012. Identification of temperature-dependent parameters in laser-interstitial thermo therapy. Math Mod Meth Appl Sci. 22:1250019.

[49] Horstmann G, Iravani J, Melville GN, Richter HG. 1977. Influence of temperature and decreasing water content of inspired air on the ciliated bronchial epithelium, Acta Oto-Laryngol. 84:124-131.

[50] He Y, Liu H, Himeno R, Sunaga J, Kakusho N, Yokota H. 2008. Finite element analysis of blood flow and heat transfer in an image-based human finger. Comp Biol Med. 38: 555-562.

[51] Hatanaka A, Umeda N, Yamashita S, Hirazawa N. 2005. A small ciliary surface glycoprotein of the monogenean parasite Neobenedenia girellae acts as an agglutination/immobilization antigen and induces an immune response in the Japanese flounder Paralichthys olivaceus. Parasitology. 131(5): 591-600.

[52] Mills Z G, Aziz B, Alexeev A. 2012. Beating synthetic cilia enhance heat transport in microfluidic channels. Soft Matter. 8(45): 11508-13.

[53] Akbar NS, Butt AW. 2015. Heat transfer analysis of Rabinowitsch fluid flow due to metachronal wave of cilia. Res Phy. 5: 92-98.

[54] Nadeem S, Sadaf H. 2015. Trapping study of nanofluids in an annulus with cilia. AIP Advances. 5(12): 127-204.

[55] Akber NS, Khan ZH, Nadeem S. 2014. Metachronal beating of cilia under influence of Hartmann layer and heat transfer. Eur Phys J Plus. 129: 176.

[56] Akbar NS, Wahid Butt A, Noor FM. 2014. Heat transfer analysis on transport of copper nanofluids due to metachronal waves of cilia. Curr Nanosci. 10(6): 807- 815

[57] Abrar MN, Haq RU, Awais M, Rashid I. 2017. Entropy analysis in a cilia transport of nanofluid under the influence of magnetic field. Nuc Eng Tech. 49(8):1680-1688.

[58] Imran A, Akhtar R, Zhiyu Z, Shoaib M. Raja MA. 2020. Heat transfer analysis of biological nanofluid flow through ductus efferentes. AIP Adv, 10(3): 035029.

[59] Manzoor, N., Maqbool, K., Bég, O.A. and Shaheen, S., 2019. Adomian decomposition solution for propulsion of dissipative magnetic Jeffrey biofluid in a ciliated channel containing a porous medium with forced convection heat transfer. *Heat Transfer—Asian Research*, *48*(2), pp.556-581.

[60] Gul F, Maqbool K, Mann AB. 2020. Thermal analysis of electroosmotic flow in a vertical ciliated tube with viscous dissipation and heat source effects. J Therm Anal Calorim: 143(3), 2111-2123.

[61] Farooq AA, Shah Z, Alzahrani EO. 2019. Heat transfer analysis of a magneto-bio-fluid transport with variable thermal viscosity through a vertical ciliated channel. Symmetry: 11(10): 1240.

[62] Pittman RN. 2011. The circulatory system and oxygen transport. In *Regulation of Tissue Oxygenation*. Morgan & Claypool Life Sciences.

[63] Abdelrasoul A, Doan H, Lohi A, Cheng CH. 2015. Mass transfer mechanisms and transport resistances in membrane separation process. Chapter. 2: 15-40.

[64] Goosen MF, Sablani SS, Al-Maskari SS, Al-Belushi RH, Wilf M. 2002. Effect of feed temperature on permeate flux and mass transfer coefficient in spiral-wound reverse osmosis systems. Desalination. 144(1-3): 367-372.

[65] Law CK. 1984. Heat and mass transfer in combustion: Fundamental concepts and analytical techniques. Prog Ener Comb Sci. 10(3): 295-318.

[66] Chern JM, Chou SR, Shang CS. 2001. Effects of impurities on oxygen transfer rates in diffused aeration systems. Water Res. 35(13): 3041-3048.

[67] Manshadi MK, Saadat M, Mohammadi M, Kamali R, Shamsi M, Naseh M, Sanati-Nezhad, A. 2019. Magnetic aerosol drug targeting in lung cancer therapy using permanent magnet. Drug Del. 26(1): 120-128.

[68] Khan NA, Sultan F. 2018. Physiological modeling and simulation of fluid flows. Compt Appr Biomed Nano-Eng. 255-277.

[69] Shaheen A, Hussain S, Nadeem S. 2016. Physiological Flow of Jeffrey Six Constant Fluid Model due to Ciliary Motion. Comm Theo Phys. 66(6): 701.

[70] Abdelsalam SI, Bhatti MM, Zeeshan A, Riaz A, Bég OA. 2019. Metachronal propulsion of a magnetised particle-fluid suspension in a ciliated channel with heat and mass transfer. Phys. Script. 94(11): 115301.

[71] Farooq AA, Shah Z, Shutaywi M, Bonyah E, Roy P. 2020. Axisymmetric mixed convective propulsion of a non-Newtonian fluid through a ciliated tubule. AIP Adv. 10(5): 055214.

[72] Shehzad SA, Abbasi FM, Hayat T, Alsaadi F. 2014. MHD mixed convective peristaltic motion of nanofluid with Joule heating and thermophoresis effects. PLoS One.;9(11):e111417.

[73] Ghasemi SE. 2017. Thermophoresis and Brownian motion effects on peristaltic nanofluid flow for drug delivery applications. J Mol Liq. 238:115-21.

[74] Sucharitha G, Sreenadh S, Lakshminarayana P, Sushma K. 2017. Brownian motion and thermophoresis effects on Peristaltic slip flow of a MHD nanofluid in a symmetric/asymmetric channel. Mat Sci Eng. 263(6): 062025.

[75] Hatami M, Mosaybidorcheh S, Jing D. 2019. Peristaltic flow and heat transfer of nanofluids in a sinusoidal wall channel: two-phase analytical study. J. Anal. 27(3):913-29.

[76] Reddy MG, Makinde OD. 2016. Magnetohydrodynamic peristaltic transport of Jeffrey nanofluid in an asymmetric channel. J Mol Liq. 223:1242-8.

[77] Kothandapani M, Prakash J. 2015. Effect of radiation and magnetic field on peristaltic transport of nanofluids through a porous space in a tapered asymmetric channel. J Mag Magn Mat. 378:152-63.

[78] Murdock J. 2006. Perturbation Methods. Math Tools Phys. 385–415.

[79] Adomian G. 1986. Nonlinear Stochastic Operator Equations: Academic Press. Can Diego, CA.

[80] Adomian G. 1994. Solving Frontier Problems of Physics: The Decomposition MethodKluwer. Boston MA.

[81] He JH. 1999. Homotopy perturbation technique. Comp Meth Appl Mech Eng. 178(3): 257-262.

[82] Vélez-Cordero JR, Lauga E. 2013. Waving transport and propulsion in a generalized Newtonian fluid. J non-New Fluid Mech, 199, 37-50.

[83] Kollberg H, Mossberg B, Afzelius BA, Philipson K, Camner P. 1978. Cystic fibrosis compared with the immotile-cilia syndrome. A study of mucociliary clearance, ciliary ultrastructure, clinical picture and ventilatory function. Scandinavian J Resp Dis. 59(6):297-306

[84] Eldabe NT, El-Sayed MF, Ghaly AY, Sayed HM. 2008. Mixed convective heat and mass transfer in a non-Newtonian fluid at a peristaltic surface with temperature-dependent viscosity. Arch App Mech. 78(8): 599-624.

[85] Akbar NS, Khan ZH. Nadeem S. 2016. Influence of magnetic field and slip on Jeffrey fluid in a ciliated symmetric channel with metachronal wave pattern. J Appl Fluid Mech. 9(2):565-72.

[86] Jyothi S, Subba RM, Gangavathi P. 2016. Hyperbolic tangent fluid flow through a porous medium in an inclined channel with peristalsis. Int J Adv Sci Res Manag. 1(4).

[87] Hayat T, Shafique M, Tanveer A, Alsaeedi A. 2016. Magnetohydrodynamic effects on peristaltic flow of hyperbolic tangent nano-fluid with slip conditions and Joule heating in an inclined channel, Int J Heat Mass Trans. 102: 54-63.

[88] Khan M, Ahmed A, Irfan M, Ahmed J. 2020. Analysis of Cattaneo–Christov theory for unsteady flow of Maxwell fluid over stretching cylinder. J Therm Anal Calorim. 1-10.

[89] Ahmed J, Khan M, Ahmad L. 2020. Effectiveness of homogeneous–hetcrogeneous reactions in Maxwell fluid flow between two spiraling disks with improved heat conduction features. J Therm Anal Calorim. 139(5): 3185-3195.

[90] Butt AW, Akbar NS, Mir NA. 2020. Heat transfer analysis of peristaltic flow of a Phan-Thien–Tanner fluid model due to metachronal wave of cilia. Biomech Model Mechanobiology. 1-9.

[91] Siddiqui AM. Zeb M. Haroon T. Azim QU. 2019. Exact solution for the heat transfer of two immiscible PTT fluids flowing in concentric layers through a pipe. Mathematics. 7(1): 81.